

ISSN 1881-7815 Online ISSN 1881-7823

BST

BioScience Trends

Volume 8, Number 2
April, 2014



www.biosciencetrends.com

BST

BioScience Trends



ISSN: 1881-7815
Online ISSN: 1881-7823
CODEN: BTIRCZ
Issues/Year: 6
Language: English
Publisher: IACMHR Co., Ltd.

BioScience Trends is one of a series of peer-reviewed journals of the International Research and Cooperation Association for Bio & Socio-Sciences Advancement (IRCA-BSSA) Group and is published bimonthly by the International Advancement Center for Medicine & Health Research Co., Ltd. (IACMHR Co., Ltd.) and supported by the IRCA-BSSA and Shandong University China-Japan Cooperation Center for Drug Discovery & Screening (SDU-DDSC).

BioScience Trends devotes to publishing the latest and most exciting advances in scientific research. Articles cover fields of life science such as biochemistry, molecular biology, clinical research, public health, medical care system, and social science in order to encourage cooperation and exchange among scientists and clinical researchers.

BioScience Trends publishes Original Articles, Brief Reports, Reviews, Policy Forum articles, Case Reports, News, and Letters on all aspects of the field of life science. All contributions should seek to promote international collaboration.

Editorial Board

Editor-in-Chief:

Masatoshi MAKUUCHI
Japanese Red Cross Medical Center, Tokyo, Japan

Co-Editors-in-Chief:

Xue-Tao CAO
Chinese Academy of Medical Sciences, Beijing, China
Rajendra PRASAD
UP Rural Institute of Medical Sciences & Research, Uttar Pradesh, India
Arthur D. RIGGS
Beckman Research Institute of the City of Hope, Duarte, CA, USA

Chief Director & Executive Editor:

Wei TANG
The University of Tokyo, Tokyo, Japan

Managing Editor:

Munehiro NAKATA
Tokai University, Hiratsuka, Japan

Senior Editors:

Xunjia CHENG
Fudan University, Shanghai, China
Yoko FUJITA-YAMAGUCHI
Tokai University, Hiratsuka, Japan
Na HE
Fudan University, Shanghai, China
Kiyoshi KITAMURA
The University of Tokyo, Tokyo, Japan

Misao MATSUSHITA
Tokai University, Hiratsuka, Japan
Takashi SEKINE
The University of Tokyo, Tokyo, Japan
Yasuhiko SUGAWARA
The University of Tokyo, Tokyo, Japan

Web Editor:

Yu CHEN
The University of Tokyo, Tokyo, Japan

Proofreaders:

Curtis BENTLEY
Roswell, GA, USA
Christopher HOLMES
The University of Tokyo, Tokyo, Japan
Thomas R. LEBON
Los Angeles Trade Technical College, Los Angeles, CA, USA

Editorial Office

Pearl City Koishikawa 603,
2-4-5 Kasuga, Bunkyo-ku,
Tokyo 112-0003, Japan
Tel: +81-3-5840-8764
Fax: +81-3-5840-8765
E-mail: office@biosciencetrends.com

BioScience Trends

Editorial and Head Office

Pearl City Koishikawa 603, 2-4-5 Kasuga, Bunkyo-ku,
Tokyo 112-0003, Japan

Tel: +81-3-5840-8764, Fax: +81-3-5840-8765
E-mail: office@biosciencetrends.com
URL: www.biosciencetrends.com

Editorial Board Members

Girdhar G. AGARWAL (Lucknow, India)	Takahiro HIGASHI (Tokyo, Japan)	Mark MEUTH (Sheffield, UK)	Koji TANAKA (Tsu, Japan)
Hirotsugu AIGA (Geneva, Switzerland)	De-Xing HOU (Kagoshima, Japan)	Satoko NAGATA (Tokyo, Japan)	John TERMINI (Duarte, CA, USA)
Hidechika AKASHI (Tokyo, Japan)	Sheng-Tao HOU (Ottawa, Canada)	Miho OBA (Odawara, Japan)	Usa C. THISYAKORN (Bangkok, Thailand)
Moazzam ALI (Geneva, Switzerland)	Yong HUANG (Ji'ning, China)	Xianjun QU (Ji'nan, China)	Toshifumi TSUKAHARA (Nomi, Japan)
Ping AO (Shanghai, China)	Hirofumi INAGAKI (Tokyo, Japan)	John J. ROSSI (Duarte, CA, USA)	Kohjiro UEKI (Tokyo, Japan)
Hisao ASAMURA (Tokyo, Japan)	Masamine JIMBA (Tokyo, Japan)	Carlos SAINZ-FERNANDEZ (Santander, Spain)	Masahiro UMEZAKI (Tokyo, Japan)
Michael E. BARISH (Duarte, CA, USA)	Kimitaka KAGA (Tokyo, Japan)	Yoshihiro SAKAMOTO (Tokyo, Japan)	Junming WANG (Jackson, MS, USA)
Boon-Huat BAY (Singapore, Singapore)	Ichiro KAI (Tokyo, Japan)	Erin SATO (Shizuoka, Japan)	Ling WANG (Shanghai, China)
Yasumasa BESSHO (Nara, Japan)	Kazuhiro KAKIMOTO (Osaka, Japan)	Takehito SATO (Isehara, Japan)	Xiang-Dong Wang (Boston, MA, USA)
Generoso BEVILACQUA (Pisa, Italy)	Kiyoko KAMIBEPPU (Tokyo, Japan)	Akihito SHIMAZU (Tokyo, Japan)	Hisashi WATANABE (Tokyo, Japan)
Shiuan CHEN (Duarte, CA, USA)	Haidong KAN (Shanghai, China)	Zhifeng SHAO (Shanghai, China)	Lingzhong XU (Ji'nan, China)
Yuan CHEN (Duarte, CA, USA)	Bok-Luel LEE (Busan, Korea)	Ri SHO (Yamagata, Japan)	Masatake YAMAUCHI (Chiba, Japan)
Naoshi DOHMAE (Wako, Japan)	Mingjie LI (St. Louis, MO, USA)	Judith SINGER-SAM (Duarte, CA, USA)	Aitian YIN (Ji'nan, China)
Zhen FAN (Houston, TX, USA)	Shixue LI (Ji'nan, China)	Raj K. SINGH (Dehradun, India)	George W-C. YIP (Singapore, Singapore)
Ding-Zhi FANG (Chengdu, China)	Ren-Jang LIN (Duarte, CA, USA)	Junko SUGAMA (Kanazawa, Japan)	Xue-Jie YU (Galveston, TX, USA)
Yoshiharu FUKUDA (Ube, Japan)	Daru LU (Shanghai, China)	Hiroshi TACHIBANA (Isehara, Japan)	Benny C-Y ZEE (Hong Kong, China)
Rajiv GARG (Lucknow, India)	Hongzhou LU (Shanghai, China)	Tomoko TAKAMURA (Tokyo, Japan)	Yong ZENG (Chengdu, China)
Ravindra K. GARG (Lucknow, India)	Duan MA (Shanghai, China)	Tadatoshi TAKAYAMA (Tokyo, Japan)	Xiaomei ZHU (Seattle, WA, USA)
Makoto GOTO (Tokyo, Japan)	Francesco MAROTTA (Milano, Italy)	Shin'ichi TAKEDA (Tokyo, Japan)	
Demin HAN (Beijing, China)	Yutaka MATSUYAMA (Tokyo, Japan)	Sumihito TAMURA (Tokyo, Japan)	
David M. HELFMAN (Daejeon, Korea)	Qingyue MENG (Beijing, China)	Puay Hoon TAN (Singapore, Singapore)	

(as of April 2014)

Review

- 68 - 74 **The role of nerve growth factor and its receptors in tumorigenesis and cancer pain.**
Wenfang Wang, Jinhua Chen, Xiuli Guo

Original Articles

- 75 - 83 **Performance of reversed transcription loop-mediated isothermal amplification technique detecting EV71: A systematic review with meta-analysis.**
Xiaoying Lei, Hongling Wen, Li Zhao, Xuejie Yu
- 84 - 92 **Overexpression of an ABC transporter and mutations of GyrA, GyrB, and ParC in contributing to high-level ciprofloxacin resistance in *Streptococcus suis* type 2.**
Jie Yao, Kexin Shang, Jinhu Huang, Wei Ran, Jam Kashif, Liping Wang
- 93 - 100 **Defect of tropomyosin-related kinase B isotype expression in ovarian clear cell adenocarcinoma.**
Yumiko Goto, Yoshie Kametani, Atsuko Kikugawa, Banri Tsuda, Masaki Miyazawa, Hiroshi Kajiwara, Yasuhisa Terao, Susumu Takekoshi, Naoya Nakamura, Satoru Takeda, Mikio Mikami
- 101 - 110 **Expression of ankyrin repeat and SOCS box containing 4 (ASB4) confers migration and invasion properties of hepatocellular carcinoma cells.**
Victor Au, Felice H Tsang, Kwan Man, Sheung Tat Fan, Ronnie TP Poon, Nikki P Lee
- 111 - 119 **Transplantation of bone marrow mesenchymal stem cells pretreated with valproic acid in rats with an acute spinal cord injury.**
Lei Chen, Xiaoyan Cui, Zhouhui Wu, Long Jia, Yan Yu, Qiulian Zhou, Xiao Hu, Wei Xu, Dandan Luo, Jie Liu, Junjie Xiao, Qiao Yan, Liming Cheng
- 120 - 125 **EPA and DHA increased PPAR γ expression and decreased integrin-linked kinase and integrin β 1 expression in rat glomerular mesangial cells treated with lipopolysaccharide.**
Wenchao Han, Hui Zhao, Bo Jiao, Fange Liu

CONTENTS

(Continued)

- 126 - 131 **Substrate specificity of human granzyme 3: Analyses of the P3-P2-P1 triplet using fluorescence resonance energy transfer substrate libraries.**
Yukiyo Hirata, Hirofumi Inagaki, Takako Shimizu, Tomoyuki Kawada
- 132 - 137 **A high-carbohydrate diet lowered blood pressure in healthy Chinese male adolescents.**
Xingchun Zhu, Jia Lin, Yongyan Song, Hui Liu, Rongrong Zhang, Mei Fan, Yuanhao Li, Rong Tian, Dingzhi Fang

Guide for Authors

Copyright

The role of nerve growth factor and its receptors in tumorigenesis and cancer pain

Wenfang Wang, Jinhua Chen, Xiuli Guo*

Department of Pharmacology, School of Pharmaceutical Sciences, Shandong University, Ji'nan, Shandong, China.

Summary

The nerve growth factor (NGF) is a growth factor that belongs to the neurotrophin family. NGF has two structurally different receptors, the p75 neurotrophin receptor (p75NTR) and the tropomyosin-related kinase A (TrkA). Interaction of NGF with its receptors regulates a variety of physiological processes of neuronal system. Recent studies have shown that NGF and its receptors were involved in the regulation of tumourigenesis by either supporting or suppressing tumor growth depending on the tumor types. This review summarizes the current views of NGF and its receptors in tumorigenesis and cancer pain.

Keywords: Nerve growth factor, tumorigenesis, cancer pain, p75NTR receptor, TrkA receptor

1. Introduction

Nerve growth factor (NGF) is a growth factor that belongs to the nerve growth factor family of neurotrophin. NGF, like the other neurotrophin family members such as brain derived neurotrophic factor (BDNF), neurotrophins-3 (NT-3), neurotrophins-4/5 (NT-4/5), and neurotrophins-6 (NT-6), binds to two structurally different types of receptors: the p75 neurotrophin receptor (p75NTR) and tropomyosin-related kinase A (TrkA) (Figure 1) (1-3) and regulates neuronal survival, differentiation and growth. Currently, NGF, released from the nerve fibers, has been found to be involved in the tumor progression, leading to generate a positive microenvironment for cancer cell survival and proliferation (4-6).

2. The molecular structure and physiological function of NGF and its receptors

2.1. NGF

NGF was first discovered by Rita Levi-Montalcini in the early 1950's for its effects on the neuronal survival, proliferation, and differentiation (7-9). NGF is not only

discovered in nervous system, but also detected and quantified in a variety of normal and neoplastic human tissues (10,11).

NGF was first isolated from the mouse submaxillary gland with the molecular weight of approximately 140 KD, which is highly homologous to human NGF (12). Each NGF is composed of 2 α subunits, 1 β subunit, 2 γ subunits ($\alpha 2\beta\gamma 2$) and also one or two zinc ions (13,14). The β subunit of NGF is a biologically active region and a non-covalently bound homodimer that can be separated into 2 identical chains of 118 amino acids. The 2 γ subunits of NGF have proteolytic activity and are members of the kallikrein family of trypsin-like proteases. The 2 α subunits are highly homologous to the γ subunit but without any enzymatic activity (15,16).

Under physiological condition, NGF regulates neuronal survival, proliferation, and differentiation in the peripheral and central nervous systems by binding to its receptors: TrkA and p75NTR. Binding to p75NTR, NGF initiates recruitment of various adaptors, which activate c-Jun N-terminal kinase (JNK) signaling pathways to promote apoptosis, and activate NF- κ B pathways to promote cell survival. By binding to TrkA, NGF initiates pro-survival PI3K/AKT and Ras/Raf signaling pathways, *via* Ras/MAPK pathway to promote cell proliferation and metastasis (Figure 2) (6,17-20).

The intracellular activation of NGF receptor binding in figure 2 occurs only as receptor homodimers. Researchers have also suggested the existence of p75NTR and TrkA complexes which has been presented

*Address correspondence to:

Dr. Xiuli Guo, Department of Pharmacology, School of Pharmaceutical Sciences, Shandong University, Ji'nan, Shandong, China.

E-mail: guoxl@sdu.edu.cn

from both cross-linking and immunoprecipitation (21). Previous research has shown that p75NTR and TrkA interact directly in surface membranes or their extracellular (EC) domains (22), but the latest research shows that TrkA and p75NTR associate physically through their intracellular (IC) domains (23). Regardless of how p75NTR and TrkA receptors associate, the coexpression of p75NTR and TrkA receptors results in the formation of high-affinity NGF binding sites. The reason is associated with p75NTR, which can contribute to increase the binding rate of NGF with TrkA and enhance TrkA activation and the number of high affinity binding sites (24). A recent report demonstrated that an endogenous intracellular domain fragment of p75NTR containing these 29 amino acids was capable of interacting with TrkA resulting in the formation of high-affinity binding sites for NGF (25). The formation of high-affinity binding sites, resulting in enhanced NGF responsiveness, is also necessary for complete outgrowth and for long-term

survival (26,27).

For a long time, NGF is always considered to be the main form for its biological activity in regulating neuronal survival, proliferation, and differentiation. However, recent studies showed that proNGF, the precursor form of NGF, is really largely exist in central nervous system tissues, and has biological functions exceeding its role as a precursor (17,28,29). ProNGF could induce cell death by binding to p75NTR with high affinity (30-32). But it shows low affinity to TrkA, another receptor of NGF (33). Moreover, proNGF could induce apoptosis by binding to p75NTR and sortilin, a specific receptor of proNGF. Sortilin is a member of the mammalian type-I transmembrane receptors containing a Vps10p domain, which plays an essential role in proNGF-induced cell death and apoptosis (34,35). Blocking sortilin can prevent induction of apoptosis by proNGF (36). Further studies showed that sortilin acted as an assistant receptor and molecular switch for p75NTR-mediated apoptosis induced by proNGF (37). This indicated that proNGF induced apoptosis by forming a stable ternary proNGF/sortilin/p75NTR complex instead of proNGF/p75NTR complex (34,38).

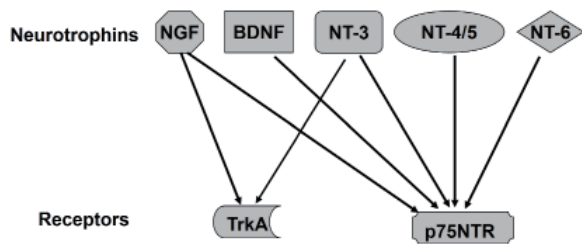


Figure 1. Neurotrophins and their preferred receptors. Neurotrophins all bind to p75NTR. TrkA is the preferred receptor for NGF. The interaction of NT-3 with TrkA requires high concentrations of the neurotrophin.

2.2. NGF receptors

p75NTR is a low affinity NGF receptor and also a member of the tumor necrosis factor (TNF) receptor superfamily. It has no tyrosine kinase activity, nor is it linked to a G-protein-coupled pathway (39). p75NTR consists of an extracellular region, which contains four cysteine-rich domains, a single transmembrane domain and an intracellular death domain. Its intracellular

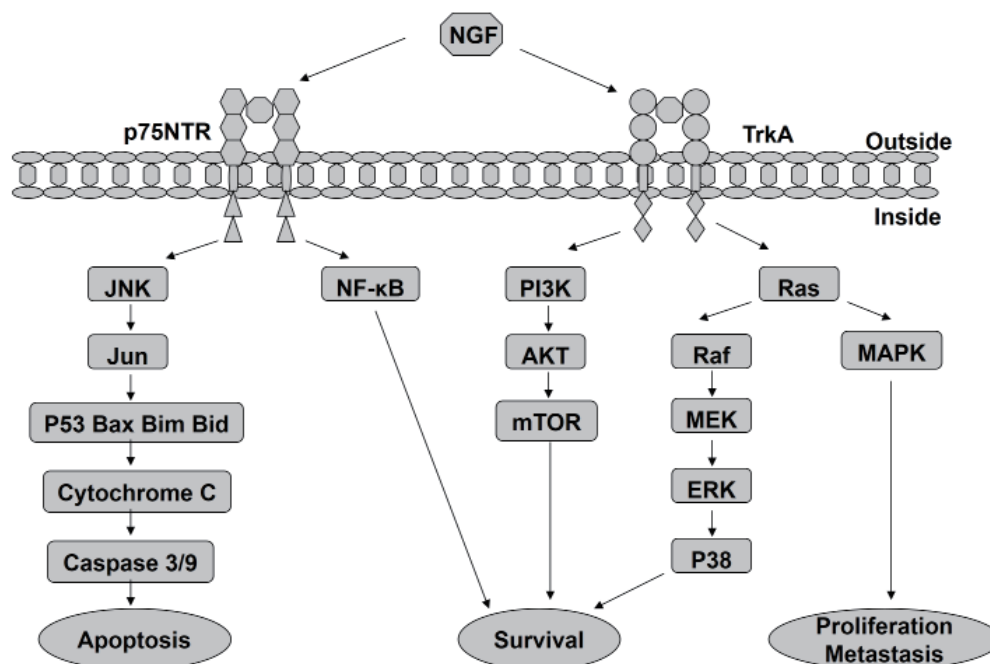


Figure 2. NGF signalling pathways. p75NTR and TrkA signalling pathways. "→" represents stimulatory modification.

domain can be phosphorylated and bind to a number of death-signalling proteins (40,41).

TrkA is a high affinity NGF receptor with tyrosine kinase activity. Unlike p75NTR which can be activated by all neurotrophin family members, TrkA is activated only by particular neurotrophins (Figure 1) (40,42-44). Like most receptor tyrosine kinases, TrkA is activated by ligand-induced formation of non-covalently associated receptor dimers (43). TrkA primarily regulates growth and differentiation of neurons in both peripheral and central nervous systems. NGF/TrkA signaling pathway supports survival and differentiation of sympathetic as well as sensory neurons responsive to temperature and pain (45).

3. Involvement of NGF and its receptors in cancer

3.1. The possible role in tumorigenesis

3.1.1. NGF prevents tumor growth through regulating innervations of perivascular nerve

Tumors require sustenance in the form of nutrients and oxygen and as well as an ability to evacuate metabolic wastes and carbon dioxide. The tumor-associated neovasculature, generated by the process of angiogenesis, addresses these needs (46). Growth of solid tumors is also dependent on their blood supply which is derived from two sources: blood vessels recruited from the pre-existing host vascular network and those resulting from the angiogenic response to cancer cells (47).

NGF facilitates innervations of perivascular nerve to regulate the blood flow in tumor neovessels and suppress tumor growth. Goda *et al.* demonstrated that NGF administration subcutaneously suppressed the growth of DU145 prostate tumors in nude mice by accelerating the maturation of neovasculatures in tumor tissues (48). Another recent study reported NGF treatment of mice implanted with DU145 prostate carcinoma cells induced innervation of perivascular nerves around tumor neovessels (49). NGF has also been shown to promote the development of new blood vessels (angiogenesis) through a direct interaction with $\alpha 9\beta 1$ integrin (50). The mechanism involved in NGF effects on tumor growth needs further investigation.

3.1.2. Involvement of NGF and p75NTR in apoptosis

p75NTR expressed in cancer cells may act as a tumor suppressor when binding to NGF and negatively regulate cell growth and proliferation (51). Dimaras and Gallie have demonstrated that p75NTR suppressed the progression of both human and TAG-RB murine retinoblastoma (52). Medulloblastoma cells overexpressing p75NTR displayed a significant increase in apoptosis (53). Non-steroidal anti-inflammatory

drugs which can induce p75NTR expression were also observed to induce apoptosis in prostate cancer cells (54,55).

Enforced p75NTR expression has been shown to inhibit gastric cancer growth *in vitro* and *in vivo* (37) by slowing cell cycle progression that results in cell accumulation of G0/G1 in prostate tumor cells (56,57) and bladder tumor cells (58). Moreover, p75NTR overexpression has been reported to induce mitochondria-mediated apoptosis through activation of a caspase-9/-7 cascade in human bladder tumor cells (59).

However, activation of the p75NTR by ligation with NGF leads to opposing effects in breast cancer. Binding of p75NTR with NGF has been shown to stimulate breast cancer cells survival signaling. The mechanism of this action is largely unknown but has been suggested to be mediated by activation of NF- κ B signaling involving BEX2. Activation of the p75NTR receptor by NGF leads to diverse and sometimes opposing effects, in particular because of intracellular adaptor molecules and expression of co-receptors (60,61).

A study by Zhao *et al.* had shown that the gene silencing technique by siRNA targeting p75NTR was capable of inducing cancer cell apoptosis (62).

3.1.3. Involvement of NGF and its receptors in metastasis

Metastasis, the spread of cancer cells from the primary neoplasm to distant organs, is the most fearsome aspect of cancer (63). p75NTR has been shown to be a tumor suppressor of NGF-stimulated migration of human prostate tumor cells (64). Jin *et al.* showed that p75NTR expression inhibited the abilities of cell invasion and metastasis of gastric cancer cells *via* inhibiting the NF- κ B signaling transduction (65). Overexpression of NGF has been shown to alter the blood vessel structure, leading to a reduction in vascular permeability and retention of cancer cells in the vasculature in lung carcinoma cells (66).

However, NGF has also been reported to promote prostate cancer cell metastasis, while intravenous gammaglobulin (IVIg), containing natural antibodies against NGF, is able to inhibit the migration of prostate cancer cell lines (67). On the other hand, TrkA overexpression promotes migration and invasion *in vitro* and enhances metastasis of xenografted breast cancer cells in immunodeficient mice (68). Further investigations are needed to elucidate the underlying mechanisms of these actions.

3.1.4. Involvement of NGF and TrkA in cancer growth

NGF/TrkA is involved in the regulating cell survival, differentiation, and proliferation, both in neuronal and non-neuronal cells (69). Recent studies demonstrated that TrkA expression was increased during the progression of medullary thyroid carcinoma and neuroblastoma (70).

Moreover, cancer cellular growth showed an association with NGF/TrkA in neuroblastomas and pancreatic cancer (71,72) and blocking the NGF/TrkA signal pathway can inhibit obviously tumor growth in prostate cancer (73). Besides, both *in vitro* and *in vivo* studies showed that TrkA stimulation can result in cellular growth in the breast cancer (45,74). TrkA appearing anti-apoptotic activities has a direct relationship with the presence of Ku70, which is the DNA repair protein and reported for its role in cell survival and carcinogenesis (69).

3.2. Involvement of NGF and TrkA in cancer pain

Pain is one of the most feared and burdensome symptoms in cancer patients and most individuals experience moderate to severe pain (75-77). Bone cancer pain is a high-risk of malignancies in patients with breast, prostate and lung cancer as these tumors have a remarkable ability to metastasize to bone (78).

NGF and its cognate TrkA receptor are believed to be a major mediator of chronic pain (79). NGF has been shown to be involved in perineural invasion (PNI), a process where cancer cells invade the surrounding nerves in pain generation in several malignancies, including breast, prostate and pancreatic cancers (80). Inhibiting the action of NGF/TrkA has been proposed to be a possible therapeutic approach to reduce PNI and block bone cancer pain (81).

NGF can promote the pathological reorganization of nearby TrkA sensory nerve fibers. The therapies of preventing this reorganization of sensory nerve fibers may provide insight into the mechanisms driving cancer pain (82,83). In a mouse model of prostate cancer-induced bone pain, both preemptive and late administration of monoclonal antibodies against NGF significantly reduced nociceptive behaviors, sensory and sympathetic nerve sprouting, and neuroma formation (84). Other studies showed that early/sustained, but not late/acute administration of a TrkA inhibitor ARRY-470 to mice markedly attenuated bone cancer pain and significantly blocked the ectopic sprouting of sensory nerve fibers and the formation of neuroma-like structures in the tumor bearing bone (85).

Both of these strategies carry its strength as well as limitations. For example, administration of monoclonal antibodies (anti-NGF or anti-TrkA) are generally selective than small inhibitors but carrying the risk of immune reactions. While small molecule inhibitors of TrkA, which are generally less expensive than monoclonal antibodies, allowing greater flexibility in dosing but generally less selective (85).

4. Discussion

NGF and its receptors are involved, directly or indirectly, in the pathogenesis of cancer and the manifesto of cancer pain through several mechanisms

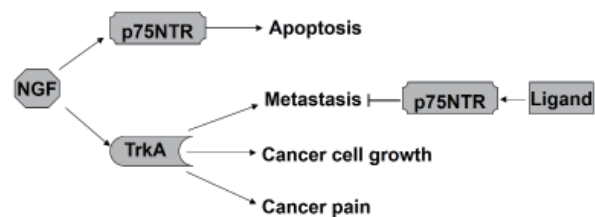


Figure 3. Effects of NGF and its receptors on tumorigenesis and cancer pain. "→" represents stimulatory modification; "←" represents inhibitory modification.

(Figure 3) such as inhibiting tumor growth, increasing apoptosis and promoting neuronal regulation of tumor blood flow. Future investigations will be provided for further insight into the actions of NGF and its receptors in cancer development and metastasis. Targeting the actions of NGF and its receptors may represent a potential direction for the treatment of tumorigenesis and cancer pain in future.

References

1. Lykissas MG, Batistatou AK, Charalabopoulos KA, Beris AE. The role of neurotrophins in axonal growth, guidance, and regeneration. *Curr Neurovasc Res.* 2007; 4:143-151.
2. Cui X, Chen L, Ren Y, Ji Y, Liu W, Liu J, Yan Q, Cheng L, Sun YE. Genetic modification of mesenchymal stem cells in spinal cord injury repair strategies. *Biosci Trends.* 2013; 7:202-208.
3. Wiesmann C, De Vos A. Nerve growth factor: structure and function. *Cell Mol Life Sci.* 2001; 58:748-759.
4. Mancino M, Ametller E, Gascón P, Almenro V. The neuronal influence on tumor progression. *Biochim Biophys Acta.* 2011; 1816:105-118.
5. Krüttgen A, Schneider I, Weis J. The dark side of the NGF family: Neurotrophins in neoplasias. *Brain Pathol.* 2006; 16:304-310.
6. Molloy NH, Read DE, Gorman AM. Nerve growth factor in cancer cell death and survival. *Cancers.* 2011; 3:510-530.
7. Levi-Montalcini R, Hamburger V. Selective growth stimulating effects of mouse sarcoma on the sensory and sympathetic nervous system of the chick embryo. *J Exp Zool.* 1951; 116:321-361.
8. Navis AR. Nerve Growth Factor. *Embryo Project Encyclopedia.* 2012; <http://hdl.handle.net/10776/1674>.
9. Aloe L. Rita Levi-Montalcini and the discovery of NGF, the first nerve cell growth factor. *Arch Ital Biol.* 2011; 149:175-181.
10. MacGrogan D, Saint-André JP, Dicou E. Expression of nerve growth factor and nerve growth factor receptor genes in human tissues and in prostatic adenocarcinoma cell lines. *J Neurochem.* 2006; 59:1381-1391.
11. Vanhecke E, Adriaenssens E, Verbeke S, Maignan S, Germain E, Berteaux N, Nurcombe V, Le Bourhis X, Hondermarck H. Brain-derived neurotrophic factor and neurotrophin-4/5 are expressed in breast cancer and can be targeted to inhibit tumor cell survival. *Clin Cancer Res.* 2011; 17:1741-1752.
12. Ullrich A, Gray A, Berman C, Dull TJ. Human β -nerve growth factor gene sequence highly homologous to that

- of mouse. *Nature*. 1983; 303:821-825.
13. Varon S, Nomura J, Shooter E. The Isolation of the Mouse Nerve Growth Factor Protein in a High Molecular Weight Form. *Biochemistry*. 1967; 6:2202-2209.
 14. Thoenen H, Barde Y. Physiology of nerve growth factor. *Physiol Rev*. 1980; 60:1284-1335.
 15. Shi E, Wang B, Sun Q. Nerve growth factor and injured peripheral nerve regeneration. *Neural Regen Res*. 2008; 3:1273-1276.
 16. Seidel MF, Herguijuela M, Forkert R, Otten U. Nerve growth factor in heumatic diseases. *Semin Arthritis Rheum*. 2010. 40:109-126.
 17. Masoudi R, Ioannou MS, Coughlin MD, Pagadala P, Neet KE, Clewes O, Allen SJ, Dawbarn D, Fahnestock M. Biological activity of nerve growth factor precursor is dependent upon relative levels of its receptors. *J Biol Chem*. 2009; 284:18424-18433.
 18. Johnson TV, Bull ND, Martin KR. Neurotrophic factor delivery as a protective treatment for glaucoma. *Exp Eye Res*. 2011; 93:196-203.
 19. Haase G, Pettmann B, Raoul C, Henderson CE. Signaling by death receptors in the nervous system. *Curr Opin Neurobiol*. 2008; 18:284-291.
 20. Hellebrand EE, Varbiro G. Development of mitochondrial permeability transition inhibitory agents: a novel drug target. *Drug Discov Ther*. 2010; 4:54-61
 21. Arrighi N, Bodei S, Zani D, Simeone C, Cunico SC, Missale C, Spano P, Sigala S. Nerve growth factor signaling in prostate health and disease. *Growth Factors*. 2010; 28:191-201.
 22. Huang CS, Zhou J, Feng AK, Lynch CC, Klumperman J, DeArmond SJ, Mobley WC. Nerve growth factor signaling in caveolae-like domains at the plasmamembrane. *J Biol Chem*. 1999; 274:36707-36714.
 23. Iacaruso MF, Galli S, Martí M, Villalta JI, Estrin DA, Jares-Erijman EA, Pietrasanta LI. Structural Model for p75^{NTR}-TrkA Intracellular Domain Interaction: A Combined FRET and Bioinformatics Study. *J Mol Biol*. 2011; 414:681-698.
 24. Barker P A. High affinity not in the vicinity?. *Neuron*. 2007; 53:1-4.
 25. Matusica D, Skeldal S, Sykes AM, Palstra N, Sharma A, Coulson EJ. An Intracellular Domain Fragment of the p75 Neurotrophin Receptor (p75^{NTR}) Enhances Tropomyosin Receptor Kinase A (TrkA) Receptor Function. *J Biol Chem*. 2013; 288:11144-11154.
 26. Nykjaer A, Willnow T E, Petersen C M. p75^{NTR}-live or let die. *Curr Opin Neurobiol*. 2005; 15:49-57.
 27. Micera A, Lambiasi A, Stampachiachiere B, Bonini S, Bonini S, Levi-Schaffer F. Nerve growth factor and tissue repair remodeling: trkA^{NGFR} and p75^{NTR}, two receptors one fate. *Cytokine Growth Factor Rev*. 2007; 18:245-256.
 28. Cuello AC, Bruno MA, Allard S, Leon W, Iulita MF. Cholinergic involvement in Alzheimer's disease. A link with NGF maturation and degradation. *J Mol Neurosci*. 2010; 40:230-235.
 29. Fahnestock M, Yu G, Michalski B, Mathew S, Colquhoun A, Ross GM, Coughlin MD. The nerve growth factor precursor proNGF exhibits neurotrophic activity but is less active than mature nerve growth factor. *J Neurochem*. 2004; 89:581-592.
 30. Feng D, Kim T, Özkan E, Light M, Torkin R, Teng KK, Hempstead BL, Garcia KC. Molecular and structural insight into proNGF engagement of p75NTR and sortilin. *J Mol Biol*. 2010; 396:967-984.
 31. Paoletti F, Covaceuszach S, Konarev PV, Gonfloni S, Malerba F, Schwarz E, Svergun DI, Cattaneo A, Lamba D. Intrinsic structural disorder of mouse proNGF. *Proteins*. 2009; 75:990-1009.
 32. Paoletti F, Konarev PV, Covaceuszach S, Schwarz E, Cattaneo A, Lamba D, Svergun DI. Structural and functional properties of mouse proNGF. *Biochem Soc Trans*. 2006; 34:605-606.
 33. Nykjaer A, Lee R, Teng KK, Jansen P, Madsen P, Nielsen MS, Jacobsen C, Kliemannel M, Schwarz E, Willnow TE. Sortilin is essential for proNGF-induced neuronal cell death. *Nature*. 2004; 427:843-848.
 34. Nykjaer A, Willnow TE. Sortilin: a receptor to regulate neuronal viability and function. *Trends Neurosci*. 2012; 35:261-270.
 35. Hermey G. The Vps10p-domain receptor family. *Cell Mol Life Sci*. 2009; 66:2677-2689.
 36. Schweigreiter R. The dual nature of neurotrophins. *Bioessays*. 2006; 28:583-594.
 37. Jin H, Pan Y, Zhao L, Zhai H, Li X, Sun L, He L, Chen Y, Hong L, Du Y. p75 neurotrophin receptor suppresses the proliferation of human gastric cancer cells. *Neoplasia*. 2007; 9:471-478.
 38. Fahnestock M, Yu G, Coughlin MD. ProNGF: A neurotrophic or an apoptotic molecule?. *Prog Brain Res*. 2004; 146:101-110.
 39. Cragnolini AB, Friedman WJ. The function of p75^{NTR} in glia. *Trends Neurosci*. 2008; 31:99-104.
 40. Bartkowska K, Turlejski K, Djavadian RL. Neurotrophins and their receptors in early development of the mammalian nervous system. *Acta Neurobiol Exp (Wars)*. 2010; 70:454-467.
 41. Skaper SD. The neurotrophin family of neurotrophic factors: An overview. *Methods Mol Biol*. 2012; 846:1-12.
 42. Hondermarck H. Neurotrophins and their receptors in breast cancer. *Cytokine Growth F R*. 2012; 23:357-365.
 43. Schecterson LC, Bothwell M. Neurotrophin receptors: old friends with new partners. *Dev Neurobiol*. 2010; 70:332-338.
 44. Skaper SD. The neurotrophin family of neurotrophic factors: an overview. *Methods Mol Biol*. 2012; 846:1-12.
 45. Nakagawara A. Trk receptor tyrosine kinases: A bridge between cancer and neural development. *Cancer Lett*. 2001; 169:107-114.
 46. Hanahan D, Weinberg RA. Hallmarks of cancer: the next generation. *Cell*. 2011; 144:646-674.
 47. Chamary V, Robson T, Loizidou M, Boulos P, Burnstock G. Progressive loss of perivascular nerves adjacent to colorectal cancer. *Eur J Surg Oncol*. 2000; 26:588-593.
 48. Goda M, Atagi S, Amitani K, Hobara N, Kitamura Y, Kawasaki H. Nerve growth factor suppresses prostate tumor growth. *J Pharmacol Sci*. 2010; 112:463-466.
 49. Sone Y, Ochi E, Matsuyama A, Fukuhara S, Goda M, Takatori S, Kawasaki H. Influence of nerve growth factor (NGF) on distribution of perivascular nerves in tumor neovasculatures of mouse corneal. *Yakugaku zasshi. Journal of the Pharmaceutical Society of Japan*. 2012; 132:157-160.
 50. Walsh EM, Kim R, Del Valle L, Weaver M, Sheffield J, Lazarovici P, Marcinkiewicz C. Importance of interaction between nerve growth factor and $\alpha 9\beta 1$ integrin in glial tumor angiogenesis. *Neuro Oncol*. 2012; 14:890-901.
 51. Reis-Filho JS, Steele D, Di Palma S, Jones RL, Savage

- K, James M, Milanezi F, Schmitt FC, Ashworth A. Distribution and significance of nerve growth factor receptor (NGFR/p75^{NTR}) in normal, benign and malignant breast tissue. *Mod Pathol.* 2006; 19:307-319.
52. Dimaras H, Gallie BL. The p75^{NTR} neurotrophin receptor is a tumor suppressor in human and murine retinoblastoma development. *Int J Cancer.* 2008; 122:2023-2029.
 53. Kuchler J, Hartmann W, Waha A, Koch A, Endl E, Wurst P, Kindler D, Mikeska T, Goodyer CG. p75^{NTR} induces apoptosis in medulloblastoma cells. *Int J Cancer.* 2010; 128:1804-1812.
 54. Wynne S, Djakiew D. NSAID Inhibition of Prostate Cancer Cell Migration Is Mediated by Nag-1 Induction via the p38 MAPK-p75^{NTR} Pathway. *Mol Cancer Res.* 2010; 8:1656-1664.
 55. Khwaja FS, Wynne S, Posey I, Djakiew D. 3, 3'-diindolylmethane induction of p75^{NTR}-dependent cell death via the p38 mitogen-activated protein kinase pathway in prostate cancer cells. *Cancer Prev Res (Phila).* 2009; 2:566-571.
 56. Khwaja F, Tabassum A, Allen J, Djakiew D. The p75^{NTR} tumor suppressor induces cell cycle arrest facilitating caspase mediated apoptosis in prostate tumor cells. *Biochem Biophys Res Commun.* 2006; 341:1184-1192.
 57. Krygier S, Djakiew D. The neurotrophin receptor p75^{NTR} is a tumor suppressor in human prostate cancer. *Anticancer Res.* 2000; 21:3749-3755.
 58. Khwaja F, Djakiew D. Inhibition of cell-cycle effectors of proliferation in bladder tumor epithelial cells by the p75^{NTR} tumor suppressor. *Mol Carcinog.* 2003; 36:153-160.
 59. Tabassum A, Khwaja F, Djakiew D. The p75^{NTR} tumor suppressor induces caspase-mediated apoptosis in bladder tumor cells. *Int J Cancer.* 2003; 105:47-52.
 60. Naderi A, Teschendorff AE, Beigel J, Cariati M, Ellis IO, Brenton JD, Caldas C. BEX2 is overexpressed in a subset of primary breast cancers and mediates nerve growth factor/nuclear factor-κB inhibition of apoptosis in breast cancer cell lines. *Cancer Res.* 2007; 67:6725-6736.
 61. Barker PA. p75^{NTR} is positively promiscuous. novel partners and new insights. *Neuron.* 2004; 42:529-533.
 62. Zhao Z, Jiang Z, Liu X, Chen Y, Jia W. Study on reversion of malignant phenotype of glioma by siRNA targeting p75 neurotrophin receptor. *Zhonghua bing li xue za zhi.* 2010; 39:400-404.
 63. Fidler IJ. The pathogenesis of cancer metastasis. the 'seed and soil' hypothesis revisited. *Nat Rev Cancer.* 2003; 3:453-458.
 64. Krygier S, Djakiew D. Neurotrophin receptor p75^{NTR} suppresses growth and nerve growth factor-mediated metastasis of human prostate cancer cells. *Int J Cancer.* 2001; 98:1-7.
 65. Jin H, Pan Y, He L, Zhai H, Li X, Zhao L, Sun L, Liu J, Hong L, Song J. p75 neurotrophin receptor inhibits invasion and metastasis of gastric cancer. *Mol Cancer Res.* 2007; 5:423-433.
 66. Seidler K, Sydykov A, Müller-Brüsselbach S, Müller R, Weißmann N, Renz H, Nockher A. Nerve Growth Factor overexpression in Clara cells suppresses metastasis and tumor growth in a mouse model of experimental lung metastasis. *Pneumologie.* 2012; 66: A603.
 67. Warrington RJ, Lewis KE. Natural antibodies against nerve growth factor inhibit *in vitro* prostate cancer cell metastasis. *Cancer Immunol Immunother.* 2011; 60:187-195.
 68. Lagadec C, Meignan S, Adriaenssens E, Foveau B, Vanhecke E, Romon R, Toillon RA, Oxombre B, Hondermarck H, Le Bourhis X. TrkA overexpression enhances growth and metastasis of breast cancer cells. *Oncogene.* 2009; 28:1960-1970.
 69. Com E, Lagadec C, Page A, El Yazidi-Belkoura I, Slomianny C, Spencer A, Hammache D, Rudkin BB, Hondermarck H. Nerve growth factor receptor TrkA signaling in breast cancer cells involves Ku70 to prevent apoptosis. *Mol Cell Proteomics.* 2007; 6:1842-1854.
 70. McGregor LM, McCune BK, Graff JR, McDowell PR, Romans KE, Yancopoulos GD, Ball DW, Baylin SB, Nelkin BD. Roles of trk family neurotrophin receptors in medullary thyroid carcinoma development and progression. *Proc Natl Acad Sci U S A.* 1999; 96:4540-4545.
 71. Brodeur GM, Minturn JE, Ho R, Simpson AM, Iyer R, Varela CR, Light JE, Kolla V, Evans AE. Trk receptor expression and inhibition in neuroblastomas. *Clin Cancer Res.* 2009; 15:3244-3250.
 72. Zhu ZW, Friess H, Wang L, Bogardus T, Korc M, Kleeff J, Büchler MW. Nerve growth factor exerts differential effects on the growth of human pancreatic cancer cells. *Clin Cancer Res.* 2001; 7:105-112.
 73. George DJ, Suzuki H, Bova GS, Isaacs JT. Mutational analysis of the TrkA gene in prostate cancer. *Prostate.* 1998; 36:172-180.
 74. Lagadec C, Meignan S, Adriaenssens E, Foveau B, Vanhecke E, Romon R, Toillon RA, Oxombre B, Hondermarck H, Le Bourhis X. TrkA overexpression enhances growth and metastasis of breast cancer cells. *Oncogene.* 2009; 28:1960-1970.
 75. Van den Beuken-van Everdingen MHJ, De Rijke JM, Kessels AG, Schouten HC, Van Kleef M, Patijn J. Prevalence of pain in patients with cancer: a systematic review of the past 40 years. *Ann Oncol.* 2007; 18:1437-1449.
 76. Ahmedzai S. New approaches to pain control in patients with cancer. *Eur J Cancer.* 1997; 33:S8-S14.
 77. Qi F, Li A, Inagaki Y, Gao J, Li J, Kokudo N, Li XK, Tang W. Chinese herbal medicines as adjuvant treatment during chemoradio-therapy for cancer. *Biosci Trends.* 2010; 4:297-307.
 78. Jimenez-Andrade JM, Mantyh WG, Bloom AP, Ferng AS, Geffre CP, Mantyh PW. Bone cancer pain. *Annals of the New York Academy of Sciences.* 2010; 1198:173-181.
 79. Watson JJ, Allen SJ, Dawbarn D. Targeting nerve growth factor in pain: what is the therapeutic potential?. *BioDrugs.* 2008; 22:349-359.
 80. Kolokythas A, Cox DP, Dekker N, Schmidt BL. Nerve growth factor and tyrosine kinase A receptor in oral squamous cell carcinoma: is there an association with perineural invasion?. *J Oral Maxillofac Surg.* 2010; 68:1290-1295.
 81. Bapat AA, Hostetter G, Von Hoff DD, Han H. Perineural invasion and associated pain in pancreatic cancer. *Nat Rev Cancer.* 2011; 11:695-707.
 82. Jimenez-Andrade JM, Bloom AP, Stake JI, Mantyh WG, Taylor RN, Freeman KT, Ghilardi JR, Kuskowski MA, Mantyh PW. Pathological sprouting of adult nociceptors in chronic prostate cancer-induced bone pain. *J Neurosci.* 2010; 30:14649-14656.

83. Mantyh WG, Jimenez-Andrade JM, Stake JI, Bloom AP, Kaczmarska MJ, Taylor RN, Freeman KT, Ghilardi JR, Kuskowski MA, Mantyh PW. Blockade of nerve sprouting and neuroma formation markedly attenuates the development of late stage cancer pain. *Neuroscience*. 2010; 171:588-598.
 84. Jimenez-Andrade JM, Ghilardi JR, Castañeda-Corral G, Kuskowski MA, Mantyh PW. Preventive or late administration of anti-NGF therapy attenuates tumor-induced nerve sprouting, neuroma formation, and cancer pain. *Pain*. 2011; 152:2564-2574.
 85. Ghilardi JR, Freeman KT, Jimenez-Andrade JM, Mantyh WG, Bloom AP, Kuskowski MA, Mantyh PW. Administration of a tropomyosin receptor kinase inhibitor attenuates sarcoma-induced nerve sprouting, neuroma formation and bone cancer pain. *Mol Pain*. 2010; 6:87.
- (Received February 24, 2014; Revised April 1, 2014; Accepted April 7, 2014)*

Performance of reversed transcription loop-mediated isothermal amplification technique detecting EV71: A systematic review with meta-analysis

Xiaoying Lei¹, Hongling Wen¹, Li Zhao¹, Xuejie Yu^{1,2,*}

¹School of Public Health, Shandong University, Ji'nan, Shandong, China;

²Department of Pathology, University of Texas Medical Branch, Galveston, Texas, USA.

Summary

Human enterovirus 71 (EV71) is the major etiological agent of hand, foot and mouth disease (HFMD), which is a common infectious disease in young children. Studies in the past have shown that reversed transcription loop-mediated isothermal amplification (RT-LAMP) was a rapid approach for the detection of EV71 in HFMD. This meta-analysis study is to evaluate the diagnostic role of RT-LAMP in detecting EV71 infection. A comprehensive literature research of PubMed, Embase, Wan Fang Data, and Chinese National Knowledge Infrastructure databases was conducted on articles aiming at the diagnostic performance of RT-LAMP in EV71 detection published before February 10, 2014. Data from selected studies were pooled to yield the summary sensitivity, specificity, positive and negative likelihood ratio (PLR, NLR), diagnostic odds ratio (DOR), and receiver operating characteristic (SROC) curve by using STATA VERSION 12.0 software. Ten studies including a total of 907 clinical samples were of high quality in this meta-analysis. Overall, the pooled sensitivity, specificity, PLR, NLR, DOR, and the area under the SROC curve was 0.99 (0.97, 1.00), 0.97 (0.94, 1.00), 5.90 (95% CI: 3.90-8.94), 0.20 (95% CI: 0.14-0.29), and 1.00 (95% CI: 0.99-1.00), respectively. The univariate analysis of potential variables showed some changes in the diagnostic performance, but none of the differences reached statistical significance. Despite inter-study variability, the test performance of RT-LAMP was consistent with real-time RT-PCR in detecting EV71. This meta-analysis suggests that RT-LAMP is a useful diagnostic tool with high sensitivity and specificity for detecting EV71.

Keywords: Human enterovirus 71 (EV71), reversed transcription loop-mediated isothermal amplification (RT-LAMP), detection, meta-analysis

1. Introduction

Human enterovirus 71 (EV71) is the major etiological agent of hand, foot, and mouth disease (HFMD), which is a febrile exanthematous disease mostly prevalent in children younger than ten years old (1,2). In recent years, EV71 associated outbreaks have been reported worldwide and its infection has become serious threat to the health of infants and young children (3-7). EV71 infection can cause various clinical manifestations

and has been associated with severe neurological and cardiopulmonary complications, such as aseptic meningitis, encephalitis, and poliomyelitis-like paralysis, resulting in higher mortality rates (8-11).

Traditional methods for EV71 detection primarily depend on virus culture and identification, and serodiagnosis, which are either time-consuming or have a high false positive rate. Recently, reverse transcription-PCR (RT-PCR) and real-time quantitative RT-PCR (qRT-PCR) assays have been developed to detect EV71 with high specificities and sensitivities (12-14). However, these methods require sophisticated instrumentations and expensive reagents, which lead a result that the methods are difficult to be applied in developing countries or in field situations (15-17). Therefore, a rapid, reliable, and cost-effective molecular

*Address correspondence to:

Dr. Xuejie Yu, Department of Hygiene Detection, School of Public Health, Shandong University, No. 44, Wenhua Xilu Road, Ji'nan, Shandong, 250012, China.

E-mail: yuxuejie@sdu.edu.cn

test should be developed to be content with the growing demand.

Loop-mediated isothermal amplification (LAMP), a nucleic acid amplification method, was first established in 2000, which has been considered as a powerful nucleic acids amplification tool because of its simplicity, speed, specificity, and cost-effectiveness (18). Since then, this method has been used widely in rapid detection for viruses, such as dengue virus, West Nile virus, Japanese encephalitis virus, Ebola virus, H1N1 influenza virus, and so on (19-23). The detection of EV71 by RT-LAMP with RNA extraction was developed recently (15-17, 24-30), however, results from a single study did not have sufficient power to demonstrate the role of RT-LAMP in the detection of EV71 infection. Therefore, we performed systematical meta-analysis to provide a more comprehensive and reliable analysis of the diagnostic accuracy of RT-LAMP for the diagnosis of EV71 infection.

2. Materials and Methods

2.1. Study protocol

This analysis was conducted with a predetermined protocol following the recommendations of Deeks *et al.* (31). Data was collected and reported according the Preferred Reporting Items for Systematic Reviews and Meta-Analyses: The PRISMA Statement (Table S1, <http://www.biosciencetrends.com/docindex.php?year=2014&kanno=2>) (32).

2.2. Search strategy

Relevant studies published before February 10, 2014 were identified from searching PubMed, Embase, Wan Fang Data, and Chinese National Knowledge Infrastructure databases using the following terms: ("enterovirus 71" OR "EV71" AND ("detection" OR ("Reverse transcription loop-mediated isothermal amplification method" OR "RT-LAMP" OR "LAMP"). Languages were not restricted.

2.3. Inclusion and exclusion criteria

Studies included in this meta-analysis had to meet the following criteria: (1) Studies detecting the nasopharyngeal swab, stool, throat swabs, and rectal swabs specimens were included; (2) Patient samples were detected using qRT-PCR method, RT-PCR or virus isolation; (3) The literature data should contain sensitivity and specificity and detection limit; (4) For the studies using the same or overlapping data by the same authors, the most recent or largest population were selected. Exclusion criteria: (1) unqualified data; (2) small scale studies with fewer than 30 patients; (3) works designated as conference abstract, letters,

case reports, editorials or reviews; (4) duplicated publications.

2.4. Data extraction and quality assessment

All selected manuscripts were reviewed by two authors (L.Z and H.L.W), independently. Any disagreement was resolved by a third person (X.J.Y). The following information was extracted from every eligible work: the first author, year of publication, country, control method, number of patients, detection limit, the number of true positive (TP), false positive (FP), false negative (FN), and true negative (TN). The qualities of all the manuscripts were assessed according to the Quality Assessment of Diagnostic Accuracy Studies (QUADAS) (Table S2, <http://www.biosciencetrends.com/docindex.php?year=2014&kanno=2>) (33). Fourteen items related to quality appraisal were used in this meta-analysis. Each of these items was scored "yes" (1 score), "no" (0 score) or "unclear" (-1 score). Disagreements were resolved by discussions and consensus.

2.5. Statistical analysis

For each selected publication, the pooled sensitivity, pooled specificity, positive likelihood ratio (PLR), negative likelihood ratio (NLR), and diagnostic odds ratio (DOR), and their 95% confidence intervals (CI) were calculated. A bivariate mixed model was adjusted to obtain a summary receiver operating characteristic (SROC) curve by summarizing the joint distribution of sensitivity and specificity with Moses linear model and the corresponding area under the curve (AUC) was calculated as a global measurement of test performance (34,35). The closer the AUC was to 1, the better the test performance. Publication bias was assessed visually using a funnel plot and tested with Egger's tests with $p < 0.10$ being considered statistically significant (36). Empty cells were handled using a 0.5 continuity correction. Meta-regression was analyzed to identify possible sources of heterogeneity. Values of $p < 0.05$ and $I^2 > 50\%$ were considered to be statistically significant. Subgroup analyses and sensitivity analysis were also performed where required. All analyses were performed with STATA 12.0 (Stata Corp LP, College Station, Texas, United States).

3. Results

3.1. Literature search

A total of 219 potential relevant manuscripts were retrieved after the primary search of the electronic databases for published work on the subject. One hundred and ninety five of these manuscripts were excluded after further review of the title and abstract for irrelevant topics, and an additional 10 manuscripts

were excluded for duplication of the reports. Then the remaining 14 manuscripts were undergoing full text review. Finally, 10 studies were included for further meta-analysis. The detailed process of this literature search is shown in Figure 1.

3.2. Study quality assessment

QUADAS list of questions were used to review the test quality of the included studies. Most of the studies satisfied a majority of the items on the list, and reports of intermediate results and withdraw cases were the most common missing items in the studies in this analysis (Table S2, <http://www.biosciencetrends.com/docindex.php?year=2014&kanno=2>). The Egger's

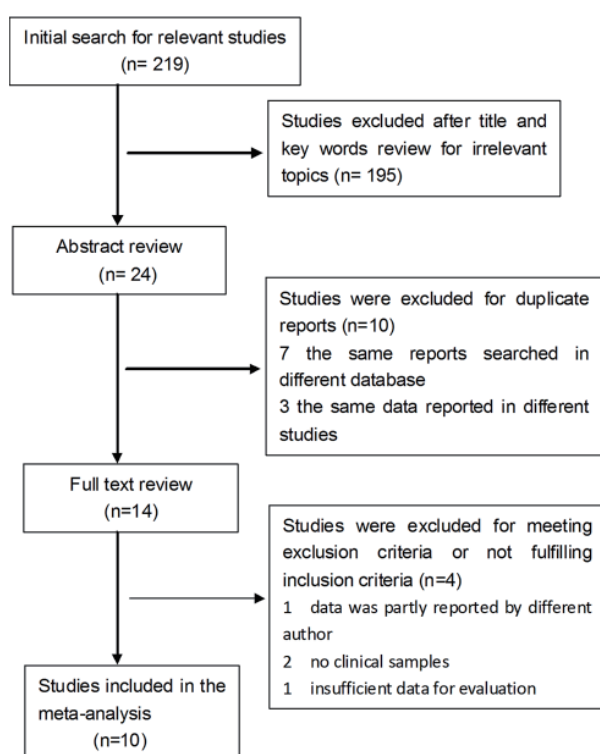


Figure 1. Flow chart describing the literature search conducted for this meta-analysis.

test revealed no significant publication bias among the included reports ($p = 0.067$).

3.3. Overall diagnostic performance of RT-LAMP

As a result, 10 eligible studies with a total of 907 samples were included in this meta-analysis, which were published from 2011 to 2012. All the samples were also detected by qRT-PCR or RT-PCR, or even virus isolation for conformation, however, the units of the detection limit of RT-LAMP varied in different studies (Table 1). The basic characteristics (TP, FP, TN, and FN) were also listed in the table.

The forest plot of sensitivity, specificity, PLR, and NLR for RT-LAMP method in the detection of EV71 infection was shown in Figures 2 and 3. The pooled sensitivity and specificity were 0.99 (95% CI: 0.97-1.00) and 0.97 (95% CI: 0.94-1.00), respectively (Figures 2 and 3). By heterogeneity analysis, I² of sensitivity, specificity, PLR, and NLR was 0.0% ($p = 0.739$), 47.5% ($p = 0.047$), 0.0% ($p = 0.994$), and 0.0% ($p = 0.998$), respectively, implicating that there was no significant heterogeneity among the samples. The pooled PLR was 5.90 (95% CI: 3.90-8.49); the pooled NLR was 0.20 (95% CI: 0.14-0.29).

The pooled DOR and the SROC curves based on summary sensitivity and specificity across all data sets were shown in Figure 4. The pooled DOR was 843.27 (95% CI: 294.19-2417.15), with individual DORs ranging from 312.00 to 41600. The results of DOR showed consistency across the included studies, without noticeable heterogeneity ($p = 0.602$, $I^2 = 0.0\%$). The point size in the SROC curve represented the proportional study weight. All the data gathered near the top left corner where both the sensitivity and specificity were the highest. The area under the curve (AUC) was 1.00 (95% CI: 0.99-1.00) indicating a high diagnostic accuracy.

In addition, we systematically removed one data set at a time, and recalculated the DOR and AUC values for the remaining studies. The changes of pooled DOR and

Table 1. Summary of the studies included in the meta-analysis

Reference number	Author	Publication year	Country	Conformation method	Samples	Detection limit	Test results				QUADAS
							TP	FP	FN	TN	
15	Shi <i>et al.</i>	2011	China	qRT-PCR	123	1PFU	56	2	0	65	
16	Nie <i>et al.</i>	2011	China	qRT-PCR	47	0.33TCID ₅₀	25	0	0	22	
17	Nie <i>et al.</i>	2012	China	qRT-PCR	145	1.6 TCID ₅₀	124	0	5	16	
24	Geng <i>et al.</i>	2011	China	qRT-PCR	58	10-5 dilution	25	8	0	25	
25	He <i>et al.</i>	2012	China	qRT-PCR	33	160 copies	24	0	0	9	
26	Jiang <i>et al.</i>	2011	China	qRT-PCR	40	0.01 PFU	26	0	2	12	
27	Li <i>et al.</i>	2012	China	qRT-PCR	41	100 copies	27	0	0	14	
28	Wang <i>et al.</i>	2012	China	RT-PCR	252	10 copies	52	0	0	200	
29	Xia <i>et al.</i>	2011	China	qRT-PCR	108	5 copies	101	0	3	4	
30	Zhao <i>et al.</i>	2011	China	RT-PCR	60	10 copies	31	4	0	26	

Abbreviations: qRT-PCR, real-time quantitative reverse transcription polymerase chain reaction; RT-PCR, reverse transcription polymerase chain reaction; PFU, plaque forming unit; TCID₅₀, 50% tissue culture infective dose; TP, true positive; FP, false positive; FN, false negative; TN, true negative.

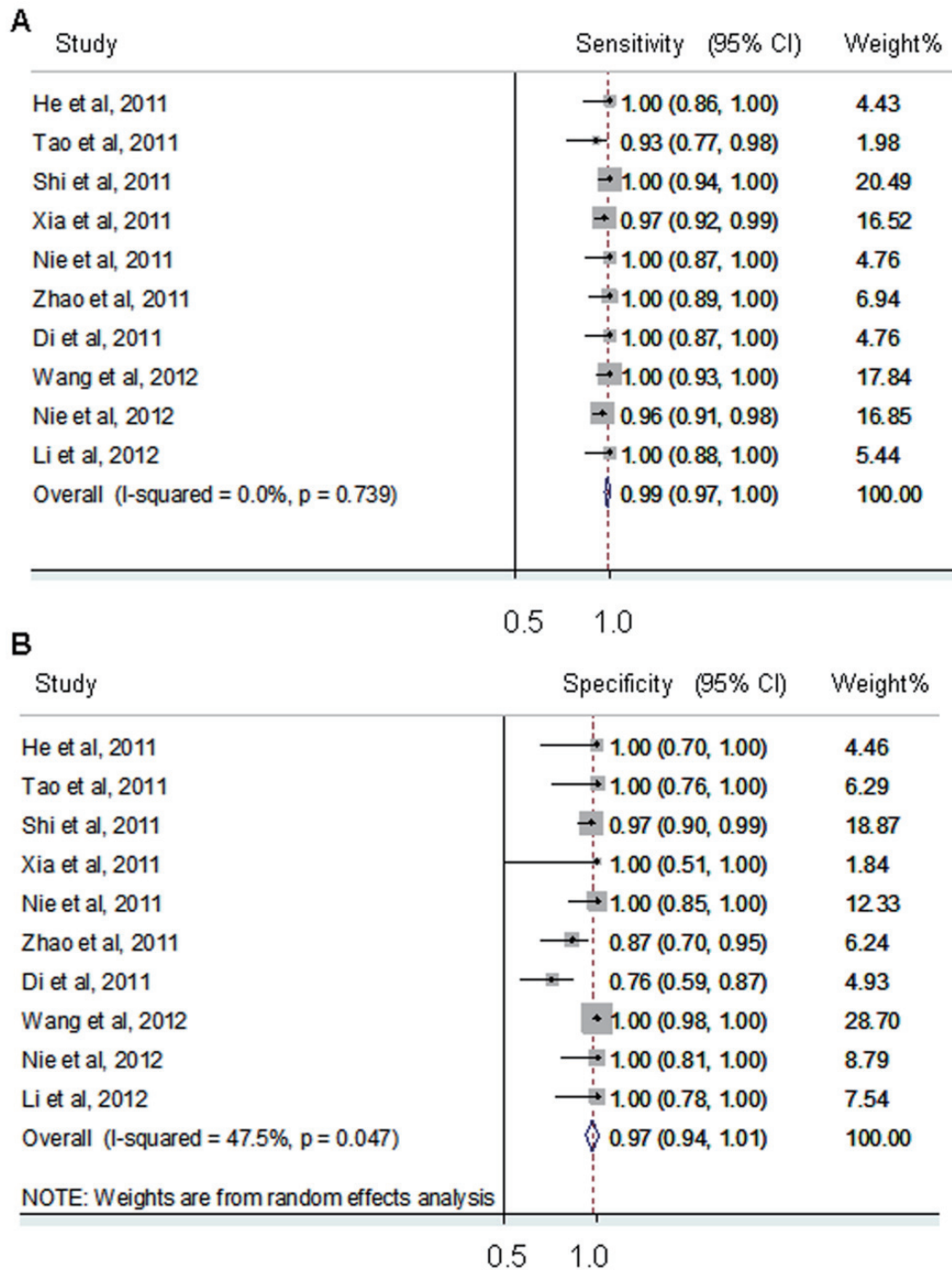


Figure 2. Forest plots of sensitivity and specificity of RT-LAMP for the detection of EV71 infection. (A) Pooled sensitivity. (B) Pooled specificity. Effect sizes were pooled by fixed-effect models. The point estimates from each study were shown as solid squares. The pooled estimates were shown as an empty diamond. Error bars represented 95% CIs.

the corresponding changes in AUC values did not show significant difference (data not shown). These results suggested that no single data set carry enough weight to significantly influence the pooled test performance reported for the ability of RT-LAMP in detection of EV71 infection.

3.4. Univariate analysis

For exploring the potential variables that may have

influenced the results, the following variables were chosen for subgroup analysis: publication year, sample size and confirmation method. In the subgroup analysis of publication year, the specificity was 0.96 for 2011, and 1.0 for 2012, thus, there was significant heterogeneity of specificity between studies published in 2011 and that published in 2012 ($p = 0.027$). Differences in the sensitivity, the PLR and NLR in this subgroup and differences in other subgroups were not statistically significant (Table 2).

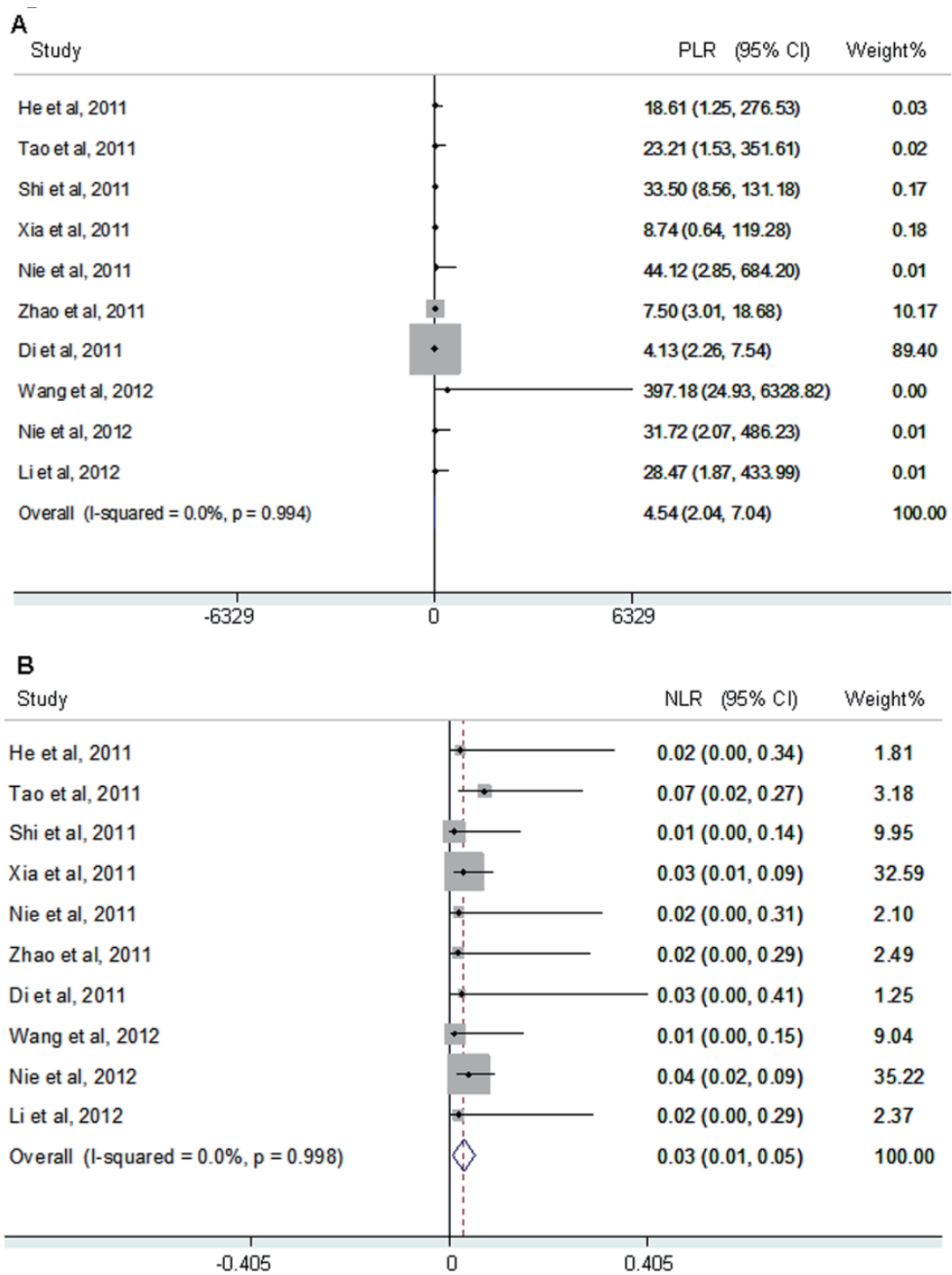


Figure 3. Forest plots of positive and negative likelihood ratios of RT-LAMP for the detection of EV71 infection. (A) Pooled positive likelihood ratio. **(B)** Pooled negative likelihood ratio. Effect sizes were pooled by fixed-effect models. The point estimates from each study were shown as solid squares. Error bars represented 95% CIs.

4. Discussion

A rapid expansion of HFMD has occurred in many provinces in China since 2008, especially in spring and summer every year. Although most of the HFMD cases without severe complications are mild and do not need much medical attention, cases infected by EV71 often lead to serious complications, or even death (37-39). Children around 3 years old are infected the most

commonly and the cases infected by EV71 may cause severe neurological disease within 2-5 days, which led to an international demand for a rapid, simple, sensitive and accurate molecular method for the diagnosis of EV71 infection. qRT-PCR and RT-PCR have been proved to be reliable nucleic acid-based methods for the detection of EV71 in laboratories, however, both methods require specialized equipment and are not cost effective. RT-LAMP is a useful molecular technique for

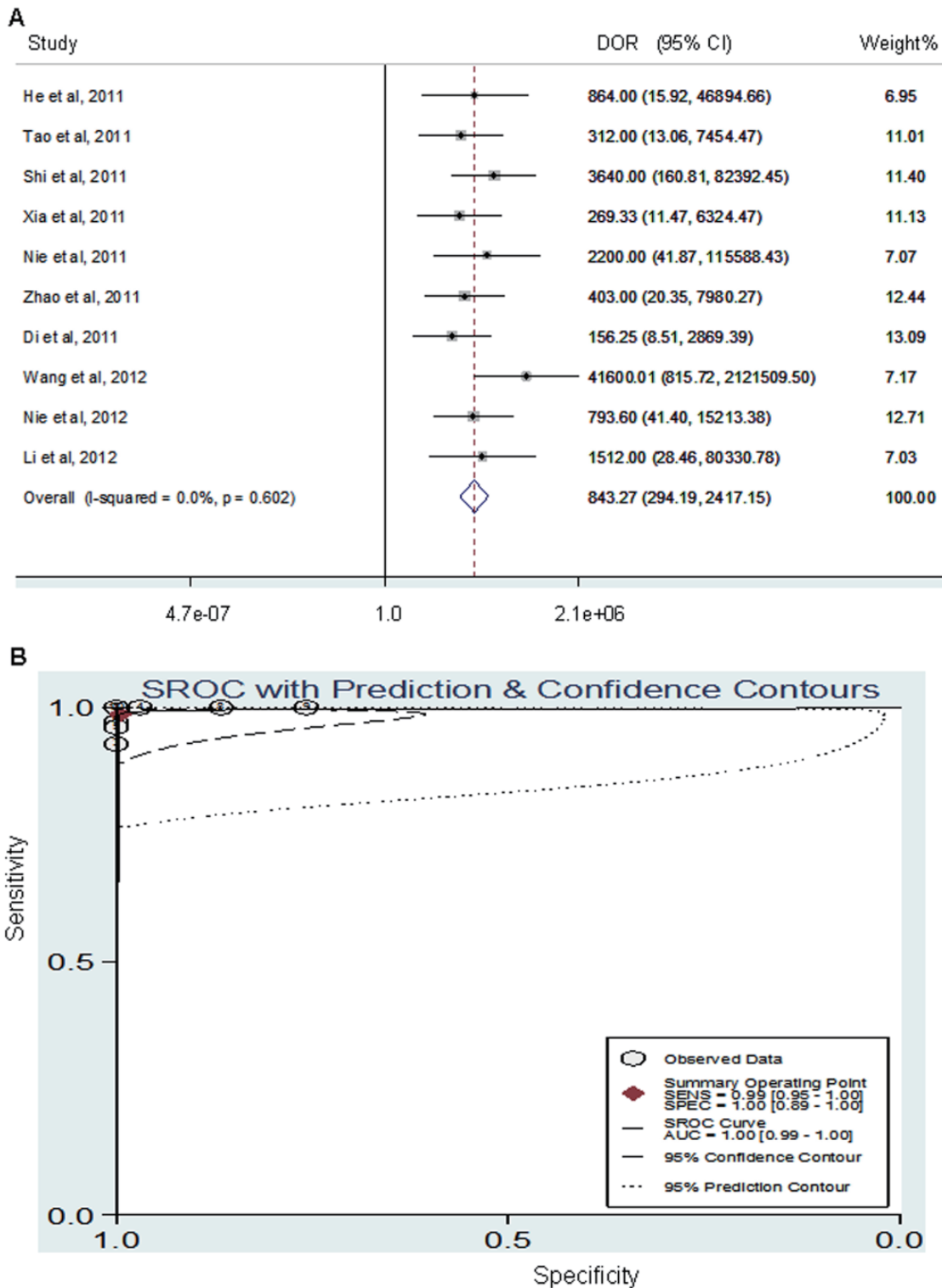


Figure 4. Overall DOR and SROC curve for all data sets describing the diagnostic performance of RT-LAMP in detecting EV71 infection. (A) Overall diamond. (B) The SROC curves for all data sets. Effect sizes were pooled by fixed-effect models. The pooled DOR is shown as an empty diamond. Each square in the SROC curve represents one study. Sample size was indicated by the size of the square.

nucleic acid research (18). To our knowledge, this is the first pooled estimation of the RT-LAMP method in detecting EV71 infection.

In this meta-analysis, 10 relevant studies with a total of 907 samples were included. Although results were not consistent across different studies, the overall

diagnostic performance of detecting EV71 RNA with RT-LAMP showed pooled sensitivity and specificity of 0.99 (95% CI: 0.97, 1.00) and 0.97 (95% CI: 0.94, 1.00), respectively. The pooled DOR and AUC of the SROC curves for all data sets were 843.27 and 1.00, respectively. The results were consistent with previous

Table 2. Subgroup analysis of potential variables influencing the test performance of RT-LAMP

Variables	Subgroup	Number of studies	Sensitivity (95%CI)	P_{h1}	Specificity (95% CI)	P_{h2}	PLR(95%CI)	P_{h3}	NLR(95%CI)	P_{h4}
Publication year	2011	7	0.99 (0.97, 1.00)	0.692	0.96 (0.93, 0.99)	0.027	4.54 (2.04, 7.03)	0.749	0.03 (-0.004, 0.06)	0.803
	2012	3	0.98 (0.96, 1.00)		1.00 (0.99, 1.00)		30.87 (-130.11, 191.86)		0.03 (-0.001, 0.07)	
Sample size	< 100	6	1.00 (0.97, 1.00)	0.513	0.96 (0.91, 1.00)	0.076	4.48 (1.98, 7.00)	0.438	0.03 (-0.03, 0.10)	0.912
	≥ 100	4	0.98 (0.97, 1.00)		1.00 (0.99, 1.00)		21.11 (-20.88, 63.10)		0.03 (0.01, 0.05)	
PCR techniques	RT-PCR	2	1.00 (0.97, 1.00)	0.325	1.00 (0.99, 1.00)	0.14	7.50 (-0.33, 15.33)	0.434	0.01 (-0.06, 0.08)	0.582
	qRT-PCR	8	0.99 (0.97, 1.00)		0.97 (0.94, 1.00)		4.21 (1.57, 6.84)		0.03 (0.01, 0.06)	

Abbreviations: CI, confidence interval; P_{h1} , P value for heterogeneity between subgroups in sensitivity; P_{h2} , P value for heterogeneity between subgroups in specificity; PLR, positive likelihood ratio; P_{h3} , P value for heterogeneity between subgroups in PLR; NLR, negative likelihood ratio; P_{h4} , P value for heterogeneity between subgroups in NLR.

studies, representing that RT-LAMP method was highly efficient in EV71 detection, regardless of the sample origin variation. In addition, the virus strains of EV71 and the sequences of EV71 were not uniform, which could be potential source of variation that may have influenced the test performance.

Infections caused by EV71 and Human coxsackievirus A16 (CVA16) shared similar clinical symptoms, and indeed, the protein sequences of the two viruses were in high similarity, therefore, frequent misdiagnosis of EV71 and CVA16 infections happened because of the difficulty in distinguishing the two viruses (40). Exact nucleotide sequences of RT-LAMP products can be derived from target DNA and primers, and restriction enzymes recognition sites were often introduced, thus, it is possible to predict the specific digestion outcomes of the samples (15). Therefore, RT-LAMP assay can provide high specificity for the detection of EV71 infection.

Heterogeneity between studies, which exists widely and could not be considered to be attributed to variances, is a potential problem in results interpretation for meta-analysis. As a result, pooled sensitivity is usually applied to assess whether the meta-analysis is influenced by any individual study. When the selected studies were removed one by one and the heterogeneity did not show significant change, the results of the analysis did not depend on one particular study absolutely. According the provided information, the univariate analysis was also carried out. Three subgroups were categorized and subgroup analysis of potential variables influencing the performance of RT-LAMP was performed. As most of the results did not show significant difference, it suggested that the conclusions are reliable.

There are several limitations in this meta-analysis. First, only 10 manuscripts met the inclusion criteria in this analysis. The sample size was so small that it limited the generalization of the results. Also, qualities of the selected manuscripts were not uniform. For example, the essential demographical data like age and

gender distributions were not presented in most studies. These factors might be potential heterogeneity sources in the analysis. In addition, the detection limits were not uniformed in the same unit in primary study. As the experiments were done by different manipulators, and the EV71 virus strain used in the studies were also different from each other, the results were not comparable with each other.

In conclusion, RT-LAMP is a simple, rapid, cheap, specific and sensitive nucleic acid detecting method and has great value in diagnosis of EV71 infection for on-site application in early stage, which could contribute to control of EV71 infection.

Acknowledgements

This study was supported by China Postdoctoral Science Foundation (2013M541923), the Independent Innovation Foundation of Shandong University (IIFSDU) (2012GN046) and the Innovation Foundation for Young Talents of the Public Health School of Shandong University (201203). The funders had no role in study design, data collection and analysis, decision to publish, or preparation of the manuscript.

References

1. Bruu AL. Enteroviruses: polioviruses, coxsackieviruses, echoviruses and newer enteroviruses. In: A practical guide to clinical virology, second edition (Haaheim LR, Pattison JR, Whitley RJ, eds.). John Wiley & Sons, Ltd, Chichester, UK, 2003; pp. 44-45.
2. Zhu D, Zhao XY, Yao Y, Dai FF, He H, Li RQ, Jin RH, Liang LC, Li N. A new factor influencing pathogen detection by molecular assay in children with both mild and severe hand, foot, and mouth disease. *Diagnostic microbiology and infectious disease*. 2013; 76:162-167.
3. Kim KH. Enterovirus 71 infection: An experience in Korea 2009. *Korean J Pediatr*. 2010; 53:616-622.
4. Lan YC, Lin TH, Tsai JD, Yang YC, Peng CT, Shih MC, Lin YJ, Lin CW. Molecular epidemiology of the 2005 enterovirus 71 outbreak in central Taiwan. *Scand J Infect Dis*. 2011; 43:345-349.

5. Li Wei A, Benjamin KW K, Kwai Peng C, Chua LT, James L, Goh KT. Epidemiology and control of hand, foot and mouth disease in Singapore, 2001-2007. *Ann Acad Med Singapore*. 2009; 38:106-112.
6. Schuffenecker I, Mirand A, Antona D, Henquell C, Chomel JJ, Archimbaud C, Billaud G, Peigue-Lafeuille H, Lina B, Bailly JL. Epidemiology of human enterovirus 71 infections in France, 2000-2009. *J Clin Virol*. 2011; 50:50-56.
7. Wen HL, Si LY, Yuan XJ, Hao SB, Gao F, Chu FL, Sun CX, Wang ZY. Complete genome sequencing and analysis of six enterovirus 71 strains with different clinical phenotypes. *Virology*. 2013; 10:115.
8. Chong CY, Chan KP, Shah VA, Ng WY, Lau G, Teo TE, Lai SH, Ling AE. Hand, foot and mouth disease in Singapore: a comparison of fatal and non-fatal cases. *Acta Paediatr*. 2003; 92:1163-1169.
9. Wang SM, Liu CC, Tseng HW, Wang JR, Huang CC, Chen YJ, Yang YJ, Lin SJ, Yeh TF. Clinical spectrum of enterovirus 71 infection in children in Southern Taiwan, with an emphasis on neurological complications. *Clin Infect Dis*. 1999; 29:184-190.
10. Yang Y, Wang H, Gong E, Du J, Zhao X, McNutt MA, Wang S, Zhong Y, Gao Z, Zheng J. Neuropathology in 2 Cases of fatal enterovirus type 71 infection from a recent Epidemic in the People's Republic of China: A histopathologic, immunohistochemical, and reverse transcription polymerase chain reaction study. *Hum Pathol*. 2009; 40:1288-1295.
11. Weng KF, Chen LL, Huang PN, Shih SR. Neural pathogenesis of enterovirus 71 infection. *Microbes Infect*. 2010; 12:505-510.
12. Fujimoto T, Yoshida S, Munemura T, Taniguchi K, Shinohara M, Nishio O, Chikahira M, Okabe N. Detection and quantification of enterovirus 71 genome from cerebrospinal fluid of an encephalitis patient by PCR applications. *Jpn J Infect Dis*. 2008; 61:497-499.
13. Tan EL, Yong LLG, Quak SH, Yeo WCA, Chow VTK, Poh CL. Rapid detection of Enterovirus 71 by real-time TaqMan RT-PCR. *J Clin Virol*. 2008; 42:203-206.
14. Xiao XL, He YQ, Yu YG, Yang H, Chen G, Li HF, Zhang JW, Liu DM, Li XF, Yang XQ, Wu H. Simultaneous detection of human enterovirus 71 and coxsackievirus A16 in clinical specimens by multiplex real-time PCR with an internal amplification control. *Arch Virol*. 2009; 154:121-125.
15. Shi W, Li K, Ji Y, Jiang Q, Shi M, Mi Z. Development and evaluation of reverse transcription-loop-mediated isothermal amplification assay for rapid detection of enterovirus 71. *BMC infectious diseases*. 2011; 11:197.
16. Nie K, Zhang Y, Luo L, Yang MJ, Hu XM, Wang M, Zhu SL, Han F, Xu WB, Ma XJ. Visual detection of human enterovirus 71 subgenotype C4 and Coxsackievirus A16 by reverse transcription loop-mediated isothermal amplification with the hydroxynaphthol blue dye. *J Virol Methods*. 2011; 175:283-286.
17. Nie K, Qi SX, Zhang Y, Luo L, Xie Y, Yang MJ, Zhang Y, Li J, Shen H, Li Q, Ma XJ. Evaluation of a direct reverse transcription loop-mediated isothermal amplification method without RNA extraction for the detection of human enterovirus 71 subgenotype C4 in nasopharyngeal swab specimens. *PloS one*. 2012; 7:e52486.
18. Notomi T, Okayama H, Masubuchi H, Yonekawa T, Watanabe K, Amino N, Hase T. Loop-mediated isothermal amplification of DNA. *Nucleic Acids Res*. 2000; 28:E63.
19. Parida M, Posadas G, Inoue S, Hasebe F, Morita K. Real-time reverse transcription loop-mediated isothermal amplification for rapid detection of West Nile virus. *J Clin Microbiol*. 2004; 42:257-263.
20. Parida M, Horioka K, Ishida H, Dash PK, Saxena P, Jana AM, Islam MA, Inoue S, Hosaka N, Morita K. Rapid detection and differentiation of dengue virus serotypes by a real-time reverse transcription-loop-mediated isothermal amplification assay. *J Clin Microbiol*. 2005; 43:2895-2903.
21. Parida MM, Santhosh SR, Dash PK, Tripathi NK, Saxena P, Ambuj S, Sahni AK, Lakshmana Rao PV, Morita K. Development and evaluation of reverse transcription-loop-mediated isothermal amplification assay for rapid and real-time detection of Japanese encephalitis virus. *J Clin Microbiol*. 2006; 44:4172-4178.
22. Kurosaki Y, Takada A, Ebihara H, Grolla A, Kamo N, Feldmann H, Kawaoka Y, Yasuda J. Rapid and simple detection of Ebola virus by reverse transcription-loop-mediated isothermal amplification. *J Virol Methods*. 2007; 141:78-83.
23. Kubo T, Agoh M, Mai LQ, Fukushima K, Nishimura H, Yamaguchi A, Hirano M, Yoshikawa A, Hasebe F, Kohno S, Morita K. Development of a reverse transcription-loop-mediated isothermal amplification assay for detection of pandemic (H1N1) 2009 virus as a novel molecular method for diagnosis of pandemic influenza in resource-limited settings. *J Clin Microbiol*. 2010; 48:728-735.
24. Geng YZ, Yao WQ, Guo JQ, Yu W, Mao LL, Chen JY, An CL. Establishment and application of RT-LAMP technique in detection of enterovirus 71 gene. *Chinese journal of Zoonoses (with English abstract)*. 2011; 27:176-179.
25. He YQ, Zong WP, Zhiyi Y, Xionghu W, Yu SY, Hong Y, Yingchun D, Guifang H. Detection of human enterovirus 71 reverse transcription loop-mediated isothermal amplification (RT-LAMP). *Lett Appl Microbiol*. 2012; 54:233-239.
26. Jiang T, Liu J, Deng YQ, Xu LJ, Li XF, Han JF, Cao RY, Qin ED, Qin CF. Development and evaluation of a reverse transcription-loop-mediated isothermal amplification assay for rapid detection of enterovirus 71. *J Clin Microbiol*. 2011; 49:870-874.
27. Li K, Shi WF, Shi D, Luo GH, Shi M, Li X, Hou XL. Rapid detection of EV71 with reverse transcription loop-mediated isothermal amplification. *J Mol Diagn Ther (Chinese with English abstract)*. 2012; 4:26-29.
28. Wang X, Zhu JP, Zhang Q, Xu ZG, Zhang F, Zhao ZH, Zheng WZ, Zheng LS. Detection of enterovirus 71 using reverse transcription loop-mediated isothermal amplification (RT-LAMP). *J Virol Methods*. 2012; 179:330-334.
29. Xia JF, Yan XF, Yu H, Qu D, Long JE. Simple and rapid detection of human enterovirus 71 by reverse-transcription and loop-mediated isothermal amplification: cryopreservation affected the detection ability. *Diagn Microbiol Infect Dis*. 2011; 71:244-251.
30. Zhao GP. Development and application of loop-mediated isothermal amplification methods for enterovirus 71 and coxsackievirus A16 detection. Dissertation, 2011, Hebei Medical University.
31. Deeks J. Systematic reviews of evaluations of diagnostic and screening tests. In: *Systematic Reviews in Health*

- Care: Meta-analysis in context (Egger M, Davey Smith G, Altman D, eds.). BMJ Publishing Group, London, 2001.
32. Moher D, Liberati A, Tetzlaff J, Altman DG. Preferred reporting items for systematic reviews and meta-analyses: The PRISMA Statement. *PLoS Med.* 2009; 6:e1000097.
 33. Whiting P, Rutjes AW, Reitsma JB, Bossuyt PM, Kleijnen J. The development of QUADAS: a tool for the quality assessment of studies of diagnostic accuracy included in systematic reviews. *BMC Med Res Methodol.* 2003; 3:25.
 34. Moses LE, Shapiro D, Littenberg B. Combining independent studies of a diagnostic test into a summary ROC curve: Data-analytic approaches and some additional considerations. *Stat Med.* 1993; 12:1293-1316.
 35. Walter S. Properties of the summary receiver operating characteristic (SROC) curve for diagnostic test data. *Stat Med.* 2002; 21:1237-1256.
 36. Egger M, Davey SG, Schneider M, Minder C. Bias in meta-analysis detected by a simple, graphical test. *BMJ.* 1997; 315:629-634.
 37. Shimizu H, Utama A, Onnimala N, Li C, Li-Bi Z, Yu-Jie M, Pongsuwanna Y, Miyamura T. Molecular epidemiology of enterovirus 71 infection in the Western Pacific Region. *Pediatr Int.* 2004; 46:231-235.
 38. Li L, He Y, Yang H, Zhu J, Xu X, Dong J, Zhu Y, Jin Q. Genetic characteristics of human enterovirus 71 and coxsackievirus A16 circulating from 1999 to 2004 in Shenzhen, People's Republic of China. *J ClinMicrobiol.* 2005; 43:3835-3839.
 39. Li P, Zhang Y, Yue YY, Song NN, Li ZH, Meng H. Complete genome sequence analysis of enterovirus 71 JN200804 strain isolated in Shandong Province. *Journal of Shandong University (Health Science) (Chinese with English Abstract).* 2011; 49:113-117.
 40. Oberste MS, Peñaranda S, Maher K, Pallansch MA. Complete genome sequences of all members of the species Human enterovirus A. *J Gen Virol.* 2004; 85:1597-1607.

(Received March 31, 2014; Revised April 10, 2014; Accepted April 14, 2014)

Overexpression of an ABC transporter and mutations of GyrA, GyrB, and ParC in contributing to high-level ciprofloxacin resistance in *Streptococcus suis* type 2

Jie Yao¹, Kexin Shang¹, Jinhu Huang¹, Wei Ran^{1,2}, Jam Kashif¹, Liping Wang^{1,*}

¹ College of Veterinary Medicine, Nanjing Agricultural University, Nanjing, Jiangsu, China;

² Department of Medical Microbiology and Parasitology, School of Basic Medical Sciences, Fudan University, Shanghai, China.

Summary

Streptococcus suis is a pathogen of zoonotic diseases. Moreover, the emergence of fluoroquinolones (FQs) resistance in this pathogen has severe consequences for pigs and human health. In this study, the molecular mechanism of FQs resistance in *S. suis* type 2 (SS2) sensitive strains isolated from pigs was assessed after *in vitro* induction of resistance against the most frequently used FQs: ciprofloxacin, norfloxacin, and enrofloxacin. Proteome analysis, sequencing and real-time RT-PCR results strongly established an overexpression of an ABC transporter protein (other than SatAB) and topoisomerase mutations in GyrA (Ser81Arg), GyrB (Glu354Lys), and ParC (Ser79Phe) in contributing to high level ciprofloxacin resistance in SS2. Due to the overexpression of the ABC transporter, intracellular ciprofloxacin concentrations were significantly lower in the resistant strains than those of sensitive strains after 20, 35, and 60 min exposures to ciprofloxacin ($p < 0.05$). It was concluded that improper use of FQs is one of the main causes of the emergence of this zoonotic pathogen as a multiresistant organism against commonly used antibiotics. The existence of an efflux-like protein is an incentive to find new drug targets to avoid the spread of FQs-resistant *S. suis* isolates in pigs and the human population.

Keywords: *S. suis*, fluoroquinolones, proteome, ABC transporter, mutations

1. Introduction

Streptococcus suis is a pathogen of zoonotic diseases. People are at great risk of infection by contact with diseased pigs or its by-products (1-6). Two outbreaks of *S. suis* have occurred in China, particularly the major epidemic that took place in 2005 in Sichuan province, which affected 204 people and caused 38 fatalities (3,6). Nevertheless, cases of *S. suis* meningitis have also been reported in patients with no history of contact with animals or their products (7).

Chemotherapy is still the most important strategy for prevention and treatment of *S. suis* infections in China and all over the world due to the lack of an effective vaccine. Fluoroquinolones (FQs) are preferred

antibacterial agents for treatment of streptococcal infections (8,9). Enrofloxacin in pigs and ciprofloxacin in humans, have remained the most preferred FQ agents for the treatment of *S. suis* infections (10). However, treatment failure in streptococcal infections is reported worldwide due to the emergence of strains resistant to FQs and other antibiotics in recent years. Such multidrug resistant streptococcal strains have become a universal problem and have severe consequences for pigs and for human health (11-15).

Resistance mechanisms to fluoroquinolones in *S. suis* are seldom studied. Only two studies have reported resistant mechanisms. One is point mutations in quinolone resistance-determining regions (QRDRs) of the *gyrA* subunit of the DNA gyrase and *parC* subunit of DNA topoisomerase IV, and another reason of developing resistance to fluoroquinolones is decreased accumulation of these FQ agents in bacterial cells mediated by SatAB (13,15).

However, in our previous studies (not published), eight FQ-susceptible strains were induced resistant

*Address correspondence to:

Dr. Liping Wang, College of Veterinary Medicine, Nanjing Agricultural University, No. 1 Weigang, Nanjing 210095, China.

E-mail: wlp71@163.com

to FQs by ciprofloxacin with a step-wise method. We found five of the resistant strains have mutations of *gyrA* and *parC* as previously reported as well as higher expression levels of *satAB*. However, the other three FQ-resistant strains selected *in vitro* have mutations in DNA gyrase and DNA topoisomerase IV, but the expression levels of *satAB* were not changed compared with their parental sensitive strains. Interestingly, the efflux pump inhibitor reserpine could decrease the MICs of ciprofloxacin and norfloxacin in these three mutants. Therefore, we considered the possibility that another efflux-mediated resistance is responsible for at least part of the resistance in *S. suis* strains and the aim of this study was to further explore the underlying molecular mechanisms involved in FQ resistance in these three lab-derived resistant strains.

2. Materials and Methods

2.1. Strains

Three strains ZY05721E, JR05730E, and JDZ05802-1E of *Streptococcus suis* type 2 (SS2) recovered from diseased swine in 2009 were used in this study. The three strains which were sensitive to enrofloxacin, ciprofloxacin, and norfloxacin were cultured in Todd-Hewitt broth (THB) with 3% calf serum at 37°C.

2.2. Antibiotics and efflux pump inhibitor

Antibiotics were obtained from different companies as follows: erythromycin and tetracycline were obtained from Amresco (Solon, OH, USA); sulfamonomethoxine, penicillin, enrofloxacin, norfloxacin, and ciprofloxacin were obtained from Sigma (St Louis, MO, USA); and efflux pump inhibitor reserpine was obtained from Fluka (USA).

2.3. Selection of ciprofloxacin-resistant mutants *in vitro* and susceptibility determination

The gradient plate method, as previously described (16) with minor modifications, was used to induce ZY05721E, JR05730E, and JDZ05802-1E to be FQ-resistant strains (named ZY05721EC, JR05730EC, and JDZ05802-

1EC) with subinhibitory concentrations of ciprofloxacin. Antimicrobial susceptibilities, either in the presence or absence of 50 µg/mL of reserpine, were done using the agar dilution method according to the recommendations of the Clinical and Laboratory Standards Institute (CLSI), and the results were determined by CLSI standards (17). Resistant mutants were subcultured in antibiotic-free medium for 10 serial passages and stored at -80°C prior to use.

2.4. Detection of FQ-resistant genes and mRNA expression of related efflux pumps

The artificially induced ciprofloxacin-resistant isolates were analyzed for mutations in quinolone resistance-determining regions (QRDRs) in *gyrA*, *gyrB*, *parC*, and *parE* by PCR and sequencing. The mRNA expression of the related efflux genes *satAB* and *smrA* as well as the identified ABC transporter gene selected by the proteome, were detected by real-time RT-PCR, as previously described (18). 16S rRNA was used as a housekeeping gene to standardize the levels of the transcripts. The genes of *satAB* and *smrA* were also sequenced and compared with their parental strains. The primers used in this study were designed by using software Primer premier 5 (Table 1).

2.5. Preparation of proteins and 2-D gel electrophoresis

The *S. suis* resistant and sensitive strains were grown to late log phase (reaching an OD₆₀₀ of 0.8) and Triton X-114 phase-separation was used to isolate lipophilic membrane proteins, using the previously described method (19). Membrane-associated proteins were desalted by using the 2-D Clean-up Kit (GE, Healthcare), and their concentrations were determined by using the 2-D Quant Kit (GE Healthcare).

2-D gel electrophoresis was performed as previously described (20). Gel assessment and data analysis were done using the Image master 2D 5.0 program (GE Healthcare). Quantitative comparison of average gels among different strains was used to designate the significantly different expressed spots; those showing at least a 2-fold change in three pairs of sensitive and resistant strains with three replicates were considered for subsequent analysis.

Table 1. Primers used for PCR amplification and qRT-PCR in this study

Name	Sequence (5'-3')	References
Amplification and sequencing		
<i>gyrA</i>	CGCCGTATTTTGTATGGGATG / GTTCCGTTAACCAGAAGGTT	This study
<i>gyrB</i>	GAAGGAGTGTCCGAATATGG / CTGGTGAAGATGTGCGTGAA	This study
<i>parC</i>	AAGGACGGCAACACTTTTGAC / AGTGGGTCTTTTTCCGTATC	This study
<i>parE</i>	TGTGGTGGACGGCATTGTG / CCTCTACTAGCGGTCCGATAT	This study
qRT-PCR		
SS2069	GTATTTTGCCTTACGCTCATCTGT/ CCTATGCTCCTTACTCTTACCACGA	This study
<i>satAB</i>	AATCCAGAACCTTGTCAT / AATAATCATCCACCAGAGT	Escudero <i>et al.</i> , 2007
16S rRNA	GTGAAGAAGGTTTTCCGGATCGT / GTAGTTAGCCGTCCTTTCTGGT	This study

2.6. Mass spectrometry analysis for protein spot analysis

Tryptic in-gel digestion was performed as described (21). The resulting peptides were air dried and analyzed with a 4800 MALDI-TOF/TOF proteomics Analyzer (Applied Biosystems, USA). The UV laser was operated at 200 Hz at a wavelength of 355 nm, and the accelerated voltage was operated at 20 kV. Protein digested by trypsin was used to standardize the mass instrument as an internal standardized mode. Data from MALDI-TOF-MS were used in a combined search next to the NCBIInr protein database using MASCOT (Matrix Science). Originally, the MASCOT server was used instead of the NCBIInr for peptide mass fingerprinting (PMF). The criteria used for protein identification were based on PMF data, including the extent of sequence coverage, number of peptides matched, and score of probability. Protein detection was assigned when the sequence coverage was greater than 15% (22,23). The identification of protein spots with a Mascot Score required a result greater than 83.

2.7. Detection of ciprofloxacin concentration in *S. suis* strains by HPLC

Accumulation of ciprofloxacin in the sensitive strain JR05730E and mutants JDZ05802-1EC, ZY05721EC, and JR05730EC was measured by HPLC. The strains were cultured in THB to an OD₆₆₀ of 0.6 and then incubated with ciprofloxacin (10 mg/L) at 37°C in a total volume of 10 mL. One milliliter suspensions during incubation were taken out at 0, 1, 2, 5, 10, 20, 35, and 60 min, respectively. Cells were centrifuged (8,000 g for 1 min), washed three times with 2 mL phosphate buffered solution (pH 7.0), adjusted the wet weight of bacteria to 40 mg, lysed by repeated freezing-thawing cycles, and the obtained suspensions were centrifuged at 12,000 g for 10 min. Proteins were precipitated from 400 µL clear supernatants using methyl cyanides. Samples were mixed, centrifuged (12,000 g for 10 min at 4°C), and supernatants were evaporated to dryness in a water bath (40°C) under a gentle stream of nitrogen gas. Residues were reconstituted in the mobile phase (0.5 mL), mixed by vortex, and an aliquot (20 µL) was

injected onto an HPLC column. The concentration of ciprofloxacin was determined by HPLC under the following conditions: a Kromasil C₁₈ column (150 mm × 4.6 mm, 5 µm), a flow rate of 1.0 mL/min, and UV detection at a wave length of 277 nm. All accumulation experiments were performed on at least three separate occasions.

2.8. Statistical analysis

All data are presented as mean ± SD and comparisons of *sataA*, *satB*, *smrA*, and *SS2069* expression as well as comparisons of the ciprofloxacin concentrations between sensitive and resistant strains was statistically analyzed using Student's *t* test. A value *p* < 0.05 was regarded as statistically significant.

3. Results

3.1. Selection of ciprofloxacin-resistant mutants *in vitro*

Minimum inhibitory concentration (MIC) of ciprofloxacin, norfloxacin, and enrofloxacin was determined in *S. suis* strains ZY05721E, JR05730E, and JDZ05802-1E. The MICs revealed that the three strains were all susceptible to enrofloxacin, ciprofloxacin, norfloxacin, and penicillin but resistant to tetracycline and sulfamonomethoxine. Subsequently, spontaneous resistant clones were obtained from these three parental sensitive isolates after stepwise induction by subinhibitory concentrations of the FQs. The final selected clones were found highly resistant to ciprofloxacin, enrofloxacin, norfloxacin, tetracycline, and sulfamonomethoxine (Table 2). The ciprofloxacin MICs of the three strains increased up to more than 128 mg/L, suggesting that the appropriate combination of stepwise induction and selection cycles are an efficient way to induce resistant mutants *in vitro*.

3.2. Mutations in the QRDRs of topoisomerase and detection of *SatAB* overexpression in resistant strains

In the three selected FQ-resistant strains, mutations showed in Table 3 were found in the QRDRs of GyrA (Ser81Arg) and ParC (Ser79Phe), together with GyrB (Asp315Asn)

Table 2. The MICs of seven antibiotics used against *S. suis* parent and induced mutants (mg•L⁻¹)

Strain	ERY	ENRO	NOR	CIP	PEN	TET	SUL
ZY05721E	0.0018	0.5	0.25	0.25	< 0.0625	16	≥ 512
JR05730E	0.0018	1	0.25	0.5	< 0.0625	128	512
JDZ05802-1E	0.0018	0.5	1	0.0625	< 0.0625	64	≥ 512
ZY05721EC	64	128	≥128	≥128	< 0.0625	16	≥ 512
JR05730EC	128	64	≥128	≥128	< 0.0625	128	512
JDZ05802-1EC	64	128	≥128	≥128	< 0.0625	64	≥ 512

ZY05721EC, JR05730EC, JDZ05802-1EC were the selected resistant strains to ciprofloxacin, norfloxacin and enrofloxacin. ERY: erythromycin; ENRO: enrofloxacin; NOR: norfloxacin; CIP: ciprofloxacin; PEN: penicillin; TET: tetracycline; SUL: sulfamonomethoxine.

in two mutants ZY05721EC and JR05730EC. However, only mutation in GyrB (Glu354Lys) was observed in the JDZ05802-1EC strain and mutation in *parE* (pro278ser) was found only in the ZY05721EC strain). The mRNA expression level of the efflux gene *satAB* was detected with and without ciprofloxacin by real-time RT-PCR, but a significant difference was not found among the parental and mutant strains (showed in Figure 2A). Furthermore, no acquired point mutations of *satAB* as well as its promoter region were found by sequencing in the wild type and mutant derivatives. Interestingly, the efflux pump inhibitor reserpine could decrease the MICs of ciprofloxacin and norfloxacin in the mutants, but it could not change the MIC of enrofloxacin (Table 4). These results indicated that other efflux pumps may be involved in ciprofloxacin and norfloxacin resistance. Therefore, the proteome method was used to investigate the new efflux mechanism associated with FQ resistance.

3.3. Proteome changes related to ciprofloxacin resistance in *S. suis*

Proteome analysis showed a consistent pattern of membrane protein expression levels on the gels under optimal 2-DE running conditions. Image analysis revealed that there were 311 ± 53 and 237 ± 53 highly reproducible protein spots observed consistently in sensitive strains and resistant mutants during the exponential growth phase, respectively. Nine numbered protein spots were common in three resistant strains with a more than 1.3-fold difference in expression level

Table 3. The mutations of QRDRs in lab-derived mutants

Isolates No.	GyrA	GyrB	ParC	ParE
ZY05721EC	Ser81Arg	Asp315Asn	Ser79Phe	Pro278Ser
JR05730EC	Ser81Arg	Asp315Asn	Ser79Phe	–
JDZ05802-1EC	–	Glu354Lys	–	–

compared with their parental strains (Figure 1). The nine spots were then characterized by MALDI-TOF-MS, and the results were compared with available data in the NCBI sequence database.

The successfully identified nine spots corresponded to nine individual proteins, and their detailed information is shown in Table 5. Eight proteins (spots 1–5 and 7–9) were upregulated in resistant strains compared with their parental sensitive strain and one protein (spot 6) was only found in two resistant strains ZY05721EC and JDZ05802-1EC. The upregulated spots mainly included six metabolic enzymes (spots 1, 2, 3, 7, 8 and 9), one putative chaperonin GroEL (spot 4), one regulatory factor (spot 6) and one ABC transporter periplasmic protein (spot 5). Among these proteins, ABC transporter periplasmic protein (spot 5), which belongs to the ATP-binding cassette transporter family, was upregulated by 50-, 22-, and 30-fold in ZY05721EC, JR05730EC, and JDZ05802-1EC, respectively. The change in the other proteins was not more than 3-fold when compared between sensitive and resistant strains.

3.4. An ABC transporter is overexpressed in the ciprofloxacin-resistant mutants

Proteome analysis of the sensitive and resistant strains revealed that the ABC transporter periplasmic protein (spot 5) may be associated with fluoroquinolone resistance in *S. suis* on the basis of its upregulation by more than 22-fold in resistant strains. The results suggested that the ABC transporter might have worked as an efflux, which helped *S. suis* to become resistant to ciprofloxacin and norfloxacin but not to enrofloxacin. Furthermore, BLAST search results (<http://www.ncbi.nlm.nih.gov/BLAST/>) also showed 100% identity with the amino acid sequence of an ABC transporter in the *S. suis* strain 05ZYH33. Therefore, we next analyzed the mRNA expression of this ABC transporter periplasmic

Table 4. Initial and final MICs of ciprofloxacin (CIP) and other antibiotics measured in the presence and absence of reserpine

Antibiotics		Initial			After selection with ciprofloxacin		
		ZY05721E	JR05730E	JDZ05802-1E	ZY05721E	JR05730E	JDZ05802-1E
CIP	Res –	0.25	0.5	0.0625	0.25	0.5	0.0625
	Res +	0.25	0.5	0.0625	0.25	0.5	0.0625
NOR	Res –	0.25	0.25	1	0.25	0.25	1
	Res +	0.25	0.25	1	0.25	0.25	1
ENRO	Res –	0.5	1	0.5	0.5	1	0.5
	Res +	0.5	1	0.5	0.5	1	0.5
ERY	Res –	0.0018	0.0018	0.0018	0.0018	0.0018	0.0018
	Res +	0.0018	0.0018	0.0018	0.0018	0.0018	0.0018
PEN	Res –	< 0.0625	< 0.0625	< 0.0625	< 0.0625	< 0.0625	< 0.0625
	Res +	< 0.0625	< 0.0625	< 0.0625	< 0.0625	< 0.0625	< 0.0625
TET	Res –	16	128	64	16	128	64
	Res +	16	128	64	16	128	64
SUL	Res –	≥ 512	512	≥ 512	≥ 512	512	≥ 512
	Res +	≥ 512	512	≥ 512	≥ 512	512	≥ 512

Bold text indicates conditions in which MIC is reduced by addition of reserpine.

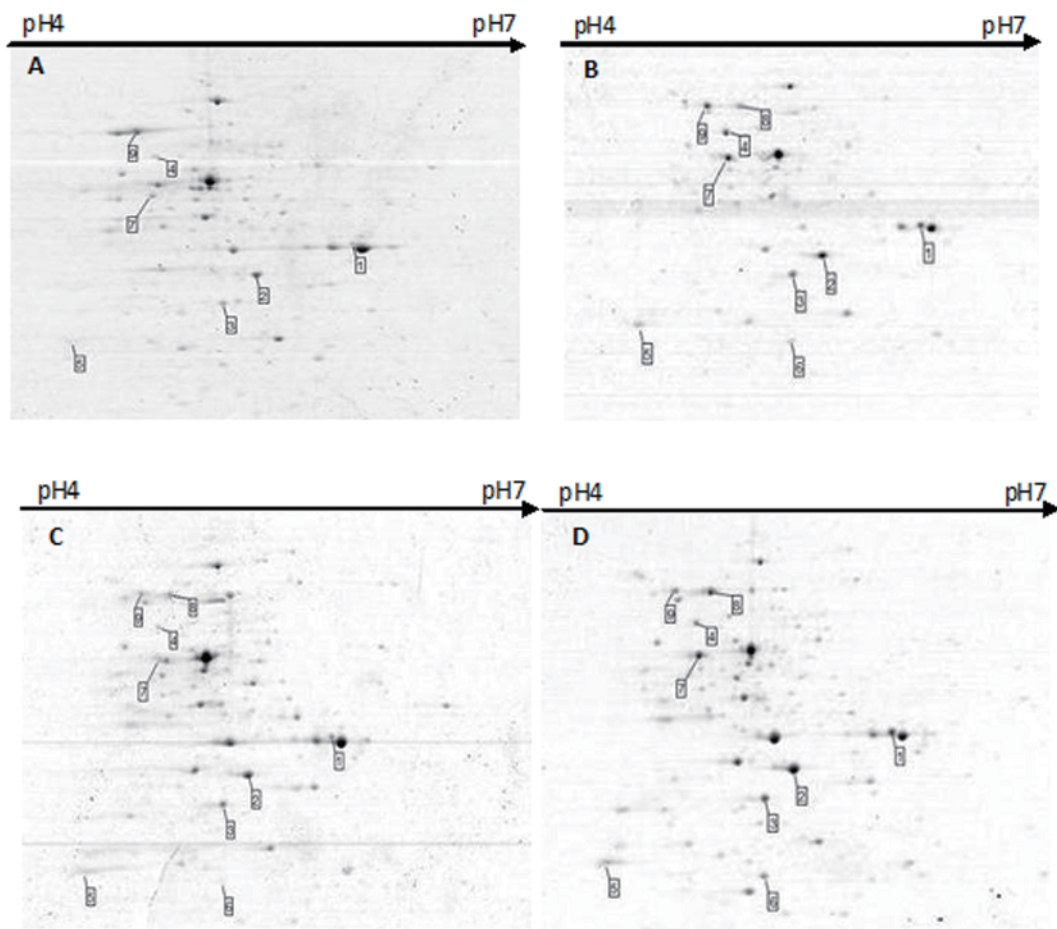


Figure 1. Coomassie Brilliant Blue G-250 stained 2-DE gel representative map of membrane proteins extracted from *S. suis* sensitive and resistant strains during the exponential growth phase. (A: JR05730; B: JR05730-EC; C: ZY05721; D: ZY05721 EC). Proteins were separated by isoelectric focusing in the *pI* range of 4–7 in the first dimension and 12% SDS-PAGE in the second dimension. Squares with numbers indicate the common upregulated proteins in three induced resistant strains compared with each parental sensitive strain. The map of the proteins came from three triplicate experiments.

Table 5. Differentially expressed proteins in *Streptococcus suis* resistant strains during exponential growth phase

Spot No. ^a	Annotation/Species	NCBI Protein Accession No.	Experimental Mw/pI	Theoretic Mw/pI	Sequence Coverage	Mascot score
1	dTDP-glucose 4,6-dehydratase/ <i>Streptococcus suis</i> 89/1591	gi 223933260	38965/5.37	38932.40/5.37	60%	251
2	L-lactate dehydrogenase/ <i>Streptococcus suis</i> 05ZYH33	gi 146318730	35400/5.05	35422.07/5.05	57%	231
3	Fructose-bisphosphate aldolase/ <i>Streptococcus suis</i> 98HAH33	gi 146320177	31250/4.90	31155.37/4.90	48%	121
4	Putative chaperonin GroEL / <i>Streptococcus suis</i> 98HAH33	gi 253751059	57037/4.70	57072.24/4.70	47%	291
5	Amino acid ABC transporter periplasmic protein/ <i>Streptococcus suis</i> 05ZYH33	gi 146319723	28609/4.42	28626.92/4.42	80%	182
6	Phosphate uptake regulator/ <i>Streptococcus suis</i> 98HAH33	gi 146320956	25097/4.96	25055.67/4.96	56%	151
7	Phosphopyruvate hydratase/ <i>Streptococcus suis</i> 98HAH33	gi 146321359	47066/4.66	47094.98/4.66	48%	222
8	L-lactate dehydrogenase/ <i>Streptococcus suis</i> 05ZYH33	gi 146318730	35400/5.05	35422.07/5.05	48%	173
9	Phosphoenolpyruvate-protein kinase/ <i>Streptococcus suis</i> 05ZYH33	gi 146318854	63045/4.60	63084.91/4.60	44%	228

Proteins were identified by MALDI-TOF. Proteins with a minimum of three matching peptides were considered positive. ^a Refers to proteins labelled in Figure 1.

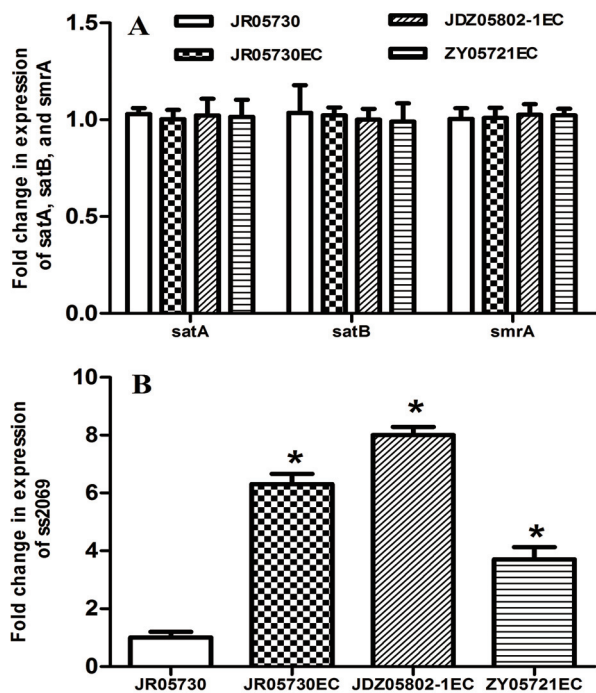


Figure 2. Expression levels of *satA*, *satB* and *smrA* (A) as well as *SS2069* gene encoding an amino acid ABC transporter (B) in sensitive and resistant strains determined by real-time RT-PCR. Pump expression was normalized against 16S RNA expression levels. Values are means \pm SD of three RNA preparations with one RT-PCR for each RNA preparation. Statistical analysis was done using the two-tailed Student's *t*-test to compare the expression levels of sensitive and resistant strains selected by antibiotics. Bars with * are significantly different from sensitive strains ($p < 0.05$).

protein corresponding gene *SS2069* (named in the *S. suis* 05ZYH33 strain) in the sensitive strain (JR05730) and resistant strains (ZY05721EC, JDZ05802-1EC, and JR05730EC) by real-time RT-PCR. The mRNA expression levels of the *SS2069* gene significantly increased by 3.7-, 6.3-, and 8.0-fold in the resistant strains ZY05721EC, JR05730EC, and JDZ05802-1EC, respectively, when compared with the sensitive strain JR05730 (Figure 2).

3.5. The accumulation of ciprofloxacin in resistant and sensitive strains

Because the overexpression of an ABC transporter was observed, the intracellular accumulation of ciprofloxacin was measured in the sensitive and resistant strains. At 1, 2, 5, 10, 20, 35, and 60 minutes after ciprofloxacin (10 μ g/mL) addition to the sensitive strain (JR05730) and resistant strains (ZY05721EC, JDZ05802-1EC, and JR05730EC), one milliliter samples were collected, and the concentration of ciprofloxacin extracted from the cells was determined by HPLC.

Intracellular ciprofloxacin concentrations reached a peak after 10 min in the three resistant strains (Figure 3). And intracellular ciprofloxacin concentrations were significantly lower in the resistant strains than in the

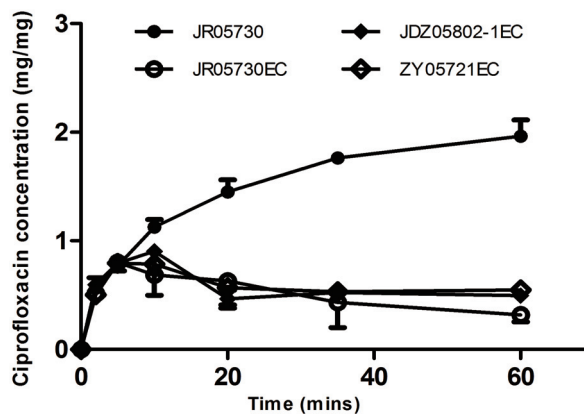


Figure 3. Intracellular accumulation of ciprofloxacin in sensitive and resistant strains of *S. suis*. At 1, 2, 5, 10, 20, 35, and 60 min after ciprofloxacin (10 μ g/mL) addition, one-milliliter samples were collected, and the concentration of ciprofloxacin extracted from cells was determined by HPLC. Each value represents the mean \pm SD from three triplicate experiments.

sensitive strain after 20, 35, and 60 min exposures to ciprofloxacin ($p < 0.05$) (Figure 3).

4. Discussion

Fluoroquinolone resistance in *S. suis* occurs by two mechanisms including mutations in the QRDRs of the *gyrA* and *parC* genes and the mediation of FQ efflux by the SatAB pump (13,15). Based on existing knowledge of FQ resistance and the related literature, the main purpose of our study was to explore the underlying molecular mechanism of FQ resistance after *in vitro* induction of fluoroquinolones in *S. suis*, due to the highly pathogenic nature and zoonotic importance. In this study, two novel findings for FQ resistance were discovered, and to the best of our knowledge they are being reported for the first time in *S. suis*: (1) A new alteration in GyrB was identified and (2) An efflux pump, other than SatAB, was identified that can pump out ciprofloxacin and norfloxacin, but not enrofloxacin, thus, conferring ciprofloxacin/norfloxacin resistance in *S. suis*.

The predicted amino acid sequences of GyrA, GyrB, ParC, and ParE exposed in all three parental susceptible isolates, showed no single amino-acid differences in their QRDRs, suggesting a high degree of protection of this region. Amino acid substitutions in the quinolone resistance-determining regions (QRDR) of GyrA, GyrB, ParC, and ParE were identified in selected resistant strains. Only one strain had a single mutation in GyrB without mutations in GyrA, ParC, or ParE. The resistance mutations in GyrA and ParC in our strains occurred at the expected hot spots (GyrA-S81Y; ParC-S79Y), which are generally similar to those reported by Escudero *et al.* (13) and those in other Gram-positive bacteria, such as *S. aureus*, *S. pneumoniae*, *S. pyogenes*, and *E. faecium* (18,24-27). It has already been demonstrated that QRDR alterations

in GyrB and ParE are associated with fluoroquinolone resistance in Gram-positive bacteria such as *S. aureus*, *S. pneumoniae*, and *E. faecium* (25,27,28), but this has not been reported in *S. suis*. The strains ZY05721EC and JR05730EC had an additional mutation Asp315Asn, and the strain JDZ05802-1EC had another amino acid substitution Glu354Lys in GyrB. Previous studies on fluoroquinolone-resistance mechanisms have identified a Ser-463 to Lys substitution in GyrB in *Salmonella* (29), and a Glu-474 to Lys substitution in GyrB in *S. pneumoniae* (30), which differ from the mutations identified in our strains. In the strain JDZ05802-1EC, only the mutation Glu354Lys in GyrB was found, strongly suggesting that this substitution is involved in FQ resistance; whether Pro278Ser is associated with FQ resistance needs to be confirmed. However, the Asp315Asn mutation has not been reported previously. Only one strain ZY05721EC had the Pro278Ser mutation in ParE. It has been reported that twenty-eight single or combination mutations were found in levofloxacin-resistant *S. pneumoniae* strains, which included the equivalent Pro454Ser mutation in ParE (31). However, they have not been able to assign any significance to the ParE mutation. In our study, the ZY05721EC strain also had mutations in GyrA, GyrB, and ParC, therefore, whether Pro278Ser in ParE is related to FQ resistance also needs to be confirmed.

The ciprofloxacin and norfloxacin-resistance phenotype can be partially reduced by the efflux pump inhibitor reserpine, indicating that a combination of ATP-binding efflux expression and target mutations may be involved in ciprofloxacin-resistance in *S. suis*. However, the enrofloxacin resistance phenotype might not be influenced by reserpine. As an ABC transporter, SatAB is the main efflux pump described in *S. suis* (15). In this study the expression level of SatAB was detected first by real-time RT-PCR; however, there was no change between parental sensitive strains and induced resistant strains. It is clear that the molecular mechanisms contributing to ciprofloxacin and norfloxacin resistance in *S. suis* comprise a complex system. Therefore, to obtain an overall view of the proteins associated with ciprofloxacin resistance in *S. suis*, comparative proteomic mapping of sensitive and resistant strains was carried out. This analysis revealed significant changes in nine differential protein spots of which most are involved in metabolism, stress and virulence. These proteins were predictable due to their common nonspecific response by bacteria when stimulated by different shock conditions, including exposure to antibiotics, toxic agents like heavy metals, oxidants, acids and bile salts (32,33). However in particular, we found a good correlation between the ciprofloxacin resistance phenotype and an increased expression level of an ABC transporter periplasmic protein. To prove the existence of efflux pump overexpression, the reaction of the parental

(JR05730) and mutant (ZY05721EC, JR05730EC, and JDZ05802-1EC) strains was examined after challenging with ciprofloxacin. The mutant strains pumped out ciprofloxacin more efficiently than the parent strains. Our results provide strong evidence that efflux pump overexpression and the change of obtaining target mutations contribute to the high number of ciprofloxacin/norfloxacin mutants selected under *in vitro* pressure on the plates (Figure 3). For an enrofloxacin resistance mechanism, target mutations were the most important and the ABC transporter was not involved in the enrofloxacin resistance mechanism in these three mutants. The characteristics of the ABC transporter identified in our study are similar to those of SatAB, recently reported by Escudero *et al.* (15). They are mainly involved in ciprofloxacin resistance development, due to an increased thickness of a methylated substituent in position C7 that blocks enrofloxacin from crossing the channels of the efflux pump; this supports the results of Takenouchi *et al.* (34). A small number of studies using different bacterial species establish that ciprofloxacin is better pumped than levofloxacin in *S. aureus* (35), probably because of its hydrophilicity (while this was demonstrated with *norA*, this pump is in the same major facilitator superfamily as *pmrA* and is the homologue of *pmrA* in *Staphylococci* and *smrA* in *S. suis*). Additional investigations on ciprofloxacin-resistance mechanisms in *S. suis* are necessary in order to protect pig production and reduce risk to human health. ABC transporters should also be given consideration as one of the factors involved in developing resistance in SS2 pathogens. Further experiments to determine the role of this possible transporter by knockout techniques are currently under way on these three resistant strains in our laboratory.

In conclusion, our study identifies the overexpression of an ABC transporter jointly with topoisomerase modification in the GyrA, GyrB, and ParC proteins, which played a significant role in ciprofloxacin/norfloxacin resistance in *S. suis* that has never been reported before. These results are useful in finding new drug targets against antibiotic resistant strains of *S. suis*.

Acknowledgements

The study was supported in part by Natural Science Foundation of Jiangsu Province of China (No. BK2012771), the Fundamental Research Funds for the Central Universities (KYZZ01105), the National Natural Science Foundation of China (No. 30972220) and A Project Funded by the Priority Academic Program Development of Jiangsu Higher Education Institutions (PAPD).

References

1. Kerdsin A, Dejsirilert S, Puangpatra P, Sripakdee S,

- Chumla K, Boonkerd N, Polwichai P, Tanimura S, Takeuchi D, Nakayama T, Nakamura S, Akeda Y, Gottschalk M, Sawanpanyalert P, Oishi K. Genotypic profile of *Streptococcus suis* serotype 2 and clinical features of infection in humans, Thailand. *Emerg Infect Dis*. 2011; 17:835-842.
2. Gottschalk M, Xu J, Calzas C, Segura M. *Streptococcus suis*: A new emerging or an old neglected zoonotic pathogen? *Future Microbiol*. 2010; 5:371-391.
 3. Tang J, Wang C, Feng Y, et al. Streptococcal toxic shock syndrome caused by *Streptococcus suis* serotype 2. *PLoS Med*. 2006; 3:e151.
 4. Huang YT, Teng LJ, Ho SW, Hsueh PR. *Streptococcus suis* infection. *J Microbiol Immunol Infect*. 2005; 38:306-313.
 5. Suankratay C, Intalapaporn P, Nunthapisud P, Arunyingmongkol K, Wilde H. *Streptococcus suis* meningitis in Thailand. *Se Asian J Trop Med*. 2004; 35:868-876.
 6. Yu H, Jing H, Chen Z, et al. Human *Streptococcus suis* outbreak, Sichuan, China. *Emerg Infect Dis*. 2006; 12:914-920.
 7. Manzin A, Palmieri C, Serra C, Saggi B, Princivalli MS, Loi G, Angioni G, Tiddia F, Varaldo PE, Facinelli B. *Streptococcus suis* meningitis without history of animal contact, Italy. *Emerg Infect Dis*. 2008; 14:1946-1948.
 8. Feldman C, Anderson R. Bacteraemic pneumococcal pneumonia: Current therapeutic options. *Drugs*. 2011; 71:131-153.
 9. Higgins R, Gottschalk M. Streptococcal diseases. In: *Diseases of swine* (Straw BE, D'Allaire S, Mengelng WL, et al.). 9th ed., Blackwell Pub., Ames, Iowa, USA, 2006; pp. 769-783.
 10. Kataoka Y, Sugimoto C, Nakazawa M, Kashiwazaki M. Detection of *Streptococcus suis* type 2 in tonsils of slaughtered pigs using improved selective and differential media. *Vet Microbiol*. 1991; 28:335-342.
 11. Seol B, Kelneric Z, Hajsig D, Madic J, Naglic T. Susceptibility to antimicrobial agents of *Streptococcus suis* capsular type 2 strains isolated from pigs. *Zentralbl Bakteriol*. 1996; 283:328-331.
 12. Marie J, Morvan H, Berthelot-Herault F, Sanders P, Kempf I, Gautier-Bouchardon AV, Jouy E, Kobisch M. Antimicrobial susceptibility of *Streptococcus suis* isolated from swine in France and from humans in different countries between 1996 and 2000. *J Antimicrob Chemother*. 2002; 50:201-209.
 13. Escudero JA, San Millan A, Catalan A, de la Campa AG, Rivero E, Lopez G, Dominguez L, Moreno MA, Gonzalez-Zorn B. First characterization of fluoroquinolone resistance in *Streptococcus suis*. *Antimicrob Agents Chemother*. 2007; 51:777-782.
 14. Palmieri C, Princivalli MS, Brenciani A, Varaldo PE, Facinelli B. Different genetic elements carrying the tet(W) gene in two human clinical isolates of *Streptococcus suis*. *Antimicrob Agents Chemother*. 2011; 55:631-636.
 15. Escudero JA, San Millan A, Gutierrez B, Hidalgo L, La Ragione RM, AbuOun M, Galimand M, Ferrandiz MJ, Dominguez L, de la Campa AG, Gonzalez-Zorn B. Fluoroquinolone efflux in *Streptococcus suis* is mediated by SatAB and not by SmrA. *Antimicrob Agents Chemother*. 2011; 55:5850-5860.
 16. Carsenti-Etesse H, Roger PM, Dunais B, Durgeat S, Mancini G, Bensoussan M, Dellamonica P. Gradient plate method to induce *Streptococcus pyogenes* resistance. *J Antimicrob Chemother*. 1999; 44:439-443.
 17. Clinical and Laboratory Standards Institute (CLSI). *Performance Standards for Antimicrobial Susceptibility Testing*; 19th informational supplement. 2010.
 18. Avrain L, Garvey M, Mesaros N, Glupczynski Y, Mingot-Leclercq MP, Pidcock LJ, Tulkens PM, Vanhoof R, Van Bambeke F. Selection of quinolone resistance in *Streptococcus pneumoniae* exposed *in vitro* to subinhibitory drug concentrations. *J Antimicrob Chemother*. 2007; 60:965-972.
 19. Malen H, Pathak S, Softeland T, de Souza GA, Wiker HG. Definition of novel cell envelope associated proteins in Triton X-114 extracts of *Mycobacterium tuberculosis* H37Rv. *BMC Microbiol*. 2010; 10:132.
 20. Wu Z, Zhang W, Lu C. Comparative proteome analysis of secreted proteins of *Streptococcus suis* serotype 9 isolates from diseased and healthy pigs. *Microb Pathog*. 2008; 45:159-166.
 21. Zhang L, Yu Z, Jiang L, Jiang J, Luo H, Fu L. Effect of post-harvest heat treatment on proteome change of peach fruit during ripening. *J Proteomics*. 2011; 74:1135-1149.
 22. Wang Y, Yang L, Xu H, Li Q, Ma Z, Chu C. Differential proteomic analysis of proteins in wheat spikes induced by *Fusarium graminearum*. *Proteomics*. 2005; 5:4496-4503.
 23. Xu H, Yang L, Xu P, Tao Y, Ma Z. cTrans: Generating polypeptide databases from cDNA sequences. *Proteomics*. 2007; 7:177-179.
 24. Leavis HL, Willems RJ, Top J, Bonten MJ. High-level ciprofloxacin resistance from point mutations in *gyrA* and *parC* confined to global hospital-adapted clonal lineage CC17 of *Enterococcus faecium*. *J Clin Microbiol*. 2006; 44:1059-1064.
 25. Oyamada Y, Ito H, Inoue M, Yamagishi J. Topoisomerase mutations and efflux are associated with fluoroquinolone resistance in *Enterococcus faecalis*. *J Med Microbiol*. 2006; 55(Pt 10):1395-1401.
 26. Pletz MWR, McGee L, Van Beneden CA, Petit S, Bardsley M, Barlow M, Klugman KP. Fluoroquinolone resistance in invasive *Streptococcus pyogenes* isolates due to spontaneous mutation and horizontal gene transfer. *Antimicrob Agents Chemother*. 2006; 50:943-948.
 27. Pidcock LJV. Mechanisms of fluoroquinolone resistance: An update 1994-1998. *Drugs*. 1999; 58:11-18.
 28. Fournier B, Hooper DC. Mutations in topoisomerase IV and DNA gyrase of *Staphylococcus aureus*: Novel pleiotropic effects on quinolone and coumarin activity. *Antimicrob Agents Chemother*. 1998; 42:121-128.
 29. Gensberg K, Jin YF, Pidcock LJ. A novel *gyrB* mutation in a fluoroquinolone-resistant clinical isolate of *Salmonella typhimurium*. *FEMS Microbiol Lett*. 1995; 132:57-60.
 30. Pan XS, Fisher LM. DNA gyrase and topoisomerase IV are dual targets of clinafloxacin action in *Streptococcus pneumoniae*. *Antimicrob Agents Chemother*. 1998; 42:2810-2816.
 31. Jones ME, Sahn DF, Martin N, Scheuring S, Heisig P, Thornsberry C, Kohrer K, Schmitz FJ. Prevalence of *gyrA*, *gyrB*, *parC*, and *parE* mutations in clinical isolates of *Streptococcus pneumoniae* with decreased susceptibilities to different fluoroquinolones and originating from Worldwide Surveillance Studies during the 1997-1998 respiratory season. *Antimicrob Agents Chemother*. 2000; 44:462-466.
 32. O'Toole R, Williams HD. Universal stress proteins and

- Mycobacterium tuberculosis*. Res Microbiol. 2003; 154:387-392.
33. Sanchez B, Champomier-Verges MC, Anglade P, Baraige F, de Los Reyes-Gavilan CG, Margolles A, Zagorec M. Proteomic analysis of global changes in protein expression during bile salt exposure of *Bifidobacterium longum* NCIMB 8809. J Bacteriol. 2005; 187:5799-5808.
 34. Takenouchi T, Tabata F, Iwata Y, Hanzawa H, Sugawara M, Ohya S. Hydrophilicity of quinolones is not an exclusive factor for decreased activity in efflux-mediated resistant mutants of *Staphylococcus aureus*. Antimicrob Agents Chemother. 1996; 40:1835-1842.
 35. Schmitz FJ, Fluit AC, Luckefahr M, Engler B, Hofmann B, Verhoef J, Heinz HP, Hadding U, Jones ME. The effect of reserpine, an inhibitor of multidrug efflux pumps, on the *in-vitro* activities of ciprofloxacin, sparfloxacin, and moxifloxacin against clinical isolates of *Staphylococcus aureus*. J Antimicrob Chemother. 1998; 42:807-810.
- (Received November 7, 2014; Revised April 10, 2014; Accepted April 14, 2014)

Defect of tropomyosin-related kinase B isotype expression in ovarian clear cell adenocarcinoma

Yumiko Goto¹, Yoshie Kametani^{2,*}, Atsuko Kikugawa³, Banri Tsuda⁴, Masaki Miyazawa¹, Hiroshi Kajiwara⁵, Yasuhisa Terao³, Susumu Takekoshi², Naoya Nakamura⁵, Satoru Takeda³, Mikio Mikami¹

¹Department of Obstetrics and Gynecology, Tokai University School of Medicine, Isehara, Kanagawa, Japan;

²Department of Immunology, Division of Basic Medical Science and Molecular Medicine, Tokai University School of Medicine, Isehara, Kanagawa, Japan;

³Department of Obstetrics and Gynecology, Juntendo University School of Medicine, Tokyo, Japan;

⁴Department of Breast and Endocrine Surgery, Tokai University School of Medicine, Isehara, Kanagawa, Japan;

⁵Department of Pathology, Tokai University School of Medicine, Isehara, Kanagawa, Japan.

Summary

Tropomyosin-related kinase B (TrkB) is a functional signal molecule that correlates with cell survival and epithelial-mesenchymal transition (EMT), which is essential for the invasiveness of malignant cancer cells. While a truncated isoform of TrkB has a dominant negative effect, full-length TrkB with its tyrosine kinase domain is predicted to play a role in cancer progression. Because ovarian clear cell adenocarcinoma (CCA) shows worse prognosis compared to other cancer types, we investigated the correlation between TrkB isoforms and the progression of CCA. Ovarian adenocarcinoma and benign tumor samples were obtained from Tokai University Hospital and Juntendo University Hospital. These samples were examined for the TrkB expression of isotype-specific proteins and mRNAs by immunohistochemistry and domain-specific semi-quantitative reverse transcription polymerase chain reaction. While TrkB mRNA expression was detected in all of the ovarian tissues and TrkB protein expression was predominant in ovarian cancer tissues, the number of tissues expressing the tyrosine kinase-truncated isoforms (T-Shc or T1) decreased according to the clinical stage of CCA. Irregular isoforms were also observed in some CCA samples. The decrease in T-Shc and T1 were less obvious in mucinous adenocarcinoma and not observed in serous or endometrioid adenocarcinoma. Decreased expression of the truncated isoforms (T-Shc and T1) was associated with CCA progression. These results demonstrate that irregular expression of TrkB isoforms is a characteristic of CCA tissues. The unique TrkB expression profile may be useful for the diagnosis of CCA subtypes.

Keywords: Tropomyosin-related kinase B, brain-derived neurotrophin factor, ovarian cancer, clear cell adenocarcinoma, isoform

1. Introduction

Brain-derived neurotrophin factor (BDNF) and its receptor tropomyosin-related kinase B (TrkB) belong to the nerve growth factor family and the Trk family,

respectively (1,2). TrkB was first reported to be a BDNF receptor and to support the growth and maintenance of the nervous system. Thereafter, TrkB and BDNF were found to be expressed in gynecological tissues including the ovary, particularly in oocytes (3,4). In the normal ovary, BDNF/TrkB signaling plays a supportive role in the growth of follicles (3) and fertilized eggs (4) through BDNF secreted from granulosa cells and cumulus cells, as it stimulates TrkB receptors expressed on oocytes. TrkB signaling reportedly promotes cell survival and epithelial-mesenchymal transition (EMT) (5,6) in head and neck squamous cell carcinoma. These features of

*Address correspondence to:

Dr. Yoshie Kametani, Department of Immunology, Division of Basic Medical Science and Molecular Medicine, Tokai University School of Medicine, 143 Shimokasuya, Isehara, Kanagawa 259-1193, Japan.

E-mail: y-kametn@is.icc.u-tokai.ac.jp

TrkB activity and its primary role as a growth factor receptor are presumably related to carcinogenesis (7,8). In fact, overexpression of TrkB has been observed in various malignant tumors, including neuroblastoma, prostate cancer, pancreatic cancers, multiple myeloma and pulmonary carcinoid tumors.

The *TrkB* gene (Figure 1) is relatively large, spanning more than 350 kbp and containing 24 exons (9). Full-length TrkB has an intracellular tyrosine kinase (TK) domain. In human neural tissue, two C-terminal truncated TrkB receptors, TrkB-T-Shc and TrkB-T1, are also expressed (10,11), and both act as dominant-negative inhibitors of the full-length receptor (12). These truncated isoforms, TrkB-T-Shc and TrkB-T1, may function in normal neuronal tissues to modulate the TrkB signal. Moreover, TrkB isoforms lacking several exons at the N-terminus have recently been predicted by in silico analysis (13).

Ovarian carcinoma is usually classified into four histopathological types: serous, endometrioid, mucinous, and clear cell adenocarcinoma (CCA). There have been many reports comparing the features of these cancer types (14). Among these ovarian cancer types, CCA accounts for more than 20% of ovarian carcinomas

in Japan, where its frequency is higher compared to western countries (15). CCA has a worse prognosis compared to other types of ovarian carcinoma, as CCA is resistant to various anti-cancer treatments, although its growth is slow. These characteristics are similar to those of cancer stem cells, which might be induced by the process of EMT (16). However, the molecular mechanisms of the worse biological behavior of CCA have not been fully clarified.

Large molecules with multiple functional domains such as TrkB can have several variants as a result of splicing or mutation of the DNA caused by oncogenesis. To date, the over-expression of TrkB protein in cancers has been evaluated by immunohistochemical analysis (17). However, any major abnormalities of the molecular structure of TrkB have not been reported in cancer tissues.

In the present study, ovarian cancer tissues were first examined for structural abnormalities in TrkB mRNA to determine whether a decrease in dominant-negative isoforms occurs with CCA progression. The results indicate that the expression of irregular TrkB variants could be a potential marker of CCA diagnosis and a target of CCA treatment.

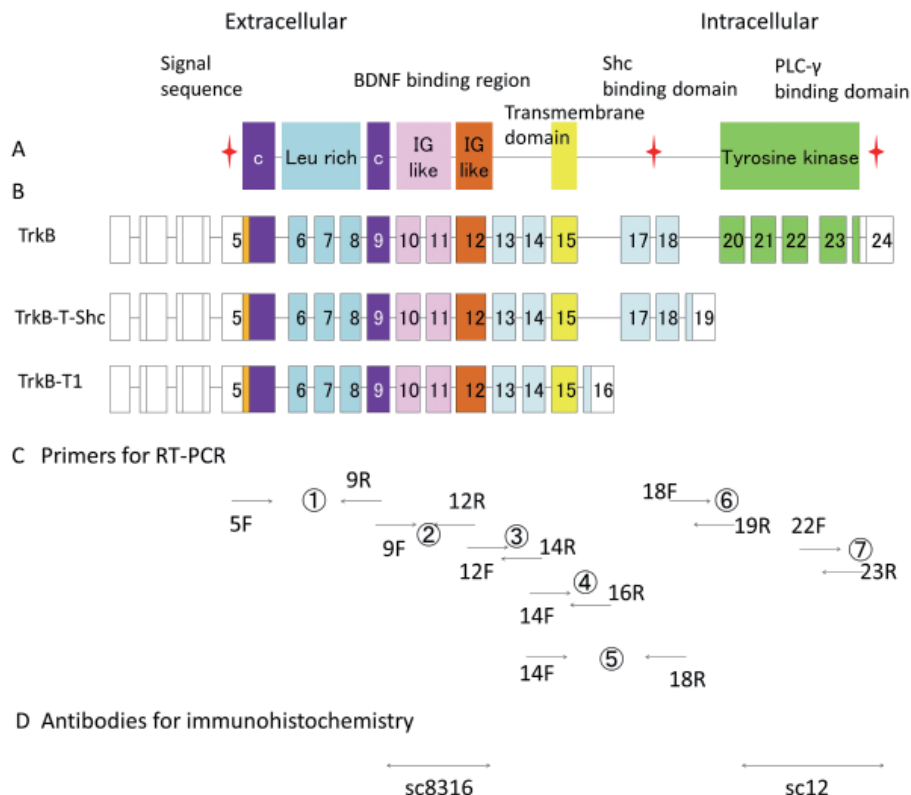


Figure 1. Predicted TrkB protein isoforms with primers and antibodies used for analysis. (A) Domains of full-length TrkB protein. c, cysteine-rich region; Leu rich, leucine-rich region; IG like, immunoglobulin-like domain. **(B)** Major splice variants of TrkB. TrkB: full-length TrkB; TrkB-T-Shc: TrkB with the Shc binding domain but without the kinase and PLC-γ domains; TrkB-T1: TrkB without functional intracellular domains. The 5' and 3' untranslated region domains are shown as empty boxes. The coding region is shown as boxes that are colored differently for each domain. **(C)** The locations of the primers for RT-PCR are shown by arrows, and the numbers indicate the amplified fragments. Thus, each primer is labeled with the exon number, and the forward (F) or reverse (R) direction is also indicated by the direction of the arrow. **(D)** Epitopes of the antibodies (sc8316 and sc12) used for immunohistochemical analysis are indicated by double-headed arrows.

2. Materials and Methods

2.1. Clinical samples

Immunohistochemical specimens of ovarian cancer ($n = 105$), endometriosis ($n = 17$), benign ovarian tumors ($n = 9$) and normal endometrium ($n = 28$) were obtained from patients who underwent surgery at Tokai University Hospital (Kanagawa, Japan) from 1994 to 2010 (Table 1A). RNA was extracted from fresh-frozen specimens of ovarian cancer tissue following reverse transcription polymerase chain reaction (RT-PCR) ($n = 47$) (Table 1B). All specimens contained at least 70% tumor tissue. Tumors were harvested peri-operatively from 2007 to 2011 at Tokai University Hospital and Juntendo University Hospital (Tokyo, Japan) and immediately frozen at -80°C . All tissues were obtained with the informed consent of the patients, and this study was approved by the Institutional Review Boards of Tokai University and Juntendo University.

2.2. Cell culture

Ovarian cancer cell lines and a neuroblastoma cell line (TGW) were purchased from American Type Culture Collection (Manassas, VA, USA). TGW was cultured at 37°C under 5% CO_2 in Glutamax with 10% fetal bovine serum (Equitech-Bio, Inc., Kerrville, TX, USA), and 10 mM all trans retinoic acid (Sigma-Aldrich, St. Louis, MO, USA) was added to induce TrkB expression. Cells were grown in 10 mm dishes (Asahi Glass Co., Ltd., Tokyo, Japan) coated with type I collagen for 6 days,

after which RNA was extracted to use as a positive control for RT-PCR.

2.3. Immunohistochemistry

Sections of formalin-fixed, paraffin-embedded tissues were stained using 2 polyclonal antibodies for TrkB (Figure 1): anti-TrkB antibody sc8316, which targets the extracellular domain near the BDNF-binding site (N: 160-340, Santa Cruz Biotechnology, Inc., Dallas, TX, USA), and anti-TrkB antibody sc12, which targets the TK domain (Santa Cruz). One monoclonal antibody was used to stain for BDNF (anti-BDNF mouse antibody, clone #35928.11; Merck, Darmstadt, Germany). Biotinylated anti-rabbit IgG (Jackson ImmunoResearch Laboratories, Inc., West Grove, PA, USA) (1:300) was used as the secondary antibody for sc8316, and biotinylated anti-mouse IgG (Fitzgerald, Acton, MA, USA) (1:200) was used for BDNF. Sections were stained by the ABC method (Vector Laboratories Inc., Burlingame, CA, USA) for the sc8316 and anti-BDNF antibodies and by the EnVision method (Dako, Glostrup, Denmark) for the sc12 antibody. EnVisionTM+ Rabbit/HRP (Dako) was used for 1 hour for sc12.

Sections of ovarian CCA specimens with strong staining for sc8316 and sc12 and sections of cerebellar tissue specimens that strongly stained for BDNF were used as positive controls. For the negative control, we used rabbit IgG (sc8316 and sc12) or mouse IgG (BDNF) in place of the primary antibodies. If more than 10% of the tumor cells were positive for TrkB or BDNF, the tumor was classified as positive.

Table 1. Clinical characteristics of the patients

A. Clinical characteristics of the patients. IHC analysis

Items	Number	Age (mean \pm S.D.)	Stage			
			I	II	III	IV/rec
Ovarian cancer	105	54.6 \pm 10.0	55	10	32	8
Mucinous	11	53.7 \pm 16.4	7	2	2	0
Serous	19	58.7 \pm 8.7	5	0	11	3
Endometrioid	25	53.1 \pm 11.3	13	3	6	3
Clear cell	50	54.0 \pm 7.7	30	5	13	2
Benign tissue	51	46.4 \pm 8.6				
Endometriosis	17	43.8 \pm 7.0				
Benign ovarian tumors	9	54.8 \pm 13.8				
Endometrium	28	45.2 \pm 5.6				

(OA: $n = 105$, EM: $n = 17$, BOT: $n = 9$, NE: $n = 28$)

B. Clinical characteristics of the patients. RT-PCR analysis

Items	Number	Age (mean \pm S.D.)	Stage			
			I	II	III	IV/rec
Ovarian cancer	47	53.6 \pm 11.8	22	6	16	4
Mucinous	8	50.8 \pm 18.5	7	1	0	0
Serous	8	62.0 \pm 12.4	1	0	7	0
Endometrioid	10	54.5 \pm 9.0	2	3	5	1
Clear cell	21	51.1 \pm 8.6	12	2	4	3

(OA: $n = 47$.)

2.4. RT-PCR and DNA sequence analysis

Total RNA was extracted using TRIzol LS reagent (Invitrogen, San Diego, CA, USA) or a Qiagen extraction kit (Qiagen, Valencia, CA, USA) from fresh-frozen tissues or cultured cells according to the manufacturer's instructions. Then, the optical density of the extracts was measured, and the concentration to use for RT-PCR was selected. The primers for TrkB (Figure 1), BDNF, and β -actin are as indicated in the Supplemental data (<http://www.biosciencetrends.com/docindex.php?year=2014&kanno=2>). Amplification involved initial reverse transcription at 50°C for 30 min and 95°C for 15 min, followed by 33 cycles of denaturation for 1 min at 94°C, annealing for 1 min at 60°C, and extension for 1 min at 72°C. Final extension was then carried out for 5 min at 72°C, after which PCR products were separated by electrophoresis on a 1% agarose gel in 1 × Tris-Borate-EDTA (TBE) and stained with 0.5 μ g/mL ethidium bromide.

Direct DNA sequencing of the PCR products was performed using the primers above and an Applied Biosystems 3500XL sequencer (Applied Biosystems, Carlsbad, CA, USA). Each sequence was compared with those registered in the National Center for Biotechnology Information (NCBI) database, and A Plasmid Editor (ApE) software was used for this analysis.

2.5. Statistical analysis

Statistical analyses were conducted using Microsoft Office Excel 2007 (Microsoft, Redmond, WA, USA). Differences were evaluated by the chi-square test for comparison among tumor subtypes or stages. The results were considered to be significant if the p -value was < 0.05 .

3. Results

We first used the extracellular domain-specific antibody (Ab) sc8316 and the intracellular domain-specific Ab sc12 to examine the localization of TrkB proteins in the tissues by immunohistochemistry. As shown in Figures 2A and 2B, the cell membrane and cytoplasm of ovarian CCA cells were clearly stained by sc8316. The invasive front of the tumor showed greater expression of TrkB (Figure 2B). As with sc8316, the cell membrane and cytoplasm were both stained by sc12 antibody (Figure 2C). These results suggest that TrkB expression was increased on CCA cells in invasive sites.

As shown in Table 2, the percentage of TrkB-positive ovarian cancers was 74.3%, which was significantly higher when compared with endometriotic tissue and normal endometrium ($p < 0.05$). Immunohistochemical analysis did not indicate a significant tissue type or clinical stage specificity. We further examined the protein expression of the intracellular domain using

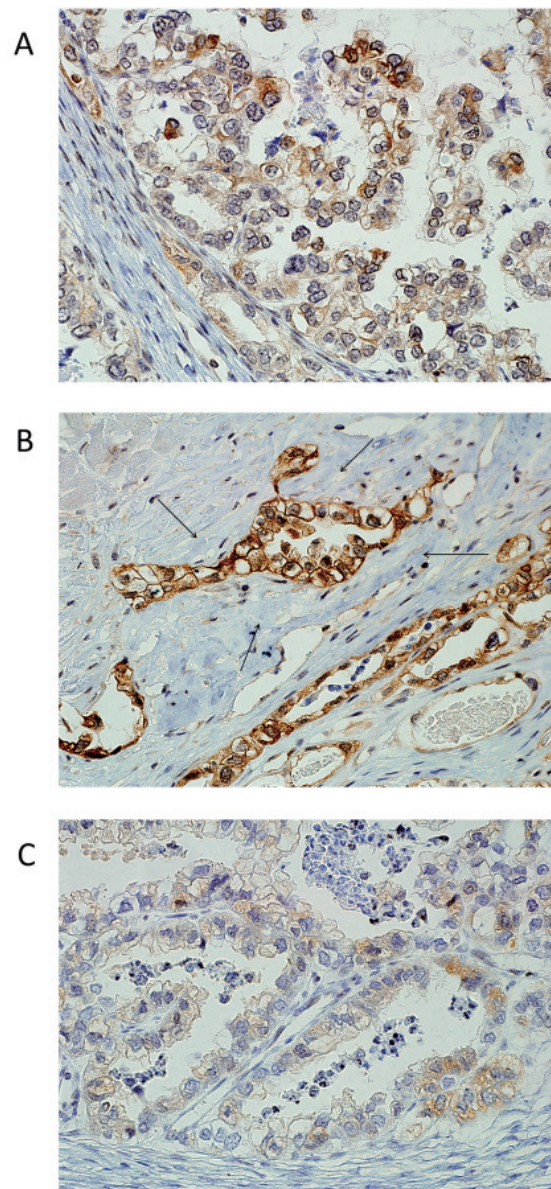


Figure 2. Immunohistochemical analysis of TrkB in ovarian cancer. (A) Representative photomicrograph of a primary clear cell adenocarcinoma stained with sc8316 (patient number 30 in Figure 4). ($\times 20$). (B) Representative photomicrograph of the invasive front of a clear cell adenocarcinoma stained with sc8316 (patient number 30 in Figure 4). Arrows indicate sites of strong TrkB expression at the invasive front. ($\times 20$). (C) Representative photomicrograph of clear cell adenocarcinoma stained with sc12 (patient number 30 in Figure 4). ($\times 20$). An Olympus AX70 optical microscope, DP2-BSW software (Ver 2.1), and DP72 camera were used.

sc12. Similar to sc8316, the cell surface and cytoplasm were stained positively by the antibody (Figure 1D). Among the 78 TrkB-positive cases, the percentage of sc8316 and sc12 double-positive cancers was 19.2% (15 cases). TK domain expression was observed in ovarian cancers and benign tumors but was not observed in the endometrium or endometriotic tissue. The percentage of sc12-positive cases did not differ among tissue types or clinical stages (Table 2).

The percentage of BDNF-positive ovarian cancers

Table 2. Immunohistochemical analysis of TrkB isoform and BDNF expression in clinical samples

Items	Expression of TrkB (sc8316)			Expression of TrkB (sc12)			Expression of BDNF		
	Negative (-)	Positive (+)	Total	Negative (-)	Positive (+)	Total	Negative (-)	Positive (+)	Total
Benign tissues									
Endometriosis	9 (52.9%)	8 (46.1%)	17	8 (100%)	0 (0%)	8	2 (11.8%)	15 (88.2%)	17
Endometrium	15 (53.6%)	13 (46.4%)	28	13 (100%)	0 (0%)	13	12 (42.8%)	16 (57.2%)	28
Ovarian tumor	1 (11.1%)	8 (88.9%)	9	6 (66.7%)	3 (33.3%)	9	1 (11.1%)	8 (88.9%)	9
Ovarian cancer									
Total	27 (25.7%)	78 (74.3%)	105	63 (80.8%)	15 (19.2%)	78	17 (16.2%)	88 (83.8%)	105
Mucinous	1 (9.1%)	10 (90.9%)	11	7 (70.0%)	3 (30.0%)	10	1 (9.1%)	10 (90.9%)	11
Serous	4 (21.0%)	15 (79.0%)	19	12 (80.0%)	3 (20.0%)	15	1 (5.3%)	18 (94.7%)	19
Endometrioid	13 (52.0%)	12 (48.0%)	25	11 (91.7%)	1 (8.3%)	12	11 (44.0%)	14 (56.0%)	25
Clear cell	9 (18.0%)	41 (82.0%)	50	33 (80.5%)	8 (19.5%)	41	4 (8.0%)	46 (92.0%)	50
Stage									
Stages I	16 (29.1%)	39 (70.9%)	55	32 (82.1%)	7 (17.9%)	39	11 (20.0%)	44 (80.0%)	55
Stages II-IV	11 (22.0%)	39 (78.0%)	50	32 (82.1%)	7 (17.9%)	39	6 (12.0%)	44 (88.0%)	50

(OA: $n = 105$, EM: $n = 17$, BOT: $n = 9$, NE: $n = 28$)

was 83.8% (88 cases). Among the TrkB-positive ovarian cancers, 88.5% (69 cases) were also BDNF positive (69 cases) (Table 2).

We then analyzed the molecular structure of the TrkB isoforms expressed in ovarian cancer. For the analyses, we selected samples (Table 1) after we confirmed TrkB protein expression by the above immunohistochemical analysis.

The RT-PCR results showed that the TGW neuroblastoma cell line expressed all domains of TrkB, as reported previously (17). The PCR products of this cell line were used as positive controls because the sequences of these products were consistent with the sequences of the TrkB domains in normal neural tissue registered in the NCBI database (NM006180.3/variant a/TrkB, NM001007097.1/variant b/TrkB-T1, NM001018064.1/variant c/TrkB lacking exon 17, NM001018065.2/variant d/TrkB-T-Shc, and NM001018066.2/variant e/TrkB-T-Shc lacking exon 17). Typical RT-PCR results are shown in Figure 3. As a result, CCA and mucinous adenocarcinoma (MA) specimens lacked TrkB domains, as shown in Figure 4A, while all the specimens of serous and endometrioid adenocarcinoma expressed all domains of normal TrkB. In CCA, the absence of the TrkB-T-Shc (exons 18-19) and TrkB-T1 (exons 14-16) isoforms was observed with high frequency (9/21 and 6/21 cases, respectively). The percentages of these truncated isoforms decreased in parallel with the clinical stage progression (Figure 5). These results indicate that the decreased level of dominant-negative isoforms correlates with CCA malignancy. Other isoforms were also observed. Prominently, amplification of the exon 9-12 fragment, which includes the BDNF-binding site, was not observed (9/21 of CCA and 2/8 of MA) during the earlier stages. Other variants lacked the exon 5-9 fragment, which is detected only in silico, or the exon 14-18 fragment, which includes the Shc-binding

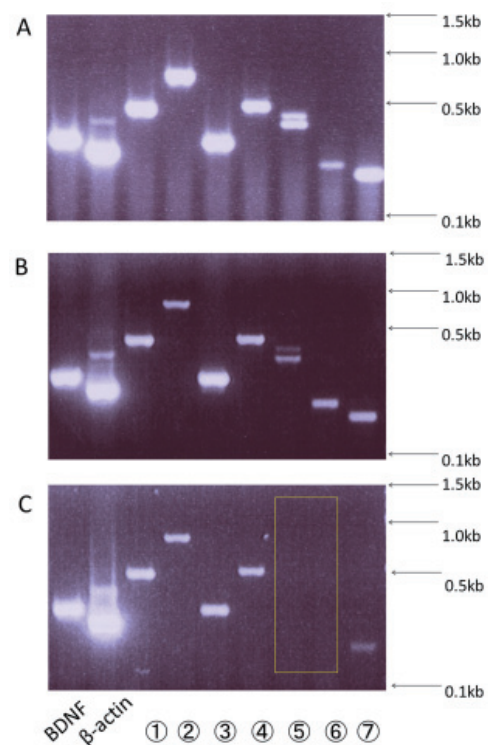


Figure 3. Semiquantitative RT-PCR analysis of ovarian cancer. (A) TGW cells (positive control). **(B)** Endometrioid adenocarcinoma (Icb) (patient number 18 in Figure 4). **(C)** Clear cell adenocarcinoma (Ica) (patient number 36 in Figure 4). The numbers below the panel indicate the PCR products shown in Figure 4.

domain. The absence of exons 18-19 (TrkB-T-Shc) was also observed in MA (1/8). The transmembrane domain (exon 12-14) and the TK domain (exon 22-23) were detected in all ovarian adenocarcinomas (OAs), suggesting the importance of these domains for TrkB expression. BDNF mRNA was expressed in all OAs, and no differences were observed in relation to the histology or clinical stage.

We then examined the expression of TrkB variants

A

	No	stage	① Exon5-9	② Exon9-12	③ Exon12-14	④ Exon14-16	⑤ Exon14-18	⑥ Exon18-19	⑦ Exon22-23	BDNF	β actin
mucinous	1	I a									
	2	I a									
	3	I a									
	4	I a									
	5	I ca									
	6	I ca									
	7	I cb									
	n=8	8	II c								
serous	9	I ca									
	10	III b									
	11	III c									
	12	III c									
	13	III c									
	14	III c						*			
	15	III c									
	n=8	16	IV								
endometrioid	17	I a									
	18	I cb									
	19	II c									
	20	II c/G1									
	21	III b/G3									
	22	III c/G2									
	23	III c						*			
	24	III c/G2									
	25	III c/G3									
	n=10	26	IV/G3					*			
clear cell	27	I a									
	28	I a									
	29	I a						*			
	30	I c									
	31	I c									
	32	I c									
	33	I c									
	34	I c									
	35	I c									
	36	I ca									
	37	I cb						*			
	38	I cb						*			
	39	II c									
	40	II cb									
	41	III b						*			
42	III c										
43	III c										
44	III c										
45	IV										
46	rec										
n=21	47	rec									

B

	No	cell line	① Exon5-9	② Exon9-12	③ Exon12-14	④ Exon14-16	⑤ Exon14-18	⑥ Exon18-19	⑦ Exon22-23	BDNF	β actin
mucinous	1	TU-OM-1									
	2	TU-OM-1/TX									
	3	TU-OM-1/CDDP/TX									
serous	4	HTOA									
	5	HUOA									
clear cell	6	HUOCA- II									
	7	W3UF									
	8	ES-2									

Figure 4. Summary of the expression of TrkB variants by ovarian adenocarcinomas and ovarian cancer cell lines. (A) Expression of TrkB variants by mucinous, serous, endometrioid, and clear cell adenocarcinomas. PCR products that were detected are shown in hatched boxes, and negative products are shown in open boxes. The asterisks in ⑤ indicate a single band (two PCR bands were observed in all other samples). **(B)** Expression of TrkB variants by mucinous, serous and clear cell adenocarcinoma cell lines. Boxes are the same as in (A). TU-OM-1/TX and TU-OM-1/CDDP/TX indicate resistance to TX and CDDP/TX, respectively.

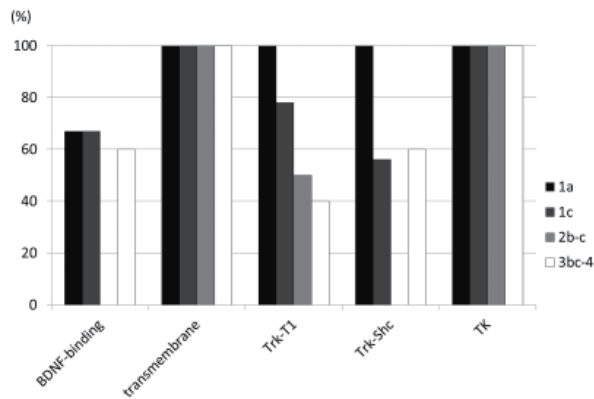


Figure 5. Expression of the TrkB domain by the clinical stage of CCA. CCA samples were categorized in 4 stages (1a: black bar, 1c: dark gray bar, 2b-c: light gray bar and 3bc-4: white bar) ($n = 21$), and the expression ratio (%) of each domain (BDNF-binding site; exon9-12, transmembrane site; exon15, TrkB-T-Shc tail; exon18-19 and TrkB-T1; exon14-16) in the 21 CCA specimens is shown in the histograms. The transmembrane domain and TK tail were expressed in all stages. The expression of the TrkB-T1 tail and TrkB-T-Shc tail (%) decreased with clinical stage progression.

in ovarian cancer cell lines. Similar to the findings in clinical specimens, the CCA cell lines (HUOCA-II, W3UF, and ES-2) lacked the TrkB-T-Shc and TrkB-T1 isoforms. The two serous adenocarcinoma cell lines (HTOA and HUOA) expressed either the TrkB-T-Shc or TrkB-T1 isoform. These results suggest that the cell lines partially maintained the TrkB isoform expression characteristics of the parental tumors (Figure 4B).

To confirm the structure of the TrkB mRNA, its cDNA sequence was analyzed. In 13/23 of tumors (2/5 MAs, 1/5 serous, 6/7 endometrioid, and 4/6 CCA), the sequence was the same as that of normal TrkB (NTrk2-NM006180), with the exception of several single nucleotide polymorphisms, suggesting that large mutations such as a frame shift did not occur at the exon level in these cancer cell lines (data not shown).

4. Discussion

TrkB, which promotes cell survival and EMT, is over-expressed in OA. Using immunohistochemistry, we demonstrated that TrkB protein expression was increased at the invasive edge (Figure 2B). However, as TrkB possesses many isoforms, including dominant negative isoforms, the overall signal level has not been clearly evaluated in association with the progression of OAs. Our results first demonstrated that although TrkB transcripts are observed in all ovarian cancer tissues, the mRNA expression of the truncated TrkB isoforms (TrkB-T-Shc and TrkB-T1) is decreased in CCA. Because these truncated isoforms are suggested to have a dominant-negative effect, their absence may indicate the augmentation of the TrkB TK signal in CCA tumor cells.

As depicted in Figure 1, the structure of the TrkB

gene includes many functional domains. The first five exons of TrkB serve as alternative transcription start sites (11). Exons 5-14 encode the extracellular domain that contains a signaling sequence for membrane localization as well as post-translationally glycosylated cysteine-rich and leucine-rich regions and two immunoglobulin-like (IG-like) domains (18). Exon 12, exon 15, and exons 20-24 encode the binding site for neurotrophins (19), the transmembrane domain, and the intracellular TK domain (20), respectively. While there is a possibility that TrkB could have more than 100 isoforms, only three isoforms, including full-length TrkB, TrkB-T-Shc and TrkB-T1, have been identified as major splice variants in previous studies. The two isoforms are mainly observed in normal neuronal tissues (11) and other tissues (20). The present analysis revealed that a significant number of CCA specimens and some MA specimens or cell lines lacked the truncated splice variants TrkB-T-Shc and TrkB-T1 (Figures 4A and 4B). The intracellular domain of full-length TrkB contains an Shc-binding domain, a TK domain and a PLC- γ -binding domain (2). While these motifs are necessary for the normal signal transduction of TrkB (2), the expression of truncated isoforms may alter the signaling cascade in cancer cells. For example, TrkB-T-Shc and TrkB-T1 suppress the activation of full-length TrkB, and the lack of these truncated isoforms may therefore augment full-length TrkB activity, leading to the suppression of anoikis and TrkB-T1 functions such as regulation of the cytoskeleton or BDNF secretion (21). Because CCA and MA are known to be more malignant than other types of ovarian cancer, loss of the dominant-negative effect of TrkB may promote EMT, which has been correlated with the characteristics of CCA.

We also found an extracellular domain variant lacking the amplification of exons 9-12 in ovarian cancer. Because this region contains the binding site for BDNF, further analysis of whether aberrant splicing of exons 9-12 influences BDNF binding is required. If this splice variant lacking exon 9-12 amplification is a constitutively active molecule that transmits signals independent of BDNF binding, there is a possibility that it could promote CCA. On the other hand, even if the BDNF binding site is intact in the region, irregular TrkB autocrine signals may be induced. These irregular TrkB signals may help to induce EMT-promoting transcription factors such as Twist-1 and Snail-1/2 in TrkB-over-expressed cancer tissues (6).

It has already been reported that BDNF is abundantly expressed in gynecological tissues (4), and we found that BDNF was highly expressed in almost all of the gynecological tissues that we analyzed, including ovarian cancers, benign ovarian tumors, and normal endometrium (data not shown). As BDNF promotes TrkB expression (22), autocrine activation of TrkB in ovarian tissues may support malignant characteristics when BDNF secretion

is augmented in the absence of dominant-negative isoforms. Our results indicate that the expression of irregular TrkB variants may be a potential marker of OA malignancy and a target of CCA treatment. The effects of TrkB isoform expression on EMT in ovarian cancer should be clarified.

Acknowledgements

This study was supported by a 2012-2013 Tokai University School of Medicine Research Grant (to Y.G.), a 2011-2012 Grant-in-Aid for Scientific Research (KAKENHI) (c) (to M.M.), a 2010-2012 Grant-in-Aid for Scientific Research (KAKENHI) (c) (to Y.K.), a 2013-2015 Grant-in-Aid for Scientific Research (KAKENHI) (c) (to Y.K.), a 2013-2014 Grant-in-Aid for Scientific Research (KAKENHI) (c) (to Y.K.), a 2013-2014 Grant-in-Aid for Scientific Research (KAKENHI) (c) (to Y.G.), and the 2012-2016 MEXT-Supported Program for the Strategic Research Foundation at Private Universities. The authors wish to thank X. Tang for providing advice and the Education and Research Support Center of Tokai University School of Medicine, H. Kamiguchi and E. Numao for their excellent technical assistance.

References

- Skaper S. The biology of neurotrophins, signalling pathways, and functional peptide mimetics of neurotrophins and their receptors. *CNS Neurolol Disord Drug Targets*. 2008; 7:46-62.
- Reichardt LF. Neurotrophin-regulated signalling pathways. *Philos Trans R Soc Lond B Biol Sci*. 2006; 361:1545-1564.
- Paredes A, Romero C, Dissen GA, DeChiara TM, Reichardt L, Cornea A, Ojeda SR, Xu B. TrkB receptors are required for follicular growth and oocyte survival in the mammalian ovary. *Dev Biol*. 2004; 267:430-449.
- Kawamura K, Kawamura N, Mulders SM, Sollewijn Gelpke MD, Hsueh AJ. Ovarian brain-derived neurotrophic factor (BDNF) promotes the development of oocytes into preimplantation embryos. *Proc Natl Acad Sci U S A*. 2005; 102:9206-9211.
- Kupferman ME, Jiffar T, El-Naggar A, Yilmaz T, Zhou G, Xie T, Feng L, Wang J, Holsinger FC, Yu D, Myers JN. TrkB induces EMT and has a key role in invasion of head and neck squamous cell carcinoma. *Oncogene*. 2010; 29:2047-2059.
- Smit MA, Geiger TR, Song JY, Gitelman I, Peeper DS. A Twist-Snail axis critical for TrkB-induced epithelial-mesenchymal transition-like transformation, anoikis resistance, and metastasis. *Mol Cell Biol*. 2009; 29:3722-3737.
- Lang K, Entschladen F, Weidt C, Zaenker KS. Tumor immune escape mechanisms: impact of the neuroendocrine system. *Cancer Immunol Immunother*. 2006; 55:749-760.
- Siu MK, Wong OG, Cheung AN. TrkB as a therapeutic target for ovarian cancer. *Expert Opin Ther Targets*. 2009; 13:1169-1178.
- Nakagawara A. Trk receptor tyrosine kinases: a bridge between cancer and neural development. *Cancer Lett*. 2001; 169:107-114.
- Klein R, Conway D, Parada LF, Barbacid M. The trkB tyrosine protein kinase gene codes for a second neurogenic receptor that lacks the catalytic kinase domain. *Cell*. 1990; 61:647-656.
- Stoilov P, Castren E, Stamm S. Analysis of the human TrkB gene genomic organization reveals novel TrkB isoforms, unusual gene length, and splicing mechanism. *Biochem Biophys Res Commun*. 2002; 290:1054-1065.
- Brodeur GM, Minturn JE, Ho R, Simpson AM, Iyer R, Varela CR, Light JE, Kolla V, Evans AE. Trk receptor expression and inhibition in neuroblastomas. *Clin Cancer Res*. 2009; 15:3244-3250.
- Luberg K, Wong J, Weickert CS, Timmusk T. Human TrkB gene: novel alternative transcripts, protein isoforms and expression pattern in the prefrontal cerebral cortex during postnatal development. *J Neurochem*. 2010; 113:952-964.
- Cho KR. Ovarian cancer update: lessons from morphology, molecules, and mice. *Arch Pathol Lab Med*. 2009; 133:1775-1781.
- Heintz AP, Odicino F, Maisonneuve P, Quinn MA, Benedet JL, Creasman WT, Ngan HY, Pecorelli S, Beller U. Carcinoma of the ovary. FIGO 26th Annual Report on the Results of Treatment in Gynecological Cancer. *Int J Gynaecol Obstet*. 2006; 95:S161-192.
- De Craene B, Berx G. Regulatory networks defining EMT during cancer initiation and progression. *Nat Rev Cancer*. 2013; 13:97-110.
- Au CW, Siu MK, Liao X, Wong ES, Ngan HY, Tam KF, Chan DC, Chan QK, Cheung AN. Tyrosine kinase B receptor and BDNF expression in ovarian cancers – Effect on cell migration, angiogenesis and clinical outcome. *Cancer Lett*. 2009; 281:151-161.
- Schneider R, Schweiger M. A novel modular mosaic of cell adhesion motifs in the extracellular domains of the neurogenic trk and trkB tyrosine kinase receptors. *Oncogene*. 1991; 6:1807-1811.
- Urfer R, Tsoulfas P, O'Connell L, Shelton DL, Parada LF, Presta LG. An immunoglobulin-like domain determines the specificity of neurotrophin receptors. *EMBO J*. 1995; 14:2795-2805.
- Middlemas DS, Lindberg RA, Hunter T. TrkB, a neural receptor protein-tyrosine kinase: Evidence for a full-length and two truncated receptors. *Mol Cell Biol*. 1991; 11:143-153.
- Fenner BM. Truncated TrkB: Beyond a dominant negative receptor. *Cytokine Growth Factor Rev*. 2012; 23:15-24.
- Haapasalo A, Sipola I, Larsson K, Akerman KE, Stoilov P, Stamm S, Wong G, Castren E. Regulation of TRKB surface expression by brain-derived neurotrophic factor and truncated TRKB isoforms. *J Biol Chem*. 2002; 277:43160-43167.

(Received January 13, 2014; Revised March 29, 2014; Accepted April 8, 2014)

Expression of ankyrin repeat and SOCS box containing 4 (ASB4) confers migration and invasion properties of hepatocellular carcinoma cells

Victor Au*, Felice H Tsang*, Kwan Man, Sheung Tat Fan, Ronnie TP Poon**, Nikki P Lee**

Department of Surgery, The University of Hong Kong, Hong Kong, China.

Summary

Ankyrin repeat and SOCS box containing 4 (ASB4) involves in physiological process of ubiquitin-mediated proteasomal degradation. Our previous study demonstrated high expression of ASB4 in hepatocellular carcinoma (HCC) cell lines. This study further reveals its clinical implications and tumorigenic properties in HCC. Analysis of 217 HCC gene expression profiles followed by validation in a separate cohort of 50 cases illustrated high ASB4 in HCC. Among the 50 cases, 54% of tumors exhibited more than 2-fold up-regulation of ASB4. Elevated ASB4 associated with low serum level of a HCC serological marker alpha-fetoprotein (AFP), postulating of its use to differentiate AFP-negative HCC. Suppression of ASB4 in PLC and MHCC97-L HCC cells hindered the cell migration and invasion. Reciprocally, enhanced migration rate was measured when ASB4 was ectopically expressed in Hep3B HCC cells. Cross comparison of results derived from *in silico* predictions of seed-matched sequences and by analyzing human HCC databases with matched microRNA and gene expression profiles, microRNA-200 (miR-200) family members including miR-200a and miR-200b were predicted to regulate ASB4 expression in HCC. MiR-200a showed inversed expression level with ASB4 in several of studied HCC cell lines. Dual luciferase reporter assay confirmed the presence of miR-200a binding site on the 3' untranslated region of ASB4. Reduced ASB4 level was noticed under the influence of miR-200a mimic treatment, for which this mimic-induced effect was neutralized with miR-200a inhibitor. In conclusion, this study demonstrates for the first time on the involvement of ASB4 in HCC and that its level is regulated by miR-200a.

Keywords: HCC, ASB4, migration, miR-200a

1. Introduction

Hepatocellular carcinoma (HCC), a major type of primary liver malignancy, ranks fifth as the most frequently diagnosed cancer in men worldwide with more than half a million new cases annually (1). Though with evolving clinical strategies including radioembolization and high-intensity focused ultrasound

to treat this cancer, current management of HCC still rely heavily on tumor resection and liver transplantation (2-4). Prognosis of HCC patients remains suboptimal especially for those patients not amendable to currently available treatments. Unlike other solid tumors with a portion of patients reacting to chemotherapeutic drugs or targeting therapies, HCC is highly resistant in nature and not responding well to most chemotherapeutic agents. Due to the heterogeneity of HCC as revealed by genome-wide studies performed in Asian cohort (5), the use of molecular targeting drug is limited at this stage. For the clinically-approved drug sorafenib, the response rate is low and survival benefit remains modest (6). Not accounting strong drug resistance property of HCC, liver tumors behave similarly as other cancers by undergoing active proliferation, division and differentiation when progress from early to advanced stage. These properties

*These authors contributed equally to this works.

**Address correspondence to:

Dr. Nikki Lee, Department of Surgery, Faculty of Medicine Building, 21 Sassoon Road, Pokfulam, Hong Kong, China.
E-mail: nikkilee@hku.hk

Professor Ronnie TP Poon, Department of Surgery, Queen Mary Hospital, Hong Kong, China.
E-mail: poontp@hku.hk

can somehow be found during normal development in the process of embryogenesis. By knowing their presence in embryonic livers and HCC, a group of oncofetal molecules have been studied. Some of them like SALL4, glypican-3, and eIF5A2 have potential use for cancer diagnosis and treatment (7-9). Ankyrin repeat and SOCS box containing 4 (ASB4) is one such molecule previously identified by our team to have expression in fetal livers and cultured HCC cells (10).

ASB4 belongs to the ASB family, for which most of its members possess two structural domains, the ankyrin repeat and the SOCS box. The presence of these domains enables ASB proteins to act as an adaptor linking other subunits of the E3 ubiquitin ligase complex, and at the same time facilitates the binding of target protein for ubiquitination and subsequent proteasomal degradation (11-13). Aside its involvement in ubiquitous protein degradation, ASB4 also involves in vascular system. During endothelial development, factor inhibiting hypoxia-inducible factor 1 (FIH) can hydroxylate ASB4 under oxygen tension, thereby promoting angiogenesis (14). A later study has then revealed the interaction of ASB4 and nuclear factor- κ B (NF- κ B) in endothelial cells (15). Other than these roles, ASB4 functions in nervous system by up-regulating the expression of proopiomelanocortin (POMC) gene in neurons in mice (16). Despite all these studies on ASB4 in normal physiology, no investigation has been performed so far to uncover the role of ASB4 in cancers. In continuation of our previous proteomic study demonstrating the link between ASB4 and liver cancer (10), this study further examines the expression and tumorigenic properties of ASB4 in HCC. Lastly, the level of ASB4 is revealed subjected to microRNA (miRNA)-based regulation.

2. Materials and Methods

2.1. Cell culture

A panel of human liver cell lines composing of immortalized normal hepatocytes MIHA and HCC cells, PLC/PRF/5 (PLC), HepG2, Hep3B, MHCC97-H (97H), MHCC97-L (97L), H2M, H2P, and Huh7, were used and cultured in Dulbecco's Modified Eagle Medium (Life Technologies, Grand Island, NY, USA) with 10% fetal bovine serum (FBS) (Life Technologies) and 1% penicillin and streptomycin (Life Technologies) (17).

2.2. Clinical specimens

Fifty pairs of HCC and adjacent non-tumor liver tissues were obtained from patients underwent hepatic resection or liver transplantation in Queen Mary Hospital, Hong Kong from September 2001 to June 2005. Non-tumor liver tissues were obtained at least 1 cm from the tumor margin. Tumors were classified according to the new AJCC staging system. The use of clinical specimens for

research was approved by the Institutional Review Board of our institute. Informed consents were obtained from patients for the use of specimens for research.

2.3. Real-time quantitative polymerase chain reaction (qPCR)

TRIzol reagent (Life Technologies) was used to extract total RNA from cultured cells and clinical specimens. Reverse transcription and qPCR were then performed as described (17). Platinum SYBR Green qPCR SuperMix-UDG with ROX (Life Technologies) and ASB4-specific primers (forward: 5'-GCC TGC CAT TCT TGT CCT AA-3'; reverse: 5'-TGC ATG AGA GTC CTT GGA GA-3') was used for qPCR under the following condition: 50°C for 2 min for 1 cycle; 95°C for 10 min for 1 cycle; 95°C for 15 sec and 60°C for 1 min for 40 cycles. Expression level of ASB4 was normalized with the expression of ribosomal RNA 18S (for clinical specimens) or β -actin (for cultured cells). For obtaining the relative expression level of putative miRNAs against ASB4, qPCR was performed using each miRNA-specific primers (Qiagen, Hilden, Germany) for miR-200a, miR-200b, miR-383, miR-498, and miR-875 under the condition as stated in the manual: 95°C for 15 min for 1 cycle; 94°C for 15 sec, 55°C for 30 sec, and 70°C for 30 sec for 40 cycles.

2.4. Ectopic expression and suppression of ASB4 in HCC cells

Ectopic expression of ASB4 was achieved by transfecting ASB4-deficient Hep3B cells using Lipofectamine 2000 (Life Technologies) and human ASB4-expressing pcDNA3.1 vector (Life Technologies). Stable cell clones with suppressed expression of ASB4 were established in ASB4-expressing PLC and 97L cells by transfecting with Lipofectamine 2000 and pGFP-V-RS vector (OriGene Technologies, Rockville, MD, USA) harboring short hairpin RNA (shRNA). By screening with three shRNAs against exon 1 (GI326178/shRNA#1) or 2 (GI326179/shRNA#2 and GI326180/shRNA#3) of human ASB4, two shRNAs with the highest knockdown efficiency in each cell line were used for PLC and 97L cells.

2.5. Cell proliferation assay

Cultured HCC cells with manipulated expression of ASB4 were seeded on 96-well plates at 1,500 cells in each well. For each day after cell seeding for five days, 10 μ L of MTT reagent was added to each well. The plate was then incubated at 37°C for 1.5 h before addition of 100 μ L DMSO after removal of medium. Plates were then read to assess the cell proliferation rate of each group as before (9,18).

2.6. Wound healing assay

Cultured HCC cells with overexpression and knockdown of ASB4 were seeded on 6-well plates until cells reached about 90% confluency. A scratch was then created in each assayed well as described (9,19). Extent of cell migration towards the created wound was followed on every 12 h till 36 h.

2.7. Cell invasion assay

HCC cells (8×10^4) with suppression of ASB4 were seeded in each BD BioCoat Matrigel Invasion Chamber (BD Biosciences, Bedford, MA, USA). To allow cell invasion through the chamber membrane, assayed cells resuspended in 0.5% FBS were placed within the chamber while medium with 2% FBS was added to the outer tank. After incubation for 48 h, 0.4% paraformaldehyde was used to fix the cells for 20 min before cells were stained with 1% crystal violet as before (17).

2.8. Prediction of miRNA targeting ASB4

Based on seed-matched sequence, miRWalk (<http://www.umm.uni-heidelberg.de/apps/zmf/mirwalk/>) (20) was used to predict potential miRNA with binding site on the 3'-untranslated region (3'UTR) of ASB4 and a sum score was used to rank each miRNA. In parallel, we also pulled out miRNA with expression negatively correlated with those of ASB4 based on our published miRNA expression array database of 97 HCC cases (21).

2.9. Luciferase reporter assay to examine the binding of miR-200a to 3'UTR of ASB4

3'UTR of ASB4 was obtained from 97L cells using primer sequences flanking the region of interest (forward: 5'-GCC TTA TGA GAC AGC AGT TCC CAA T-3' and reverse: 5'-GAA AGG AGA CAG AAG AGC TTT ATT T-3') before cloning into pMIR-REPORT Luciferase vector (Life Technologies), while pRL-TK vector (Promega, Madison, WI, USA) was used as background control. In addition to transfecting with these two vectors, H2M HCC cells were co-transfected with miR-200a mimic (Qiagen) and/or miR-200a inhibitor (Qiagen). Lipofectamine 2000 was used as transfecting agent. After 48 h, cells were harvested and suspended in Reporter Lysis Buffer (Promega) and subjected to dual luciferase reporter assay as before (18,19).

2.10. Assessment of ASB4 expression upon ectopic expression of miR-200a

Cellular miR-200a level was induced by transfecting 97L HCC cells using miR-200a mimic using Lipofectamine 2000. To support for the specificity of this experiment, exogenously induced miR-200a level was neutralized using miR-200a inhibitor as above in parallel

experiments. The resultant effect of miR-200a mimic and inhibitor on ASB4 expression was assessed using qPCR as above.

2.11. Statistical analyses

Statistical analyses were performed using SPSS version 16 (SPSS Inc., Chicago, IL, USA) as described (9). Independent *t*-test was used to compare between experimental groups. Paired *t*-test was performed for comparing expression between tumors and adjacent non-tumor tissues. Clinicopathological features including HBsAg status, serum alpha-fetoprotein (AFP) level, presence of venous infiltration, tumor size, tumor differentiation and tumor stage were analyzed using Pearson's chi-squared test. A *p*-value < 0.05 was considered as statistical significance.

3. Results

3.1. High expression of ASB4 in HCC tumors and its correlation with low serum AFP level

Involvement of ASB4 in HCC was revealed by analyzing its expression in HCC clinical specimens. Retrospective analysis of published gene expression array database (22-24) associated high expression of ASB4 with tumor tissues when compared to the non-tumor tissues in 217 HCC cases ($p = 0.0013$) (Figure 1A, upper panel). Validation of the gene expression array data was achieved by detecting the level of ASB4 in a separate cohort of 50 cases using qPCR. A significant up-regulation of ASB4 was observed in HCC tumors when compared to their adjacent non-tumor counterparts ($p = 0.011$) (Figure 1A, lower panel). Among these 50 pairs of tissues, 27 cases with tumors having more than 2-fold induction in ASB4 expression, accounting for 54% of total studied cases. Clinical correlation was undertaken for these two cohorts of subjects separately. For each cohort, patients were further segregated into two groups based on expression of ASB4 in tumors, high expression of ASB4 denoted the top 20% of cases with highest expression. ASB4 expression did not correlate well with most of the studied clinical parameters including HBsAg status, tumor size, presence of venous infiltration, tumor differentiation and tumor stage. Unexpectedly, ASB4 expression was markedly correlated with serum AFP level both in the gene expression array cohort (Table 1a) and qPCR validation cohort (Table 1b), such that high expression of ASB4 linked to low serum AFP level condition.

3.2. Role of ASB4 in conferring migration and invasion properties of HCC cells

To provide further evidence to support the tumorigenic properties of ASB4 in HCC, next we examined the phenotypic effects of HCC cells when ASB4 level was

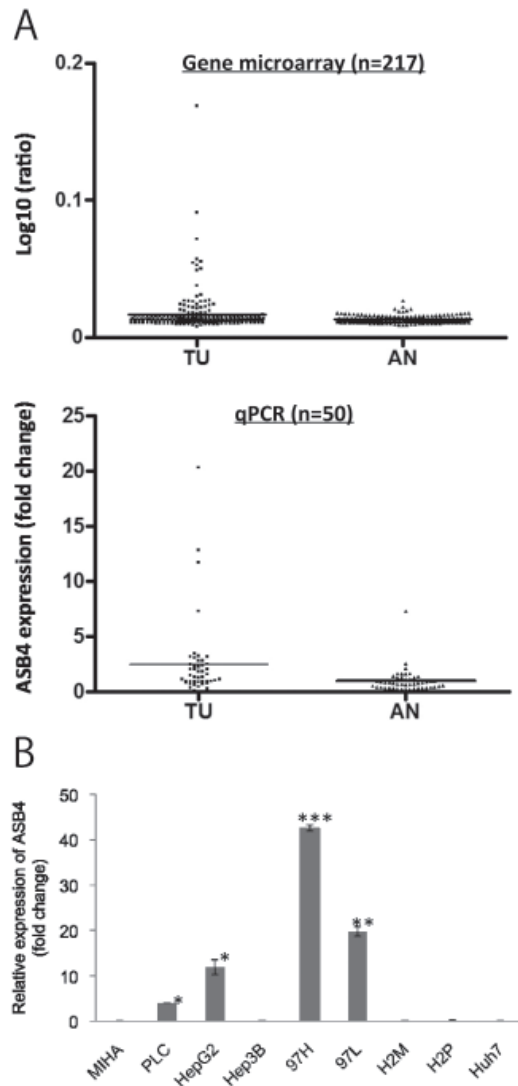


Figure 1. High expression of ASB4 in HCC tumors and cultured cell lines. (A) Gene expression array of 217 HCC cases was re-analyzed for the expression of ASB4 in tumors and adjacent non-tumor tissues. Validation was further performed in a separate cohort of 50 cases using qPCR. Both assays show significant up-regulation of ASB4 in tumors when compared to the non-tumor tissues. For gene expression array, log₁₀ (ratio) of ASB4 in each sample was obtained by subtracting with the mean log₁₀ (intensity) of ASB4 across all non-tumor tissues ($p = 0.0013$). For qPCR, the expression of ASB4 was obtained by normalization with ribosomal RNA 18S. The fold change was then determined by normalizing with the average value of non-tumor tissues ($p = 0.011$). (B) Differential expression of ASB4 was observed in our human cell line panel using qPCR. Among the eight HCC cell lines, four cell lines, PLC, HepG2, 97H and 97L, were found to have high expression of ASB4. The expression levels were normalized to average of the cell line panel. Representative set among 4 sets of experiments is shown. *, $p < 0.05$; **, $p < 0.01$; ***, $p < 0.001$. AN, adjacent non-tumor tissues; TU, tumor.

manipulated. For this purpose, ASB4 was suppressed in two HCC cells having high expression of ASB4, PLC and 97L (Figure 1B), by treating them with shRNA to generate stable clones with suppressed level of ASB4. When assessed using qPCR, individual shRNA exerted different degrees of ASB4-suppressing efficiencies in different cell lines, such that shRNA#2 led to the most

Table 1a. Clinical correlation of ASB4 in 217 HCC cases*

Clinicopathological features	Patient number	ASB4 expression		p-value
		Low	High	
HBsAg				0.142
Negative	30	21	9	
Positive	187	153	34	
Serum AFP level (ng/mL)				0.003
< 50 ng/mL	97	69	28	
≥ 50 ng/mL	120	105	15	
Serum AFP level (ng/mL)				0.011
< 100 ng/mL	108	79	29	
≥ 100 ng/mL	109	95	14	
Tumor size (cm)				0.466
< 5 cm	66	51	15	
≥ 5 cm	151	123	28	
Venous infiltration				0.865
Absent	107	85	22	
Present	110	89	21	
Tumor differentiation ^{a,b}				0.53
Well	37	26	11	
Moderately	114	92	22	
Poorly	38	31	7	
Undifferentiated	2	2	0	
Tumor stage ^c				0.893
Stage I	92	72	20	
Stage II	64	51	13	
Stage IIIA	45	37	8	
Stage IIIB	14	12	2	
Stage IV	2	2	0	

*, Analysis of gene expression array database; ^a, Calculation was performed based on available data; ^b, Determined based on Edmonson grading; ^c, Tumor was staged using new AJCC system.

Table 1b. Clinical correlation of ASB4 in 50 HCC cases*

Clinicopathological features	Patient number	ASB4 expression		p-value
		Low	High	
HBsAg ^a				0.8
Negative	7	6	1	
Positive	42	33	9	
Serum AFP level (ng/mL)				0.011
< 50 ng/mL	21	13	8	
≥ 50 ng/mL	29	27	2	
Serum AFP level (ng/mL)				0.035
< 100 ng/mL	24	16	8	
≥ 100 ng/mL	26	24	2	
Tumor size (cm)				0.258
< 5 cm	13	12	1	
≥ 5 cm	37	28	9	
Venous infiltration				0.707
Absent	16	12	4	
Present	34	28	6	
Tumor differentiation ^{a,b}				0.177
Well	6	3	3	
Moderately	28	22	6	
Poorly	9	8	1	
Undifferentiated	0	0	0	
Tumor stage ^c				0.189
Stage I	9	7	2	
Stage II	16	15	1	
Stage IIIA	12	10	2	
Stage IIIB	13	8	5	
Stage IV	0	0	0	

*, Based on qPCR data generated in this study; ^a, Analyses were performed based on available data; ^b, Tumor differentiation was determined based on Edmonson grading; ^c, Tumor was staged using new AJCC system.

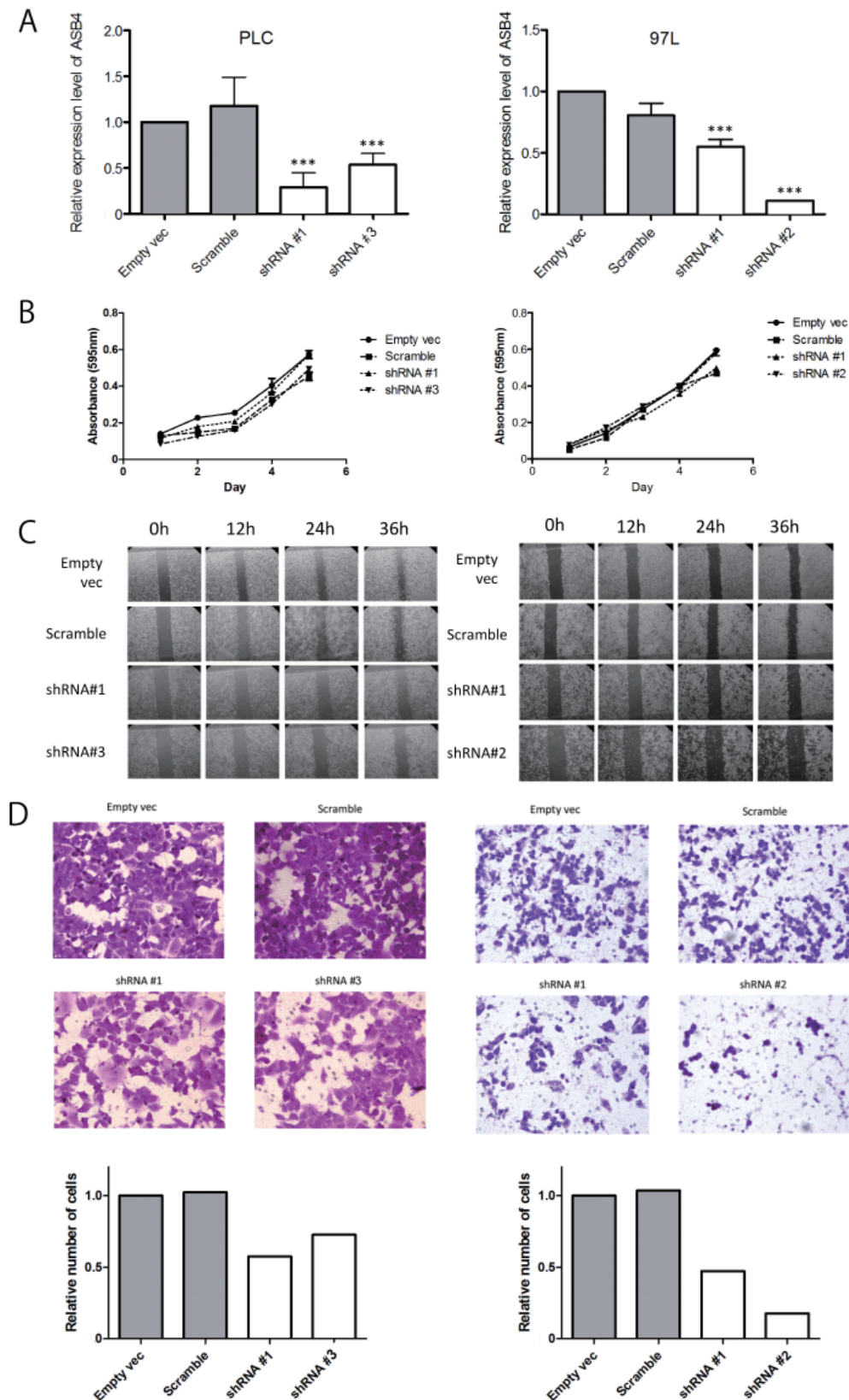


Figure 2. Suppression of ASB4 inhibits migration and invasion of PLC and 97L cells. (A) PLC and 97L cells were transfected with ASB4-targeting shRNAs to develop stable cell clones with suppression of ASB4. In parallel, cells were transfected with scrambled shRNA (Scramble) and empty vector (Empty vec) as negative controls. Expression of ASB4 in Scramble and shRNA was normalized against the expression in Empty vec. (B) Using MTT assay, no significant difference in proliferation rate was observed when ASB4 was suppressed in PLC and 97L cells. (C) After suppression of ASB4, shRNA clones adopted slower migration rate towards the artificially created wounds when compared to Empty vec and Scramble cells. Photos of the same positions of each were taken at three time points (12 h, 24 h and 36 h) after scratching on the cell monolayer. (D). 48 h after seeding cells on the inner chamber, invaded cells from each experiment group were stained and counted. Less number of invaded cells was recorded for shRNA clones when compared to Empty vec and Scramble groups. Original magnification, 200 \times . The number of invaded cells in each group was counted and normalized to Empty vec in the bar chart. ***, $p < 0.001$.

prominent suppression of ASB4 in 97L rather than others (Figure 2A). Using MTT assay, we failed to observe any significant deviation in proliferation rates of ASB4-suppressed PLC and 97L cells when compared to their parallel controls transfected with empty vector or scrambled shRNA (Figure 2B). Intriguingly, suppressing ASB4 in PLC and 97L cells retarded the migration of these cells towards artificially created wounds in confluent cell monolayers. ASB4 seems to determine the migration ability of HCC cells, as shRNA#2-transfected cells with most significant knockdown in ASB4 level were incapable to close the wound even after 36 hours of incubation (Figure 2C). Besides cell migration, ASB4 is also responsible for regulating the invasive properties of HCC cells. For those PLC and 97L cells with suppressed level of ASB4, fewer number of cells successfully invaded through the Matrigel-coated membrane of the invasion chamber. Such drop in numbers also corresponded to the extent of ASB4 suppression. Similar to the observation of wound-healing assay, transfection of shRNA#2 into 97L cells resulted in the least number of cells with penetrative properties (Figure 2D).

Using opposite approach against the knockdown experiment, ectopic expression of ASB4 was performed in ASB4-deficient Hep3B cells by transient transfection of ASB4-expressing vector (Figure 3A). As in Figure 2B, MTT assay was unable to detect significant changes in the proliferation of ASB4-expressing Hep3B cells in comparison to those cells transfected with empty vector (Figure 3B). Migration rate of Hep3B cells enhanced dramatically after transfection of ASB4-expressing vector, as the artificially created wound was nearly closed after 36 hours (Figure 3C). Based on this set of knockdown and overexpression experiment, it is conclusive to know for the role of ASB4 in conferring migration and invasion properties of HCC cells, despite the involvement of ASB4 in cell proliferation is rather limited.

3.3. Regulation of ASB4 by miR-200a

MiRNA belongs to a class of small molecule capable of regulating dozens of cancer-related molecules *via* its binding to the 3'UTR of target molecules (25,26). Based on the above findings pointing to the role of ASB4 in HCC, we hypothesize ASB4 might also be subjected to this kind of post-translational regulation. To prove for this notion, potential miRNAs binding to the 3'UTR of ASB4 were predicted bioinformatically. Table 2 shows 11 miRNAs carrying seed-matched sequences for 3'UTR of ASB4. Taking advantage of our miRNA database of 97 HCC cases with matched gene expression profile (21-24) and by performing correlation analysis using ASB4 expression level, 3 miRNAs negatively correlated with ASB4 expression were identified on top of the list (Table 3). Cross comparison of miRNAs in Table 2 and 3 pointed to miR-200 family members (miR-200a and

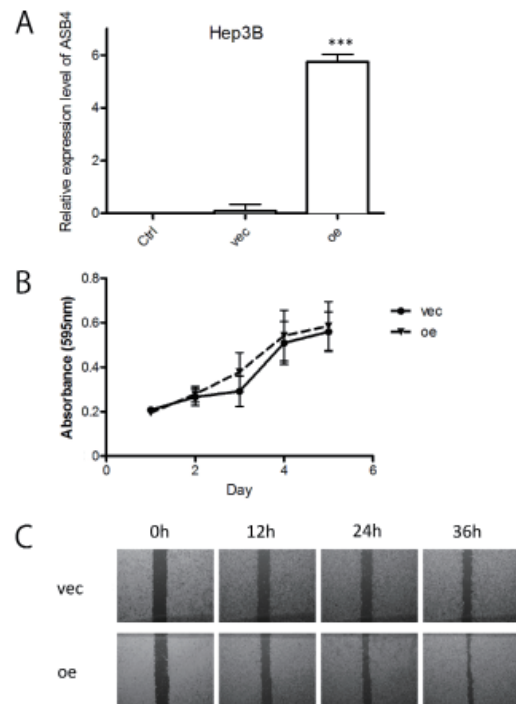


Figure 3. Overexpression of ASB4 promotes migration of Hep3B cells. (A) Transient transfection of ASB4 was performed in Hep3B cells. By means of qPCR, a significant induction in the level of ASB4 was observed in ASB4-overexpressing cells (oe) when compared to no treatment control (Ctrl) and cells transfected using empty vector (vec). ASB4 expression in oe and vec was normalized to Ctrl. (B) No significant difference in cell proliferation was observed between oe and vec group with or without overexpression of ASB4 when assessed using MTT assay. (C) Wound-healing assay was performed using vec and oe cells, in which overexpression of ASB4 enhanced the migration of cells towards the artificially created wound. Photos of the same positions of each were taken 12 h, 24 h and 36 h after scratching of the cell monolayer. ***, $p < 0.001$.

miR-200b) as potential miRNAs regulating ASB4 in HCC. These two miRNAs together with those miRNAs (miR-383, miR-498, and miR-875) absent from our miRNA expression database (21) were subjected to qPCR to detect their relative expressions in our cell line panel as in Figure 1B (Figure 4A). Amongst these five miRNAs, miR-200a, miR-200b, and miR-383 displayed a general, yet not perfect, trend for its expression negatively correlated to ASB4 level in this cell line panel. Of note, some cell lines having negligible levels of both studied miRNA and ASB4 were not taken into account for consideration. Applying these selection criteria has then put our focus on miR-200a for validation study.

In understanding whether miR-200a could interact with 3'-UTR of ASB4, H2M cells lacking both miR-200a and ASB4 were transfected with vector harboring 3'UTR of ASB4. Co-transfection with miR-200a mimic reduced the luciferase activity. This reduction was further enhanced when a higher amount of miR-200a mimic was used. On the contrary, the reduction in luciferase activity was rescued when miR-200a inhibitor was co-transfected with mimic (Figure 4B). This data has demonstrated exogenous addition of miR-200a can bind specifically to

Table 2. miRNAs with potential binding sites on 3'UTR of ASB4

MicroRNA	StemLoop ID	DIANAmT	miRanda	miRDB	miRWalk	RNAhybrid	PICTAR4	PICTAR5	PITA	RNA22	Targetscan	SUM
hsa-miR-498	hsa-mir-498	1	1	0	1	0	0	1	1	1	1	7
hsa-miR-143	hsa-mir-143	1	1	0	1	0	0	1	1	1	1	7
hsa-miR-200a	hsa-mir-200a	1	1	0	1	0	0	1	0	1	1	6
hsa-miR-875-3p	hsa-mir-875	1	1	1	1	0	0	1	0	0	1	6
hsa-miR-148b	hsa-mir-148b	1	1	0	1	0	0	1	0	1	1	6
hsa-miR-648	hsa-mir-648	1	1	1	1	0	0	1	0	0	1	6
hsa-let-7f	hsa-let-7f-2	1	1	0	1	0	0	1	0	1	1	6
hsa-miR-218	hsa-mir-218-2	1	1	0	1	0	0	1	0	1	1	6
hsa-let-7a	hsa-let-7a-3	1	1	0	1	0	0	1	0	1	1	6
hsa-miR-331-5p	hsa-mir-331	1	1	1	1	0	0	1	0	0	1	6
hsa-miR-383	hsa-mir-383	1	1	0	1	0	0	1	0	1	1	6

Table 3. miRNAs with expression negatively correlated with those of ASB4 in 97 HCC cases

miRNA	Spearman R	p-value (R)	ASB4 (T)	ASB4 (NT)	ASB4 (NT/T)	p-value (T versus NT)
HSA-MIR-138	-0.314	0.002	0.022638	0.039637	1.750929	0.000676
HSA-MIR-200B	-0.334	0.001	0.990351	1.505138	1.519802	0.027175
HSA-MIR-375	-0.242	0.020	1.063168	1.653897	1.555631	0.023164

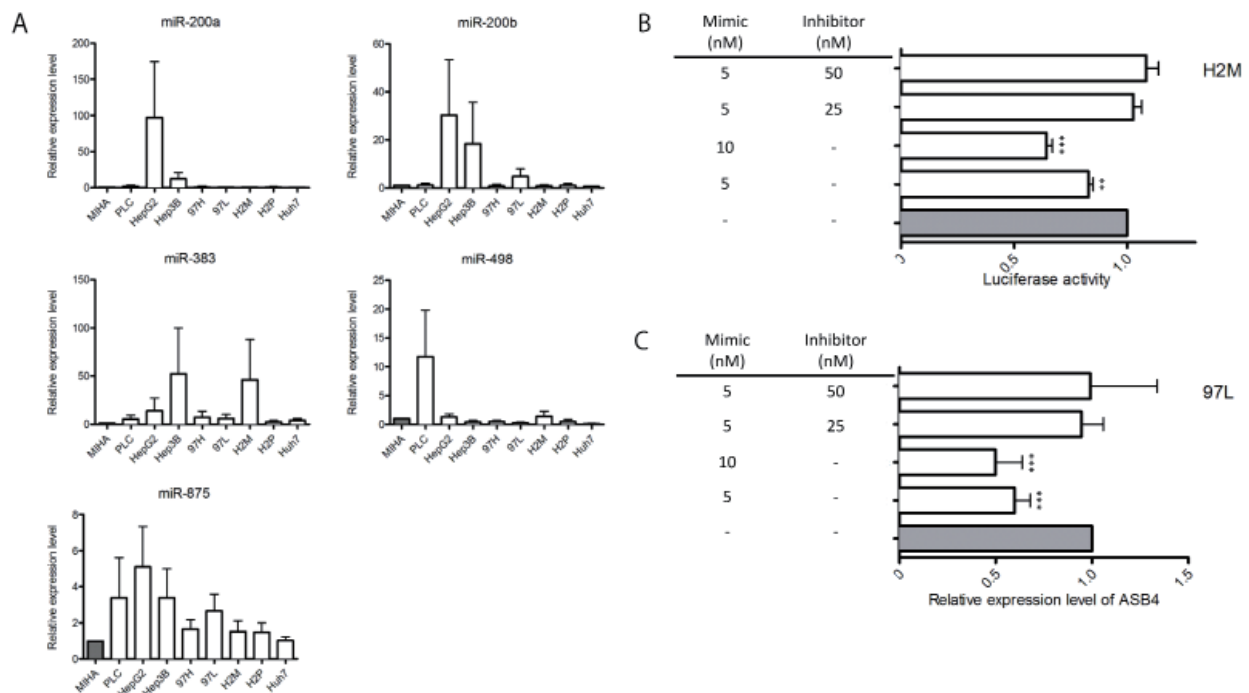


Figure 4. MiR-200a binds and suppresses the level of ASB4. (A) Five miRNAs chosen based on the selection criteria mentioned in the result section were subjected to qPCR to determine their expression in our panel of liver cell line. Differential expression of each miRNA was observed. For each cell line, expression of each miRNA in HCC cells was normalized against immortalized normal hepatocyte MIHA. **(B)** Luciferase reporter assay was performed to investigate whether miR-200a would bind to 3'UTR of ASB4 in H2M cells lacking both of these molecules. Transfection of H2M cells with miR-200a mimic and 3'UTR of ASB4 reduced luciferase activity in a dose-dependent manner, while addition of miR-200a inhibitor restored the drop in activities. Luciferase activity of each treatment was normalized to control cells transfected with 3'UTR of ASB4. **(C)** After transfecting ASB4-expressing 97L cells with miR-200a mimic, ASB4 suppression was measured. The specificity of this reaction was confirmed when this ASB4-suppressing effect was neutralized with the addition of miR-200a inhibitor. The relative expression of each treatment group was normalized to control cells without any treatment. **, $p < 0.01$; ***, $p < 0.001$.

3'UTR of ASB4.

Following the luciferase reporter assay, plan has been devoted to examine whether miR-200a mimic can reduce the endogenous level of ASB4. For this, 97L cells were used due to its absence of miR-200a and its expression of ASB4. By means of qPCR, dose-dependent reduction in ASB4 level was observed in

97L cells after transfection with miR-200a mimic. The specificity of this reaction was confirmed as co-transfecting cells with both miR-200a mimic and inhibitor ruled out the ASB4-reducing effects of miR-200a (Figure 4C). Together with the luciferase reporter assay result, miR-200a can bind to 3'UTR of ASB4 and reduce its level.

4. Discussion

Involvement of ASB4 in HCC was first hinted in our previous proteomic study of developing mouse livers (10). Expression of ASB4 was detected in fetal mouse livers, but was absent in adult mouse livers. In the same study, ASB4 was found to have negligible expression in an immortalized normal hepatocyte line MIHA and differential expression was noticed in several HCC cell lines. The high expression of ASB4 in metastatic 97L and 97H cell lines has prompted us to include more cell lines in this study, among the three additional cell lines one of them H2M is a metastatic line. Although we would expect H2M cells also possess high level of ASB4, no measurable level of ASB4 was detected in this pair of cell line (primary H2P and metastatic H2M). Only PLC cells had detectable level of ASB4. The differential expression of ASB4 in our cell line panel has implicated that a subset of HCCs requires specifically the function of this molecule to maintain its tumor properties. To follow on this statement, ASB4 level was measured in clinical specimens of HCC. Our earlier investigation failed to detect ASB4 under the stated experimental condition (10), for which this problem was remedied by using another set of qPCR primer in this study. The primer used in our previous setting can detect both variants 1 and 2 of ASB4, while the current primer can only recognize variant 1. 54% of patients are found to have ASB4-overexpressing tumors. However, high expression of ASB4 does not correlate with most of the examined clinicopathological parameters including presence of venous infiltration and tumor stages. Despite that, high expression of ASB4 was found associating with low serum level of AFP. Elevated AFP level has been used as a serological marker for HCC detection and used in most clinical centers, together with ultrasound, around the world for routine surveillance of HCC (27,28). Nevertheless, using AFP as a marker for HCC fails to cover all HCC cases because around 20-50% of cases have comparable AFP level as healthy individuals (29-31). Continuing efforts have identified supplemental markers for AFP in detecting AFP-negative subjects. Prominent molecule like dickkopf-1 is proven to supersede or complement AFP for this purpose (32). Apart diagnosis, AFP also has clinical value in classifying poor prognostic cases such as those with large tumor size and with portal vein thrombus (29,30). Its level negatively correlated with those of AFP, ASB4 might be another attractive candidate for HCC prognostication.

Embryogenesis and tumorigenesis are distinct cellular processes. Yet, they share certain common pathways and possess a pool of oncofetal molecules. The first and most well-known example of liver oncofetal molecule is AFP (33). Its clinical applicability in HCC surveillance is well recognized (34). Despite that, measurement of serum AFP suffers from its own limitation in sensitivity

and specificity. To improve this clinical situation, other oncofetal molecules soluble in circulation like glypican-3 and GP73 have been tested for their potential use, or in combination with serum AFP, in detecting HCC (35-37). Adding value to the clinical usefulness of oncofetal molecules, some of them have also been examined for their therapeutic potentials. Representative candidates include cadherin-17 and survivin, for which suppression of their levels is known as a way to counteract liver tumorigenesis in both *in vitro* and *in vivo* experimental settings (17,38). In this study, an alleviation of migration and invasion in HCC cells was clearly shown upon ASB4 suppression, providing a solid evidence for the involvement of ASB4 in the presentation of these tumor phenotypes. Interestingly, we did not observe any variation in proliferation of HCC cells after ASB4 suppression. This undoubtedly supports for the selective involvement of ASB4 in cell migration and invasion.

ASB4 is shown to express in a subset of HCC based on the qPCR data derived from cultured cells and clinical specimens. Next, we might want to understand what factor leads to its upregulation in ASB4-expressing HCC. MiRNAs execute their biological functions *via* binding on the 3'UTR of target molecules, thereby interfering target gene expressions under normal and diseased conditions (39). A growing number of reports have further complicated the current network of miRNA in HCC (40,41). MiRNAs participate in tumorigenesis by modulating the balance between oncogene and tumor suppressor gene (42,43). Attempt has been made to investigate whether ASB4, an oncofetal molecule, is subjected to miRNA-based regulation. Results derived from this study have confirmed the ASB4-inhibiting effect of miR-200a. Indeed, down-regulation of miR-200a is observed in HCC and that suppression of miR-200a promotes tumor phenotypes of HCC cells (44). Notably, overexpression of miR-200a in HCC cells did not alter cell proliferation, but is able to decrease cell migration by increasing E-cadherin (45). These earlier studies are in support for our observations showing exogenous addition of miR-200a reduces ASB4 level. We have also indicated that suppression of ASB4 alleviates migration and invasion, but not proliferation, of HCC cells, for which this result highly resembles to those exhibited by overexpressing miR-200a. This is the first study that deciphers miRNA-based regulatory mechanism of ASB4. Apart from this mode of regulation, there is only one study so far describing ASB4 as a downstream molecule of NF- κ B and TNF- α signaling pathway in endothelial cells (15). In conclusion, the current study confirms the tumorigenic properties of ASB4 and introduces a novel regulatory mechanism for this molecule in HCC.

Acknowledgements

This work was supported in part by Seed Funding

Programme for Basic Research by The University of Hong Kong, Hong Kong.

References

- Jemal A, Bray F, Center MM, Ferlay J, Ward E, Forman D. Global cancer statistics. *CA Cancer J Clin.* 2011; 61:69-90.
- Wong TC, Poon RT. Hepatobiliary malignancies: lessons from Asia. *Dig Dis.* 2013; 31:130-137.
- Lau WY, Sangro B, Chen PJ, Cheng SQ, Chow P, Lee RC, Leung T, Han KH, Poon RT. Treatment for hepatocellular carcinoma with portal vein tumor thrombosis: the emerging role for radioembolization using yttrium-90. *Oncology.* 2013; 84:311-318.
- Chan AC, Cheung TT, Fan ST, Chok KS, Chan SC, Poon RT, Lo CM. Survival analysis of high-intensity focused ultrasound therapy versus radiofrequency ablation in the treatment of recurrent hepatocellular carcinoma. *Ann Surg.* 2013; 257:686-692.
- Kan Z, Zheng H, Liu X, *et al.* Whole genome sequencing identifies recurrent mutations in hepatocellular carcinoma. *Genome Res.* 2013; 23:1422-1433.
- Thomas M. Molecular targeted therapy for hepatocellular carcinoma. *J Gastroenterol.* 2009; 44 (Suppl 19):136-141.
- Yong KJ, Gao C, Lim JS, *et al.* Oncofetal gene SALL4 in aggressive hepatocellular carcinoma. *N Engl J Med.* 2013; 368:2266-2276.
- Yao M, Yao DF, Bian YZ, Zhang CG, Qiu LW, Wu W, Sai WL, Yang JL, Zhang HJ. Oncofetal antigen glypican-3 as a promising early diagnostic marker for hepatocellular carcinoma. *Hepatobiliary Pancreat Dis Int.* 2011; 10:289-294.
- Lee NP, Tsang FH, Shek FH, Mao M, Dai H, Zhang C, Dong S, Guan XY, Poon RT, Luk JM. Prognostic significance and therapeutic potential of eukaryotic translation initiation factor 5A (eIF5A) in hepatocellular carcinoma. *Int J Cancer.* 2010; 127:968-976.
- Lee NP, Leung KW, Cheung N, Lam BY, Xu MZ, Sham PC, Lau GK, Poon RT, Fan ST, Luk JM. Comparative proteomic analysis of mouse livers from embryo to adult reveals an association with progression of hepatocellular carcinoma. *Proteomics.* 2008; 8:2136-2149.
- Kile BT, Schulman BA, Alexander WS, Nicola NA, Martin HM, Hilton DJ. The SOCS box: A tale of destruction and degradation. *Trends Biochem Sci.* 2002; 27:235-241.
- Kohroki J, Nishiyama T, Nakamura T, Masuho Y. ASB proteins interact with Cullin5 and Rbx2 to form E3 ubiquitin ligase complexes. *FEBS Lett.* 2005; 579:6796-6802.
- Linossi EM, Nicholson SE. The SOCS box-adapting proteins for ubiquitination and proteasomal degradation. *IUBMB Life.* 2012; 64:316-323.
- Ferguson JE, 3rd, Wu Y, Smith K, Charles P, Powers K, Wang H, Patterson C. ASB4 is a hydroxylation substrate of FIH and promotes vascular differentiation *via* an oxygen-dependent mechanism. *Mol Cell Biol.* 2007; 27:6407-6419.
- Bode M, Wu Y, Pi X, Lockyer P, Dechyapirom W, Portbury AL, Patterson C. Regulation of ankyrin repeat and suppressor of cytokine signalling box protein 4 expression in the immortalized murine endothelial cell lines MS1 and SVR: a role for tumour necrosis factor alpha and oxygen. *Cell Biochem Funct.* 2011; 29:334-341.
- Li JY, Chai BX, Zhang W, Wang H, Mulholland MW. Expression of ankyrin repeat and suppressor of cytokine signaling box protein 4 (Asb-4) in proopiomelanocortin neurons of the arcuate nucleus of mice produces a hyperphagic, lean phenotype. *Endocrinology.* 2010; 151:134-142.
- Liu LX, Lee NP, Chan VW, *et al.* Targeting cadherin-17 inactivates Wnt signaling and inhibits tumor growth in liver carcinoma. *Hepatology.* 2009; 50:1453-1463.
- Zhu R, Wong KF, Lee NP, Lee KF, Luk JM. HNF1 α and CDX2 transcriptional factors bind to cadherin-17 (CDH17) gene promoter and modulate its expression in hepatocellular carcinoma. *J Cell Biochem.* 2010; 111:618-626.
- Fatima S, Lee NP, Tsang FH, Kolligs FT, Ng IO, Poon RT, Fan ST, Luk JM. Dickkopf 4 (DKK4) acts on Wnt/ β -catenin pathway *via* influencing β -catenin in hepatocellular carcinoma. *Oncogene.* 2012; 31:4233-4244.
- Dweep H, Sticht C, Pandey P, Gretz N. miRWalk--database: prediction of possible miRNA binding sites by "walking" the genes of three genomes. *J Biomed Inform.* 2011; 44:839-847.
- Luk JM, Burchard J, Zhang C, *et al.* DLK1-DIO3 genomic imprinted microRNA cluster at 14q32.2 defines a stemlike subtype of hepatocellular carcinoma associated with poor survival. *J Biol Chem.* 2011; 286:30706-30713.
- Lamb JR, Zhang C, Xie T, *et al.* Predictive genes in adjacent normal tissue are preferentially altered by sCNV during tumorigenesis in liver cancer and may rate limiting. *PLoS One.* 2011; 6:e20090.
- Ivanovska I, Zhang C, Liu AM, *et al.* Gene signatures derived from a c-MET-driven liver cancer mouse model predict survival of patients with hepatocellular carcinoma. *PLoS One.* 2011; 6:e24582.
- Hao K, Luk JM, Lee NP, Mao M, Zhang C, Ferguson MD, Lamb J, Dai H, Ng IO, Sham PC, Poon RT. Predicting prognosis in hepatocellular carcinoma after curative surgery with common clinicopathologic parameters. *BMC Cancer.* 2009; 9:389.
- Ceppi P, Peter ME. MicroRNAs regulate both epithelial-to-mesenchymal transition and cancer stem cells. *Oncogene.* 2014; 33:269-278.
- Heneghan HM, Miller N, Kerin MJ. MiRNAs as biomarkers and therapeutic targets in cancer. *Curr Opin Pharmacol.* 2010; 10:543-550.
- Marrero JA. Multidisciplinary management of hepatocellular carcinoma: Where are we today? *Semin Liver Dis.* 2013; 33 Suppl 1:S3-10.
- Lee NP, Cheung ST, Poon RT, Fan ST, Luk JM. Genomic and proteomic biomarkers for diagnosis and prognosis of hepatocellular carcinoma. *Biomark Med.* 2007; 1:273-284.
- Farinati F, Marino D, De Giorgio M, Baldan A, Cantarini M, Cursaro C, Rapaccini G, Del Poggio P, Di Nolfo MA, Benvegno L, Zoli M, Borzio F, Bernardi M, Trevisani F. Diagnostic and prognostic role of alpha-fetoprotein in hepatocellular carcinoma: both or neither? *Am J Gastroenterol.* 2006; 101:524-532.
- Tangkijvanich P, Anukulkarnkusol N, Suwangool P, Lertmaharit S, Hanvivatvong O, Kullavanijaya P,

- Poovorawan Y. Clinical characteristics and prognosis of hepatocellular carcinoma: analysis based on serum alpha-fetoprotein levels. *J Clin Gastroenterol.* 2000; 31:302-308.
31. Nomura F, Ohnishi K, Tanabe Y. Clinical features and prognosis of hepatocellular carcinoma with reference to serum alpha-fetoprotein levels. Analysis of 606 patients. *Cancer.* 1989; 64:1700-1707.
32. Shen Q, Fan J, Yang XR, *et al.* Serum DKK1 as a protein biomarker for the diagnosis of hepatocellular carcinoma: a large-scale, multicentre study. *Lancet Oncol.* 2012; 13:817-826.
33. Terentiev AA, Moldogazieva NT. Alpha-fetoprotein: a renaissance. *Tumour Biol.* 2013; 34:2075-2091.
34. Maluccio M, Covey A. Recent progress in understanding, diagnosing, and treating hepatocellular carcinoma. *CA Cancer J Clin.* 2012; 62:394-399.
35. Filmus J, Capurro M. Glypican-3 and alphafetoprotein as diagnostic tests for hepatocellular carcinoma. *Mol Diagn.* 2004; 8:207-212.
36. Hippo Y, Watanabe K, Watanabe A, *et al.* Identification of soluble NH₂-terminal fragment of glypican-3 as a serological marker for early-stage hepatocellular carcinoma. *Cancer Res.* 2004; 64:2418-2423.
37. Marrero JA, Romano PR, Nikolaeva O, Steel L, Mehta A, Fimmel CJ, Comunale MA, D'Amelio A, Lok AS, Block TM. GP73, a resident Golgi glycoprotein, is a novel serum marker for hepatocellular carcinoma. *J Hepatol.* 2005; 43:1007-1012.
38. Zhang R, Ma L, Zheng M, Ren J, Wang T, Meng Y, Zhao J, Jia L, Yao L, Han H, Li K, Yang A. Survivin knockdown by short hairpin RNA abrogates the growth of human hepatocellular carcinoma xenografts in nude mice. *Cancer Gene Ther.* 2010; 17:275-288.
39. Yates LA, Norbury CJ, Gilbert RJ. The long and short of microRNA. *Cell.* 2013; 153:516-519.
40. Huang S, He X. The role of microRNAs in liver cancer progression. *Br J Cancer.* 2011; 104:235-240.
41. Szabo G, Bala S. MicroRNAs in liver disease. *Nat Rev Gastroenterol Hepatol.* 2013; 10:542-552.
42. Farazi TA, Spitzer JI, Morozov P, Tuschl T. miRNAs in human cancer. *J Pathol.* 2011; 223:102-115.
43. Baer C, Claus R, Plass C. Genome-wide epigenetic regulation of miRNAs in cancer. *Cancer Res.* 2013; 73:473-477.
44. Yuan JH, Yang F, Chen BF, Lu Z, Huo XS, Zhou WP, Wang F, Sun SH. The histone deacetylase 4/SP1/microRNA-200a regulatory network contributes to aberrant histone acetylation in hepatocellular carcinoma. *Hepatology.* 2011; 54:2025-2035.
45. Hung CS, Liu HH, Liu JJ, Yeh CT, Chang TC, Wu CH, Ho YS, Wei PL, Chang YJ. MicroRNA-200a and -200b Mediated Hepatocellular Carcinoma Cell Migration Through the Epithelial to Mesenchymal Transition Markers. *Ann Surg Oncol.* 2013; 20:360-368.

(Received January 29, 2014; Revised April 1, 2014, Accepted April 8, 2014)

Transplantation of bone marrow mesenchymal stem cells pretreated with valproic acid in rats with an acute spinal cord injury

Lei Chen^{1,2,*}, Xiaoyan Cui^{1,*}, Zhou Rui Wu², Long Jia², Yan Yu², Qiulian Zhou³, Xiao Hu², Wei Xu², Dandan Luo¹, Jie Liu¹, Junjie Xiao³, Qiao Yan¹, Liming Cheng^{1,2,**}

¹ Translational Center for Stem Cell Research, Tongji Hospital, Department of Regenerative Medicine, Tongji University School of Medicine, Shanghai, China;

² Department of Spinal Surgery, Tongji Hospital, Tongji University School of Medicine, Shanghai, China;

³ College of Life Sciences, Shanghai University, Shanghai, China.

Summary

This study aimed to investigate whether valproic acid (VPA) pretreatment enhances the therapeutic effectiveness of mesenchymal stem cells derived from bone marrow (BMSCs) transplanted into rats with an acute spinal cord injury (SCI). BMSCs were pretreated with VPA before transplantation and then intravenously injected 1 week after SCI. Before transplantation, levels of CXC chemokine receptor 4 (CXCR4) expression in BMSCs were tested using quantitative real-time PCR and Western blotting. Stromal derived factor-1 (SDF-1), the unique ligand of CXCR4, was quantified using RT-PCR and immunofluorescence. The locomotor function of rats with an SCI was evaluated using the Basso, Beattie, and Bresnahan (BBB) locomotor rating scale. Fluorescence microscopy and hematoxylin-eosin (HE) staining were also performed to evaluate pathophysiological changes after transplantation. On day 7 after SCI, the level of SDF-1 expression peaked. CXCR4 expression increased significantly in BMSCs pretreated with VPA. After intravenous transplantation, BrdU-labeled BMSCs were noted at the spinal injury site, and this was especially true for BMSCs pretreated with VPA. More significant functional improvement was observed in rats receiving BMSCs pretreated with VPA than in other groups of rats. AMD3100 partially inhibited improvement. This study demonstrates that pretreatment with VPA before transplantation enhances the therapeutic benefits of BMSCs in terms of greater cell migration and better neurological outcomes after traumatic SCI. The mechanism of this enhancement may be related to the SDF-1/CXCR4 axis. Therefore, pretreatment of BMSCs with VPA warrants further study in relation to the treatment of traumatic SCI.

Keywords: Mesenchymal stem cells derived from bone marrow, spinal cord injury, valproic acid, stromal derived factor-1, CXC chemokine receptor 4

1. Introduction

Spinal cord injury (SCI) is a serious hazard to human health. It usually causes severe neurological dysfunction and disability. However, effective ways to

treat SCI have not been available until now. One reason is because a complex series of pathophysiological changes, such as local inflammation and glutamate cytotoxicity, results in the apoptosis of neurons and oligodendrocyte glial cells and the reactivation of astrocytes that in turn lead respectively to disconnection of neuronal circuits, demyelination, and glial scar formation (1).

Over the past few decades, stem cell therapy has offered promise as a strategy to treat SCI. Mounting evidence has shown that mesenchymal stem cells derived from bone marrow (BMSCs) can improve

*These authors contributed equally to this works.

**Address correspondence to:

Dr. Liming Cheng, Department of Spinal Surgery, Tongji Hospital, Tongji University School of Medicine, 389 Xincun Road, Shanghai 200065, China.
E-mail: chlm.d@163.com

recovery in SCI models by regulating host immunity, secreting neurotrophic factors, and differentiating into neurons (1-3). BMSC therapy has several advantages over therapy with other types of stem cells, including greater availability, less likelihood of immune rejection, and fewer ethical issues.

The systemic administration of BMSCs provides a therapeutic benefit in rats with a SCI (4). However, this treatment seems to have more limited therapeutic effectiveness than local direct injection because of the uneven distribution of BMSCs *in vivo* after intravenous injection (5). Ninety-nine percent of intravenously injected MSCs adhere to the lungs, while only 2-3% of adhering MSCs are released into the circulation (6). Numerous experiments have shown that BMSCs will preferentially migrate to sites of inflammation after intravenous administration (4,7-9). A way to promote the migration of exogenous BMSCs to the injury site has yet to be determined. One proven way is *via* chemotactic factors that mediate the homing of BMSCs. Stromal derived factor-1 (SDF-1) and its cellular receptor CXC chemokine receptor 4 (CXCR4) have been found to direct the migration of BMSCs in models of stroke, SCI, and cardiomyopathy (7-9).

Previous studies found that valproic acid (VPA) affected the structure of chromatin and gene expression as an inhibitor of histone deacetylase (HDAC) activity (10). Short-term (3 h) exposure of MSCs to a relatively high concentration (2.5 mM) of VPA markedly increased CXCR4 transcript and protein levels and it enhanced SDF-1-mediated MSCs migration (11). Thus, the current study sought to investigate whether BMSCs pretreated with VPA would enhance the migration of BMSCs to improve functional recovery in an experimental rat model of SCI.

2. Materials and Methods

2.1. Isolation, culture, identification, and differentiation of BMSCs

The use of rats in this study was approved by the Ethical Committee of Tongji Hospital. All experimental procedures were conducted in accordance with the Guide for the Care and Use of Laboratory Animals (NIH Pub, revised 2011).

BMSCs were isolated and identified as described previously (4,7). Briefly, primary BMSCs were harvested from tibias and femurs of 3-week-old Sprague-Dawley rats under aseptic conditions and then purified and passaged in dulbecco's modified eagle medium (DMEM, Gibco, St. Louis, MO, USA) supplemented with 10% fetal bovine serum (FBS, Gibco). Cells were maintained at 37°C in a humidified atmosphere with 5% carbon dioxide, and the medium was changed every 3 days. Upon reaching 80 to 90% confluence, adherent cells were detached with 0.25%

Trypsin-EDTA (Gibco) and replated at a ratio of 1:3 in regular growth medium for continued passaging. Upon the third passage, the BMSCs were trypsinized and then filtered through a stainless steel mesh filter into single-cell suspensions. These suspensions were stained with fluorescein isothiocyanate-labeled antibodies for flow cytometric analysis, including rat anti-CD29, CD45, CD73, CD90, and CD106 (BD Pharmingen, San Diego, USA). BMSCs that had been passaged 4 times were harvested for the following experiments.

To ascertain differentiation, BMSCs that were passaged 4 times were divided into 3 groups: (i) untreated BMSCs; (ii) BMSCs pretreated with VPA, and (iii) BMSCs pretreated with VPA and AMD3100.

BMSCs were incubated with 2.5 mmol/L of VPA (Sigma-Aldrich, P4543-10G, St. Louis, MO, USA), a small molecule compound that is an histone deacetylase (HDAC) inhibitor, for 3 h and then washed with fresh medium to yield BMSCs pretreated with VPA. BMSCs pretreated with VPA were also treated with 20 μ mol/L AMD3100 (Sigma-Aldrich) for 6 h and then washed with fresh medium to yield BMSCs pretreated with VPA and AMD3100. All 3 groups of cells were plated in 6-well tissue culture plates and growth medium was replaced. Cells were then fed by completely replacing the medium with fresh BMSC osteogenic/adipogenic differentiation medium (Cyagen Biosciences Inc., California, USA) or growth medium supplemented with 10 ng/mL b-fibroblast growth factor (bFGF, Gibco) and 10 ng/mL epidermal growth factor (EGF, Gibco) (12). After differentiation, cells were fixed and subjected to Alizarin red staining, Oil red O staining, and immunofluorescence staining.

2.2. VPA and AMD3100 pretreatment and BrdU labeling of BMSCs *in vitro*

BMSCs that had been passaged 4 times were divided into 3 groups (1×10^6 cells in each group): (i) untreated BMSCs; (ii) BMSCs pretreated with VPA; and (iii) BMSCs pretreated with VPA and AMD3100. All groups of cells were labeled with 10 μ mol/L of BrdU for 3 days. Cells were then harvested for subsequent experiments.

2.3. Model of acute SCI

Adult Sprague-Dawley rats weighing 180 to 200 g were chosen to create an SCI model. Rats were anesthetized with an intraperitoneal injection of 2% pentobarbital sodium (60 mg/kg). A laminectomy was performed at the T10 level using a micromanipulator, and then the spinal cord was exposed without scratching the dura mater. Rats were placed on the fixation plate of an IH-0400 impactor (Precision Systems and Instrumentation, Kentucky, USA), and then the vertebral bodies at T9 and T11 were grasped with 2 adjustable forceps

to immobilize the spine. The impact force of the impactor was set at 200 kDynes. Gentamycin (5 mg/kg) was injected *via* intraperitoneal injection in the first 3 days after SCI. Rats were left on heated pads until they awoke. Upon awakening, each rat's bladder was manually expressed twice a day, and the rat's locomotion was evaluated (13,14). To evaluate the expression of SDF-1 at the injury site on days 1 and 7 after SCI, RT-PCR and immunohistochemical analysis were performed on injured spinal cords and normal spinal cords.

2.4. BMSC transplantation

Rats were randomly divided into four groups: rats receiving DMEM (sham), rats receiving untreated BMSCs, rats receiving BMSCs pretreated with VPA, and rats receiving BMSCs pretreated with VPA and AMD3100. Cells were injected into the tail vein with a scalp vein needle. In rats receiving DMEM, only 0.5 mL of DMEM was injected intravenously into the tail vein 7 days after SCI. The other groups of rats were injected with 1×10^6 of the corresponding cells in 0.5 mL DMEM. After injection, a cotton ball soaked in alcohol was pressed on the wound to prevent bleeding.

2.5. Behavioral test

Hind limb locomotion was evaluated using the Basso, Beattie, and Bresnahan (BBB) locomotor rating scale on days 1, 3, 7, 14, and 28 after SCI (12). During the evaluation, rats were placed in an open field and observed for 5 minutes at each time point by 2 observers who were blind to the experimental protocol. The BBB locomotor rating scale ranges from 0 to 21 points, with 0 points indicating no spontaneous hind limb movement and 21 points indicating normal hind limb movement. Observers completed their ratings independently.

2.6. q-PCR analysis

Total RNA was isolated from cells and injured spinal cords with TRIzol reagent (Gibco-Invitrogen, Carlsbad, CA, USA). Injured spinal cord segments were first homogenized. RNA concentrations were quantified using ultraviolet spectroscopy. As outlined in the instruction manual, reverse transcription was performed in a 20 μ L reaction system with 4 mg of total RNA treated by RNase-free DNase I (TaKaRa Bio, Inc., Otsu, Japan). The PCR primers were synthesized from Invitrogen as follows: β -Actin forward primer, CACCCGCGAGTACAACCTTC; β -Actin reverse primer, CCCATACCCACCATCACACC; rCXCR4 forward primer: CCTTCTGGGCAGTGGACG; and CXCR4-reverse primer, GGACAATGGCAAGGTAGCG. Reverse transcription was performed with a SYBR Premix Ex Taq Kit (TaKaRa Bio) in a real-time fluorescence

quantitative PCR system (ABI 7800, USA). The reaction mixture was a 20- μ L mixture containing 10 μ L of SYBR Premix Ex Taq TM (Takara Bio), 0.4 μ L of each primer, and 2 μ L of cDNA. In accordance with the instruction manual, the cycling conditions were as follows: an initial cycle of heating at 95°C for 15 sec, followed by 40 cycles at 95°C for 5 sec and 40 cycles at 60°C for 31 sec. After PCR, the RT-PCR system automatically analyzed the fluorescence signal and converted it to the cycle threshold (Ct) value. Each sample was analyzed in triplicate.

2.7. Western blot analysis of CXCR4 in BMSCs

All groups of BMSCs were cleaved in radio-immunoprecipitation assay (RIPA, Sigma-Aldrich) buffer supplemented with a protease inhibitor and phosphatase inhibitor cocktail (Sigma) for 30 min at 4°C. Protein homogenates were then centrifuged at 12,000 g for 15 min at 4°C to collect the supernatant. The protein concentration was determined using a bicinchoninic acid (BCA) protein assay kit and Bio-Rad spectrophotometer. The samples were separated using sodium dodecyl sulfate polyacrylamide gel electrophoresis (SDS-PAGE) and then transferred to polyvinylidene fluoride (PVDF) membranes. Membranes were blocked with 5% albumin from bovine serum (BSA, Sigma-Aldrich) and incubated with goat anti-CXCR4 polyclonal antibody (1:1,000; Abcam, London, England). Finally, blots were incubated with rabbit anti-goat IgG (1:2,000; Jackson, Lancaster, USA) conjugated with horseradish peroxidase. Protein signals were detected in an X-ray developing darkroom. The results were expressed as relative integrated intensity compared to β -actin.

2.8. Immunohistochemical analysis

To label and track BMSCs, the rate of BrdU labeling *in vitro* was analyzed and the distribution of grafted MSCs in the spinal cord was determined using immunofluorescence. The spinal cord, dissected 5 days after the transplantation of BMSCs, was frozen and sectioned before staining. Sections or cells were fixed with 4% paraformaldehyde (PFA) for 20 min. After rinsing with tris-buffered saline (TBS), samples were permeabilized with 0.3% Triton in TBS for 15 min at room temperature (RT). They were then rinsed 3 times with TBS for 30 min at RT. Samples were incubated in 2 N HCl for 30 min at 37°C followed by 0.1 M sodium tetraborate (pH 8.5) for 10 min at 37°C. After they were rinsed 3 times with TBS, the samples were incubated in a blocking buffer (1% BSA and 10% goat normal serum in 0.3% Triton X-100-TBS) for 1 h at RT. Samples were then incubated in rat anti-BrdU (1:200) diluted with blocking buffer overnight at 4°C. After they were rinsed 3 times with TBS, sections were incubated for 1

h at RT with Goat Anti-Rat IgG Cy3 (1/1,000, Abcam). Sections were then rinsed 3 times in TBS-0.05% Tween 20. Sections or cells were finally coverslipped with 4',6-diamidino-2-phenylindole (DAPI) mounting medium (Sigma-Aldrich). Each spinal sample was cut into 3 slices, and results represented the average for the slices.

2.9. Hematoxylin and eosin (HE) staining to estimate the volume of injured tissue

Four weeks after SCI, all rats were anesthetized and transcardially perfused with PBS followed by 4% PFA until blood had been removed. Six spinal cords were dissected from 6 rats in each group and these spinal cords were immersed in 4% PFA for 2 days until they sank. Each spinal cord was embedded in paraffin and sectioned into 3 slices. Cross-sections (5 μ m) were cut and stained with HE. A cross-section of the injured spinal cord was obtained using a microscope camera, and its area was measured using the image analysis software NIH Image. The injured area consisted of all meaningful (> 100 μ m) cavities present at the injury site. The total area of the spinal cord was divided by the area of injured tissue to yield a ratio of the injured area/entire area. This ratio represented the final result.

2.10. Statistical analysis

Data were statistically analyzed and expressed as mean values \pm S.D. Differences between the means of different groups were assessed with one-way analysis of variance (ANOVA) followed by Tukey's post-hoc test. Scores on the BBB locomotor rating scale on different days were analyzed using repeated-measures ANOVA. A *p* value < 0.05 was considered statistically significant. All analyses were performed using SPSS 16.0 software.

3. Results

3.1. Isolation, culture, characterization, and differentiation of rat BMSCs

About 7-10 days after isolation, BMSCs cultured as plastic adherent cells proliferated consistently and were passaged to cover 80-90% of the plate. Cells passaged 3 times had consistent morphological features of being flat and spindle-shaped (Figure 1A). The proliferative activity of BMSCs decreased with passaging. Flow cytometry analysis indicated that BMSCs passaged 3 times expressed CD29, CD73, and CD90 but not CD45 or CD106 (Figure 1B). Upon induction, BMSCs consistently differentiated into osteogenic/adipogenic/neurogenic cells, indicating that the BMSCs were multipotent. Certain concentrations of VPA and AMD3100 did not markedly affect the differentiation of BMSCs into other cell types (Figures 1D, 1E, and 1F).

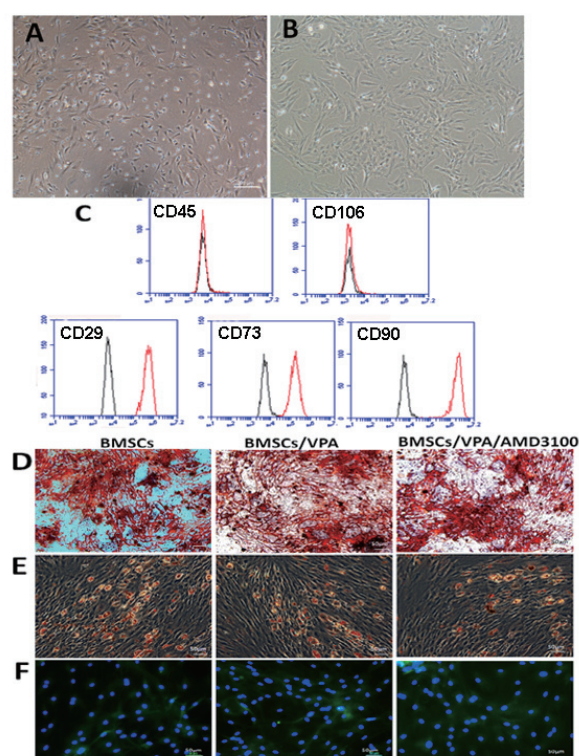


Figure 1. Morphology, phenotypic characterization, and differentiation of rat BMSCs. (A) Primary BMSCs after 7 days of culturing (magnification: $\times 100$, bar = 200 μ m). (B) BMSCs passaged 3 times (magnification: $\times 100$, bar = 200 μ m). (C) Flow cytometric analysis of cultured BMSCs with the cell surface markers CD29, CD45, CD73, CD90, and CD106. (D) Analysis of osteogenic differentiation using Alizarin red staining. (E) Analysis of adipogenic differentiation using Oil red O staining. (F) Neural cell differentiation indicated by immunostaining. The figure shows the staining of GFAP since NeuN was negative (data not shown). [magnification: $\times 200$, bar = 50 μ m].

3.2. VPA and AMD3100 affected CXCR4 expression and did not affect BrdU labeling of BMSCs

Pretreating BMSCs with 2.5 mmol/L of VPA and 20 μ mol/L of AMD3100 had no apparent negative effect on their morphology, such as nuclear shrinkage or formation of cytoplasmic vacuoles. RT-PCR results suggested that VPA increased the expression of CXCR4 in BMSCs about 2.25 ± 0.20 -fold while VPA and AMD3100 increased the expression of CXCR4 1.44 ± 0.12 -fold (Figure 2A). BMSCs pretreated with VPA had significant greater (*p* < 0.05) expression of CXCR4 than other groups of cells, and the same was true according to the results of Western blotting (Figure 2B).

BrdU-labeled BMSCs had proliferative activity at a rate of 80-90%. VPA and AMD3100 did not significantly affect BMSC proliferation and BrdU labeling (Figure 2C).

3.3. Changes in SDF-1 levels at the spinal injury site

Compared to normal spines, injured spines had 2.01 ± 0.29 times more expression of SDF-1 on day 1 post-

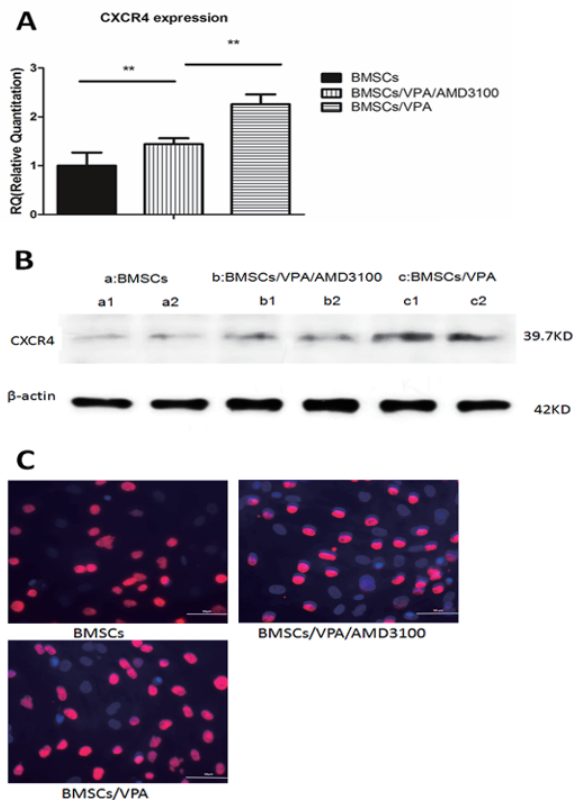


Figure 2. CXCR4 expression and BrdU immunofluorescence. (A) mRNA expression of CXCR4 in each group. Data are the mean \pm S.D. ($n = 6$). BMSCs pretreated with VPA had significantly greater CXCR4 expression than other groups. $** p < 0.01$ indicates significant differences between groups (one-way ANOVA). (B) CXCR4 and β -actin in each group ($n = 6$) were detected with Western blotting. The blots were 2 representative examples from 6 experiments per group. (C) BrdU (Cy3)-DAPI staining indicated no significant differences in BrdU-labeled BMSCs among the groups (magnification: $\times 400$, bar = 50 μ m).

injury and 3.03 ± 0.47 times more expression on day 7 post-injury (Figure 3A). Immunofluorescent staining of spinal cord sections indicated that normal spinals expressed a slight amount of SDF-1 although expression was marked on day 7 post-injury (Figure 3B). Fluorescence was more marked in gray matter, which may be related to astrocyte activation.

3.4. Pretreatment with VPA enhanced the migration of BMSCs to the spinal injury site

Five days after intravenous transplantation, BMSCs that were grafted to the injured spinal cord were tracked using BrdU immunostaining (Figure 4). The number of labeled cells at the injury site was as follows: no labeled cells in the control group, 12.67 ± 2.08 cells per slice in rats receiving untreated BMSCs, 33.33 ± 6.1 cells per slice in rats receiving BMSCs pretreated with VPA, and 14 ± 2.65 cells per slice in rats receiving BMSCs pretreated with VPA and AMD3100. There were significant differences ($p < 0.05$) in the number of cells in rats receiving BMACs pretreated with VPA and rats receiving untreated BMSCs and there were

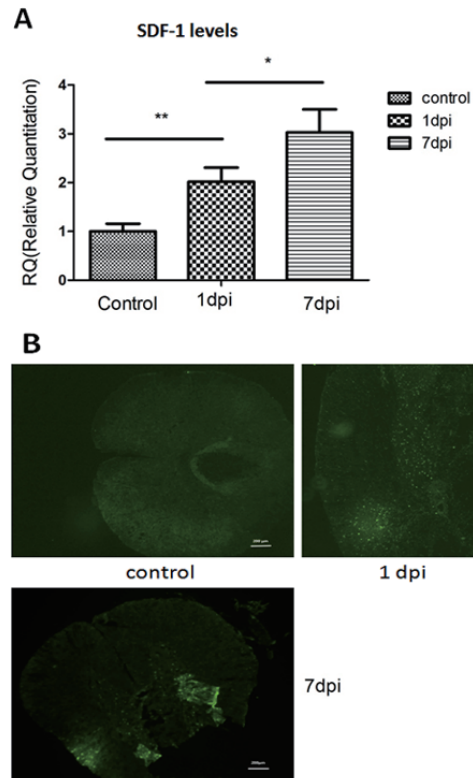


Figure 3. RT-PCR and immunofluorescence of SDF-1 at the spinal injury site. (A) RT-PCR. About 3 centimeters of the injured spinal cord was removed from each rat on days 1 and 7 after SCI, and these injured spinal cords were compared to normal spinal cords ($n = 6$ in each group). $** p < 0.01$ indicates significant differences between groups, $* p < 0.05$ for day 1 post-injury versus day 7 post-injury (one-way ANOVA). (B) Immunofluorescent staining. Normal spinal cords had slight expression of SDF-1 that increased on day 1 post-injury and peaked on day 7 post-injury (magnification: $\times 40$, bar = 200 μ m).

significant differences ($p < 0.05$) in the number of cells in rats receiving BMSCs pretreated with VPA and rats receiving BMSCs pretreated with VPA and AMD3100.

3.5. Spared tissue after SCI

The injured portion of the spinal cord was embedded in paraffin and stained with HE on day 28 post-injury. Slices were then analyzed using the methods described previously (15). The ratio of the injured area/total area was calculated and the results were expressed as a mean value. Staining indicated that rats receiving BMSCs pretreated with VPA had relatively smaller cavities and scar tissue formation compared to rats receiving BMSCs and rats receiving BMSCs pretreated with VPA and AMD3100 (Figure 5).

3.6. Neurological outcomes

The recovery of hind limb function in all rats was assessed in an open field test using the BBB Locomotor Rating Scale. Wild-type (WT) rats had a score of 21 points during evaluation. Injured rats had complete hind

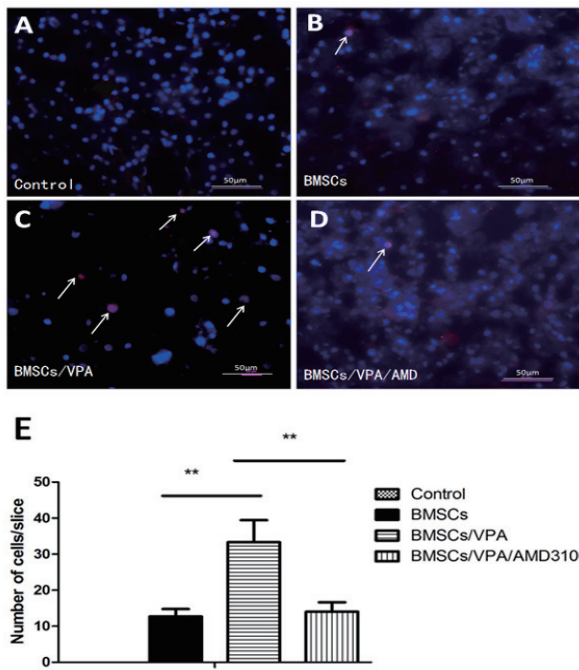


Figure 4. BrdU immunostaining of BMSCs grafted to the spinal injury site. (A) Control group. (B) Rats receiving untreated BMSCs. (C) Rats receiving BMSCs pretreated with VPA. (D) Rats receiving BMSCs pretreated with VPA and AMD3100 (magnification: $\times 400$, bar = 50 μm). BrdU-labeled BMSCs were stained red by Cy3 and blue by DAPI. Rats receiving BMSCs pretreated with VPA had significantly more BMSCs than other groups of rats. (E) Calculation of the average number of BMSCs at the spinal injury site. $** p < 0.01$ indicates significant differences between groups (one-way ANOVA) ($n = 6$).

limb paraplegia immediately after SCI. The recovery of motor function was most pronounced 1-2 weeks after SCI, and especially on days 10-14 post-injury. All of the groups of rats had relatively few changes in their score on the BBB Locomotor Rating Scale from day 14 post-injury to day 28 post-injury (Figure 6A). On day 28 post-injury, the control group had a score of 4.17 ± 0.75 points on the BBB Locomotor Rating Scale, rats receiving untreated BMSCs had a score of 6.33 ± 0.82 points, rats receiving BMSCs pretreated with VPA had a score of 9.5 ± 1.05 points, and rats receiving BMSCs pretreated with VPA and AMD3100 had a score of 7 ± 0.89 points. Rats receiving BMSCs pretreated with VPA had a more marked recovery than other groups of rats ($p < 0.05$). Moreover, there were significant differences ($p < 0.05$) between rats receiving untreated BMSCs or BMSCs pretreated with VPA and AMD3100 and the control group.

4. Discussion

BMSC transplantation *via* the tail vein is a useful way to treat SCI (4,16). However, the uneven distribution of exogenous BMSCs *in vivo* has seriously hindered further research. Recent studies have found that systemic infusion of BMSCs resulted in their distribution to a

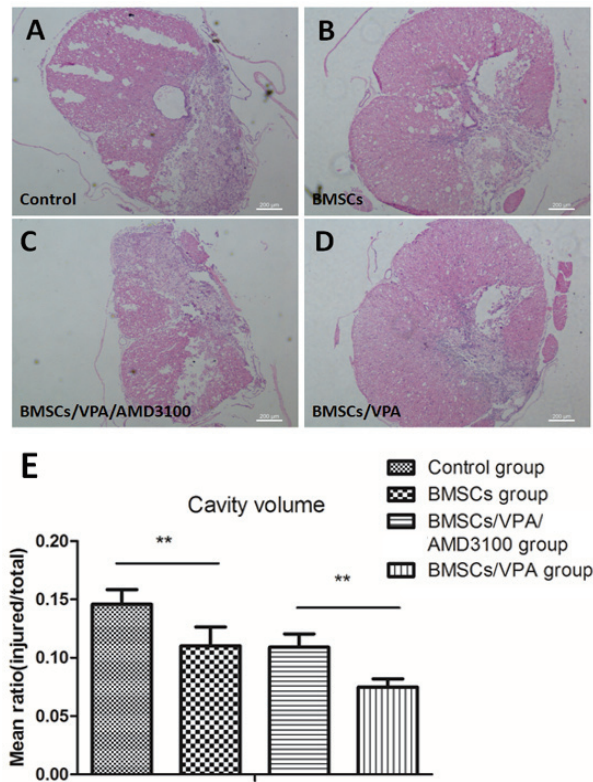


Figure 5. HE staining to estimate the volume of injured tissue and spared tissue. (A) Control group. (B) Rats receiving untreated BMSCs. (C) Rats receiving BMSCs pretreated with VPA and AMD3100. (D) Rats receiving BMSCs pretreated with VPA (magnification: $\times 40$, bar = 50 μm). (E) The mean ratio of the injured area/total area for all groups of rats. Compared to the control group, other groups of rats had a cavity with a smaller volume. $** p < 0.01$ indicates significant differences between groups (one-way ANOVA) ($n = 6$).

wide range of tissues in nonhuman primates and that these BMSCs may migrate to the site of an SCI (17). The current study confirmed that exogenous BMSCs migrated to the spinal injury site and that pretreatment with VPA enhanced the therapeutic benefits of BMSCs in terms of greater cell migration and improved neurological recovery. These results also indicate that SDF-1/CXCR4 plays an important role in the migration of BMSCs to the spinal injury site.

BMSCs can be harvested, cultured, and grown *in vitro* and exhibit low immunogenicity (4). BMSCs were isolated from the tibias and femurs of rats and passaged 3 times, resulting in a consistent morphology and phenotype. Cells passaged 3 times had consistent morphological features of being flat and spindle-shaped. The results of flow cytometry indicated that BMSCs were positive for CD29, CD73, and CD90 and negative for CD45 and CD106, and these findings agree with the results of previous studies (7,18). Moreover, an attempt was made to analyze the multipotency of BMSCs by inducing osteogenic and adipogenic cell differentiation. As noted in other sources, BMSCs were able to differentiate into osteoblasts and adipocytes with a high level of efficiency (15).

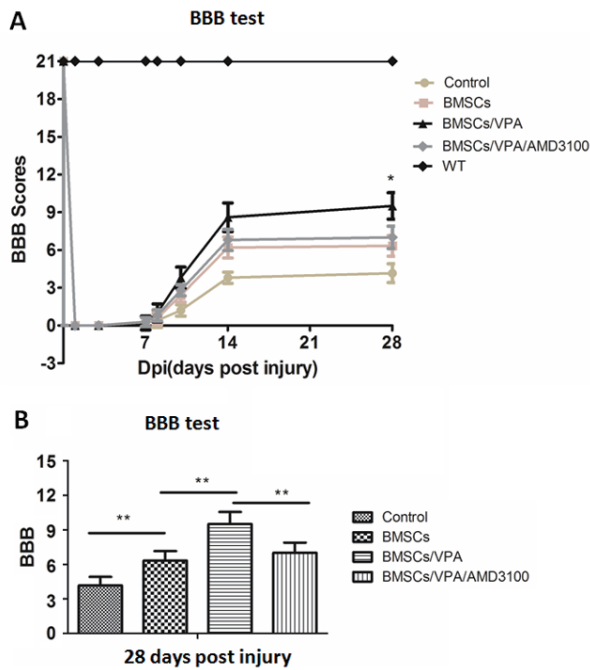


Figure 6. Evaluation of the recovery of hind limb function using the BBB Locomotor Rating Scale. (A) Functional recovery was similar for all of the groups of rats. Rats receiving BMSCs pretreated with VPA had a better recovery than did other groups of rats. Significant differences were noted between the control group and rats receiving BMSCs pretreated with VPA ($p < 0.0001$), and significant differences ($p < 0.0001$) were also noted between rats receiving BMSCs pretreated with VPA and rats receiving BMSCs pretreated with VPA and AMD3100. **(B)** On day 28 post-injury, the score on the BBB Locomotor Rating Scale peaked for all of the groups of rats. Rats receiving BMSCs/VPA had a significantly higher score than rats receiving BMSCs and rats receiving BMSCs pretreated with VPA and AMD3100. Rats receiving untreated BMSCs had a significantly higher score than the control group. ** $p < 0.01$ indicates significant differences between groups.

VPA has been widely used as an anticonvulsant for over 40 years and is believed to act *via* g-aminobutyric acid (GABA) metabolism. A study has indicated that VPA inhibits HDAC, altering the structure of chromatin and neuronal gene expression (10). In previous studies, VPA increased the expression of glial cell line-derived neurotrophic factor (GDNF) and brain-derived neurotrophic factor (BDNF) in astrocytes to protect neurons (19). A recent study showed that VPA promoted the BDNF and GDNF expression of BMSCs and that it also improved the ability of BMSCs to migrate (20). Studies have indicated that VPA increases the expression of CXCR4 by inhibiting HDAC, thus improving the ability of BMSCs to migrate. Results of one study indicated that short-term (3 h) exposure of MSCs to a relatively high concentration (2.5 mM) of VPA markedly increased CXCR4 transcript and protein levels (11). The current study found that pretreatment with 2.5 mM of VPA for 3 h significantly increased the CXCR4 expression of BMSCs. This study also examined the effects of certain concentrations of VPA on the rate of BrdU labeling of BMSCs. Results

indicated that the rate of labeling differed little among 3 groups of cells, thus ruling out the effect of different drugs on the BrdU labeling of MSCs.

Various chemokines and receptors are involved in the migration of BMSCs, and the involvement of SDF-1 and its cognate receptor CXCR4 in BMSC migration to injured tissues is well documented (8,21). Though high levels of SDF-1 were expressed by meningeal cells in both intact and injured spinal cords, the level of SDF-1 was elevated at the site following SCI and a gradient arose to guide immune and stem cells to the injury site. The current study found little expression of SDF-1 in the normal spinal cord, an increased level on day 1 post-injury, and the highest level on day 7 post-injury. This agrees with the results of a previous study (22). Only a small proportion of BMSCs expresses functionally active CXCR4 receptor on their surface and this expression diminished with passage, but CXCR4 is key to mediating specific migration of these cells (23,24). Overexpression of CXCR4 by genetic modification enhances the ability of MSCs to respond to SDF-1-induced chemotaxis *in vitro* and promotes MSC recruitment around the ischemic core *in vivo* (25).

To explore the hypothesis that VPA promotes the migration of MSCs, BMSC transplantation *via* tail vein injection was performed on rats with an SCI 7 days after injury. The transplantation consisted of 1×10^6 BrdU-labeled BMSCs, and the injured segments of the spinal cord were analyzed using immunofluorescence and HE staining. BrdU immunostaining indicated that rats receiving BMSCs pretreated with VPA or BMSCs pretreated with VPA and AMD3100 had relatively more MSCs at the injury site than rats receiving untreated BMSCs. Pretreatment with VPA and AMD3100 largely suppressed the homing ability of BMSCs, indicating that SDF-1/CXCR4 played an important role in the migration of BMSCs. In rats receiving untreated BMSCs, few BMSCs were present at the injury site. This may be related to the low level of CXCR4 expression on the surface of BMSCs.

BMSCs had more of a therapeutic effect on motor recovery of rats with an SCI with a greater number of BMSCs at the injury site. The BBB Locomotor Rating Scale is a general method of evaluating behavior and can accurately assess changes in behavior after SCI. HE staining also indicated that injured rats with better motor recovery had a smaller cavity in the spinal cord. Pretreatment of BMSCs with VPA may enhance the therapeutic effects of BMSCs in SCI by increasing BMSC migration, which is closely related to SDF-1/CXCR4. However, the mechanism of action of BMSCs in SCI therapy has yet to be fully elucidated (1-3). One possible mechanism is *via* the secretion of growth factors, like BDNF and GDNF, by BMSCs to reduce lesion volume and promote axonal regrowth of the injured spinal cord (26). More BMSCs may maintain an effective concentration of growth factors. Another

possible mechanism is *via* the differentiation of BMSCs into neurons, which may serve to rebuild neural circuits (27,28). Moreover, VPA may promote the secretion of TGF- β , BDNF, and bFGF by BMSCs (20). TGF- β plays an important role in immunosuppression by inhibiting the activity of T cells (CD4, CD8) and dendritic cells (29). Previous studies also indicated that BDNF and bFGF were factors that induced BMSCs to transform into neural cells (30). Thus, an increase in the aforementioned autocrine factors of MSCs might result in enhanced immunosuppression and transformation of BMSCs into neural cells that help to repair SCI. Compared to a study by Cho *et al.* (20), the current study used a relatively low concentration of VPA. This may have a limited effect on the aforementioned factors secreted by MSCs. A high concentration of VPA could result in apoptosis of BMSCs (11).

In summary, the current study indicates that BMSC transplantation *via* the tail vein is a minimally invasive and useful way to provide SCI therapy. However, the therapeutic effectiveness of BMSCs is limited. Pretreatment with VPA can enhance the therapeutic benefits of BMSCs in terms of greater cell migration and better neurological outcomes after traumatic SCI. The mechanism of this enhancement may be related to growth factors, axons, and neuron transdifferentiation from BMSCs at the injury site (31). Therefore, pretreatment of BMSCs with VPA warrants further study in relation to the treatment of traumatic SCI.

Acknowledgements

This project was supported by a grant (81330030) from the State Key Program of the National Natural Science Foundation of China, a grant (XBR2013094) from the Shanghai Public Health System as part of a Project supporting Excellent Academic Leaders of Shanghai, a grant (2012M520933) from the National Science Foundation for Post-doctoral Scientists of China, a grant (20124y147) for Youth Projects of the Shanghai Municipal Health Bureau, and a grant (2012KJ016) from the Fundamental Research Funds for Central Universities.

References

- Fuhrmann T, Montzka K, Hillen LM, Hodde D, Dreier A, Bozkurt A, Woltje M, Brook GA. Axon growth-promoting properties of human bone marrow mesenchymal stromal cells. *Neurosci Lett.* 2010; 474:37-41.
- Uccelli A, Benvenuto F, Laroni A, Giunti D. Neuroprotective features of mesenchymal stem cells. *Best Pract Res Clin Haematol.* 2011; 24:59-64.
- Nakajima H, Uchida K, Guerrero AR, Watanabe S, Sugita D, Takeura N, Yoshida A, Long G, Wright KT, Johnson WE, Baba H. Transplantation of mesenchymal stem cells promotes an alternative pathway of macrophage activation and functional recovery after spinal cord injury. *J Neurotrauma.* 2012; 29:1614-1625.
- Osaka M, Honmou O, Murakami T, Nonaka T, Houkin K, Hamada H, Kocsis JD. Intravenous administration of mesenchymal stem cells derived from bone marrow after contusive spinal cord injury improves functional outcome. *Brain Res.* 2010; 1343:226-235.
- Vaquero J, Zurita M, Oya S, Santos M. Cell therapy using bone marrow stromal cells in chronic paraplegic rats: Systemic or local administration? *Neurosci Lett.* 2006; 398:129-134.
- Lee RH, Pulin AA, Seo MJ, Kota DJ, Ylostalo J, Larson BL, Semprun-Prieto L, Delafontaine P, Prockop DJ. Intravenous hMSCs improve myocardial infarction in mice because cells embolized in lung are activated to secrete the anti-inflammatory protein TSG-6. *Cell Stem Cell.* 2009; 5:54-63.
- Wang Y, Deng Y, Zhou GQ. SDF-1 α /CXCR4-mediated migration of systemically transplanted bone marrow stromal cells towards ischemic brain lesion in a rat model. *Brain Res.* 2008; 1195:104-112.
- Askari AT, Unzek S, Popovic ZB, Goldman CK, Forudi F, Kiedrowski M, Rovner A, Ellis SG, Thomas JD, DiCorleto PE, Topol EJ, Penn MS. Effect of stromal-cell-derived factor 1 on stem-cell homing and tissue regeneration in ischaemic cardiomyopathy. *Lancet.* 2003; 362:697-703.
- Jaerve A, Bosse F, Muller HW. SDF-1/CXCL12: Its role in spinal cord injury. *Int J Biochem Cell Biol.* 2012; 44:452-456.
- Gottlicher M, Minucci S, Zhu P, Kramer OH, Schimpf A, Giavara S, Sleeman JP, Lo Coco F, Nervi C, Pelicci PG, Heinzel T. Valproic acid defines a novel class of HDAC inhibitors inducing differentiation of transformed cells. *EMBO J.* 2001; 20:6969-6978.
- Tsai LK, Leng Y, Wang Z, Leeds P, Chuang DM. The mood stabilizers valproic acid and lithium enhance mesenchymal stem cell migration *via* distinct mechanisms. *Neuropsychopharmacology.* 2010; 35:2225-2237.
- Bae KS, Park JB, Kim HS, Kim DS, Park DJ, Kang SJ. Neuron-like differentiation of bone marrow-derived mesenchymal stem cells. *Yonsei Med J.* 2011; 52:401-412.
- Kawabe J, Koda M, Hashimoto M, Fujiyoshi T, Furuya T, Endo T, Okawa A, Yamazaki M. Neuroprotective effects of granulocyte colony-stimulating factor and relationship to promotion of angiogenesis after spinal cord injury in rats: laboratory investigation. *J Neurosurg Spine.* 2011; 15:414-421.
- Basso DM, Beattie MS, Bresnahan JC. A sensitive and reliable locomotor rating scale for open field testing in rats. *J Neurotrauma.* 1995; 12:1-21.
- Quertainmont R, Cantinieaux D, Botman O, Sid S, Schoenen J, Franzen R. Mesenchymal stem cell graft improves recovery after spinal cord injury in adult rats through neurotrophic and pro-angiogenic actions. *PLoS One.* 2012; 7:e39500.
- Mohammad-Gharibani P, Tiraihi T, Delshad A, Arabkheradmand J, Taheri T. Improvement of contusive spinal cord injury in rats by co-transplantation of gamma-aminobutyric acid-ergic cells and bone marrow stromal cells. *Cytotherapy.* 2013; 15:1073-1085.
- Devine SM, Cobbs C, Jennings M, Bartholomew A, Hoffman R. Mesenchymal stem cells distribute to a wide range of tissues following systemic infusion into nonhuman primates. *Blood.* 2003; 101:2999-3001.
- Lin WP, Chen XW, Zhang LQ, Wu CY, Huang ZD, Lin JH. Effect of neuroglobin genetically modified bone marrow mesenchymal stem cells transplantation on spinal

- cord injury in rabbits. PLoS One. 2013; 8:e63444.
19. Wu X, Chen PS, Dallas S, Wilson B, Block ML, Wang CC, Kinyamu H, Lu N, Gao X, Leng Y, Chuang DM, Zhang W, Lu RB, Hong JS. Histone deacetylase inhibitors up-regulate astrocyte GDNF and BDNF gene transcription and protect dopaminergic neurons. *Int J Neuropsychopharmacol.* 2008; 11:1123-1134.
 20. Cho GW, Kang BY, Kim KS, Kim SH. Effects of valproic acid on the expression of trophic factors in human bone marrow mesenchymal stromal cells. *Neurosci Lett.* 2012; 526:100-105.
 21. Song C.H, Honmou O, Furuoka H, Horiuchi M. Identification of chemoattractive factors involved in the migration of bone marrow-derived mesenchymal stem cells to brain lesions caused by prions. *J Virol.* 2011; 85:11069-11078.
 22. Takeuchi H, Natsume A, Wakabayashi T, Aoshima C, Shimato S, Ito M, Ishii J, Maeda Y, Hara M, Kim SU, Yoshida J. Intravenously transplanted human neural stem cells migrate to the injured spinal cord in adult mice in an SDF-1- and HGF-dependent manner. *Neurosci Lett.* 2007; 426:69-74.
 23. Son BR, Marquez-Curtis LA, Kucia M, Wysoczynski M, Turner AR, Ratajczak J, Ratajczak MZ, Janowska-Wieczorek A. Migration of bone marrow and cord blood mesenchymal stem cells *in vitro* is regulated by stromal-derived factor-1-CXCR4 and hepatocyte growth factor-c-met axes and involves matrix metalloproteinases. *Stem Cells.* 2006; 24:1254-1264.
 24. Wynn RF, Hart CA, Corradi-Perini C, O'Neill L, Evans CA, Wraith JE, Fairbairn LJ, Bellantuono I. A small proportion of mesenchymal stem cells strongly expresses functionally active CXCR4 receptor capable of promoting migration to bone marrow. *Blood.* 2004; 104:2643-2645.
 25. Yu X, Chen D, Zhang Y, Wu X, Huang Z, Zhou H, Zhang Z. Overexpression of CXCR4 in mesenchymal stem cells promotes migration, neuroprotection and angiogenesis in a rat model of stroke. *J Neurol Sci.* 2012; 316:141-149.
 26. Gu W, Zhang F, Xue Q, Ma Z, Lu P, Yu B. Transplantation of bone marrow mesenchymal stem cells reduces lesion volume and induces axonal regrowth of injured spinal cord. *Neuropathology.* 2010; 30:205-217.
 27. Zeng R, Wang LW, Hu ZB, Guo WT, Wei JS, Lin H, Sun X, Chen LX, Yang LJ. Differentiation of human bone marrow mesenchymal stem cells into neuron-like cells *in vitro*. *Spine (Phila Pa 1976).* 2011; 36:997-1005.
 28. Tan Y, Uchida K, Nakajima H, Guerrero AR, Watanabe S, Hirai T, Takeura N, Liu SY, Johnson WE, Baba H. Blockade of interleukin 6 signaling improves the survival rate of transplanted bone marrow stromal cells and increases locomotor function in mice with spinal cord injury. *J Neuropathol Exp Neurol.* 2013; 72:980-993.
 29. Jones BJ, McTaggart SJ. Immunosuppression by mesenchymal stromal cells: from culture to clinic. *Exp Hematol.* 2008; 36:733-741.
 30. Sanchez-Ramos J, Song S, Cardozo-Pelaez F, Hazzi C, Stedeford T, Willing A, Freeman TB, Saporta S, Janssen W, Patel N, Cooper DR, Sanberg PR. Adult bone marrow stromal cells differentiate into neural cells *in vitro*. *Exp Neurol.* 2000; 164:247-256.
 31. Zhao T, Yan W, Xu K, Qi Y, Dai X, Shi Z. Combined treatment with platelet-rich plasma and brain-derived neurotrophic factor-overexpressing bone marrow stromal cells supports axonal remyelination in a rat spinal cord hemi-section model. *Cytherapy.* 2013; 15:792-804.

(Received February 2, 2014; Revised April 4, 2014;
Accepted April 8, 2014)

EPA and DHA increased PPAR γ expression and decreased integrin-linked kinase and integrin β 1 expression in rat glomerular mesangial cells treated with lipopolysaccharide

Wenchao Han¹, Hui Zhao², Bo Jiao^{2,*}, Fange Liu^{1,3,*}

¹ Department of Pediatrics, the Second Affiliated Hospital of Shandong University, Ji'nan, Shandong, China;

² Department of Pharmacology, School of Pharmaceutical Science, Shandong University, Ji'nan, Shandong, China;

³ Department of Pediatrics, Qilu Hospital of Shandong University, Ji'nan, Shandong, China.

Summary

Fish oil containing n-3 polyunsaturated fatty acids (n-3 PUFAs) including eicosapentaenoic acid (EPA) and docosahexaenoic acid (DHA) is known to prevent the progression of nephropathy and retard the progression of kidney disease. This study sought to investigate the underlying mechanisms of EPA and DHA in terms of peroxisome proliferator-activated receptor γ (PPAR γ), integrin-linked kinase (ILK), and integrin β 1 expression in glomerular mesangial cells (GMCs) because of their critical roles in the development and progression of nephropathy. Lipopolysaccharide (LPS) significantly reduced the expression of PPAR γ and increased the expression of ILK at the mRNA level and at the protein level in GMCs as indicated by real-time PCR and Western blotting. In addition, LPS increased integrin β 1 expression in GMCs at the mRNA level. Treatment with EPA and DHA significantly increased the expression of PPAR γ and decreased the expression of ILK and integrin β 1 in GMCs. These data suggest that the renoprotective effects of EPA and DHA may be related to their potential to increase the expression of PPAR γ and decrease the expression of ILK and integrin β 1.

Keywords: Eicosapentaenoic acid, docosahexaenoic acid, mesangial cells, PPAR γ , integrin-linked kinase, integrin

1. Introduction

Glomerular diseases are a leading cause of chronic and end-stage kidney failure worldwide, and an array of glomerular diseases is distinguished by glomerular mesangial cell (GMC) injury, including membranoproliferative glomerulonephritis, IgA nephropathy, and diabetic nephropathy. In a pathophysiological state, GMCs typically lead to expansion of the mesangial matrix and they undergo cell proliferation and hypertrophy and apoptosis. The phenomena are closely correlated with deterioration

of renal function, so GMCs have long been considered an important factor in progressive renal failure (1).

Integrin-linked kinase (ILK) is known to be a widely expressed serine/threonine protein kinase localized to focal adhesion plaques and centrosomes (2,3). ILK plays a fundamental role in the regulation of cell survival, proliferation, and migration by connecting the cytoplasmic domains of β -integrins to the actin cytoskeleton, mediating integrin signaling in diverse cell types (3). An increase in the ILK level in the mesangium is associated with diffuse mesangial expansion. ILK is a downstream mediator of integrin β 1 activity, and integrin/ILK signal pathways are involved in the regulation of cell adhesion, changes in cell morphology, and extracellular matrix (ECM) deposition (4). Overexpression of ILK can result in ECM remodeling and cell proliferation by GMCs (5).

Peroxisome proliferator-activated receptors (PPARs) are members of the nuclear hormone receptor family consisting of three subtypes (α , δ , and γ) with distinct and overlapping expression patterns (6). These lipid-

*Address correspondence to:

Dr. Fange Liu, Department of Pediatrics, the Second Affiliated Hospital of Shandong University, Ji'nan, Shandong, China.

E-mail: liufe@sdu.edu.cn

Dr. Bo Jiao, Department of Pharmacology, School of Pharmaceutical Science, Shandong University, Ji'nan, Shandong, China.

E-mail: jiaob@sdu.edu.cn

sensitive receptors regulate many important physiological processes including glucose and lipid metabolism, energy homeostasis, cell proliferation, inflammation, immunity and reproduction (7). PPAR γ is expressed in several types of tissue, including kidney tissue. In addition to regulating glucose and lipid metabolism, PPAR γ has antiinflammatory and anti-fibrotic action in kidney diseases (8).

Eicosapentaenoic acid (EPA, C20:5 n-3) and docosahexaenoic acid (DHA, C22:6 n-3), which belong to the n-3 polyunsaturated fatty acid (PUFA) family, are the main components of fish oil from deep sea fish. Fish oil, a type of PPAR γ natural ligand, has been reported to slow the progress of kidney disease. A diet rich in n-3 PUFA, like EPA and DHA, has been associated with reduced triacylglycerol (TAG) levels, anti-inflammatory action, pulmonary disease (9), and a lowered risk of cardiovascular disease and mortality (10-13). A higher dietary intake of PUFA may protect against progression of chronic kidney disease (14). Clinical trials have provided conflicting results with regard to the efficacy of n-3 PUFA in treating IgA nephropathy, although *in vitro* and *in vivo* experimental studies have indicated that n-3 PUFA act on inflammatory pathways involved in the progression of kidney disease (15).

Despite increasing knowledge of the beneficial effects of fish oil in treating nephropathy, the exact mechanisms underlying its renoprotective effects are not fully understood. Previous studies by the current authors showed that EPA and DHA inhibited the proliferation of GMCs induced by lipopolysaccharide (LPS) (16). Furthermore, the protective effects of EPA and DHA on the kidney were found to be related to their action to suppress TGF- β 1 and MCP-1 expression in GMCs (17). In addition, EPA and DHA may protect GMCs by regulating the imbalance of MMP and TIMP expression (18). The present study sought to examine the effects of EPA and DHA on the expression of PPAR γ , ILK, and integrin β 1 in rat GMCs in order to further investigate the renoprotective action of fish oil.

2. Materials and Methods

2.1. Chemicals and antibodies

EPA, DHA, and LPS were purchased from Sigma-Aldrich (St. Louis, MO, USA). RPMI 1640 and fetal bovine serum (FBS) were purchased from Life Technologies (Carlsbad, CA, USA). Rabbit anti-rat ILK and rabbit anti-rat PPAR γ were from Santa Cruz Biotechnology (Dallas, TX, USA). Monoclonal antibody against β -actin was purchased from

Beijing Jing Mei Biotechnology (Beijing, China). All primers were synthesized by BioSune (Shanghai, China). Green real-time PCR master mix was purchased from Toyobo Biotech (Shanghai, China).

2.2. Cell culture

Rat GMCs (HBZY-1) were purchased from the Chinese Center for Typical Culture Collection (Wuhan, Hubei, China). GMCs were routinely cultured in RPMI-1640 media supplemented with 10% FBS. For experiments, GMCs were divided into six groups: *i*) Control group: cells were cultured in RPMI-1640 during the entire study; *ii*) LPS group: cells were treated with 10 μ g/mL LPS; *iii*) Low-dose EPA group: cells were treated with 10 μ g/mL LPS and 10 μ mol/L EPA; *iv*) High-dose EPA group: cells were treated with 10 μ g/mL LPS and 100 μ mol/L EPA; *v*) Low-dose DHA group: cells were treated with 10 μ g/mL LPS and 10 μ mol/L DHA; *vi*) High-dose DHA group: cells were treated with 10 μ g/mL LPS and 100 μ mol/L DHA. Each experiment was repeated three times.

2.3. RNA isolation and quantitative real-time polymerase chain reaction (PCR)

After incubation for 24 h or 48 h, GMCs were harvested and total RNA was extracted using TRIzol reagent (Invitrogen, Carlsbad, CA, USA) according to the manufacturer's protocol. Complement DNA (cDNA) was synthesized using a Super Script III first strand cDNA synthesis Kit (Invitrogen). Real-time PCR was performed with SYBR Green PCR Master Mix kits (Applied Biosystems, Foster City, CA, USA) and an ABI Prism 7900HT Sequence Detection System (Applied Biosystems, Foster City, CA, USA). Gene-specific primer sequences are listed in Table 1.

β -Actin was used as an internal control to quantify mRNA expression. The relative expression of the target gene = intensity of fluorescence of target gene fragments/intensity of fluorescence of the β -actin gene. Cycling conditions were 94°C, 3 min, followed by 40 cycles of 94°C, 30 sec; 60°C, 30 sec; and 72°C, 1 min.

2.4. Western blotting

After incubation for 24 h or 48 h, cells were harvested and lysed. The protein concentration was determined using the Coomassie Brilliant Blue method. Equal amounts of lysate proteins from whole-cell lysates were loaded onto

Table 1. Primer pairs used in RT-PCR

Gene	Forward (5'-3')	Reverse (5'-3')
PPAR γ	AACCGGAACAAATGCCAGTA	TGGCAGCAGTGGGAAGAATCG
ILK	CTTCTGTGGGAAGTGGTGAC	CACATGGGGGAAATACCTG
Integrin β 1	AGGAGGAGTAAAGTAAAGTAG	AACCACCATAACAAAATGGG
β -Actin	GGCTGTATCCCTCCATCG	CCAGTTGGTAACAATGCCATGT

10% gels and separated using SDS-PAGE. Then gels were transferred to a polyvinylidene difluoride membrane. After blocking for 2 h at room temperature in blocking buffer, the membrane was incubated overnight with rabbit anti-rat PPAR γ or rabbit anti-rat ILK. Blots were washed and then incubated with a secondary goat antibody raised against rabbit IgG conjugated to horseradish peroxidase. After further washing, the bound antibodies were visualized using an ECL kit, and band densities were measured using TINA imaging software (Raytest, Straubenhardt, Germany). The level of β -actin protein served as a protein loading control.

2.5. Statistical analysis

Data are expressed as mean \pm SD. One-way ANOVA followed by Dunnett's test was performed using SPSS/Win11.0 software (SPSS, Inc., Chicago, IL, USA). A significant difference was defined as $p < 0.05$.

3. Results

3.1. EPA and DHA increased PPAR γ expression in GMCs

The effects of EPA and DHA on PPAR γ expression were examined at the mRNA level and at the protein level in GMCs treated with LPS.

PPAR γ protein expressed by GMCs was evaluated using Western blotting. Exposure of cultured GMCs to 10 μ g/mL LPS induced a significant decrease in PPAR γ expression in comparison to that in the control group ($p < 0.01$ at 24 h and 48 h, Figure 1). Incubation GMCs cultured with 10 μ g/mL LPS and treated with EPA (100 μ mol/L) or DHA (100 μ mol/L) for 24 h resulted in a significant increase in PPAR γ protein expression ($p < 0.01$, vs. LPS group, Figure 1A). In addition, incubation of GMCs treated with 100 μ mol/L of EPA or 10 μ mol/L or 100 μ mol/L of DHA for 48 h markedly increased the expression of PPAR γ ($p < 0.05$ or $p < 0.01$, vs. LPS group, Figure 1B).

Levels of PPAR γ mRNA in GMCs were determined using real-time PCR. As shown in Figure 2, the ratio of the

level of PPAR γ mRNA to the level of β -actin mRNA was determined to be 1.0 for the control group, and this value decreased dramatically to 0.68 (24 h, $p < 0.05$) and 0.31 (48 h, $p < 0.01$) for the LPS group. Incubation of GMCs treated with EPA (10 μ mol/L and 100 μ mol/L) or DHA (10 μ mol/L and 100 μ mol/L) for 24 h (Figure 2A) and 48 h (Figure 2B) resulted in a significant increase in PPAR γ mRNA expression in comparison to that in the LPS group ($p < 0.05$ or $p < 0.01$).

3.2. EPA and DHA reduced ILK expression in GMCs

The rise in the ILK level in the mesangium is associated with diffuse mesangial expansion. Whether EPA or DHA is able to diminish ILK expression in GMCs was ascertained at the mRNA level and at the protein level.

ILK protein expressed by GMCs was evaluated using Western blotting. Exposure of cultured GMCs to 10 μ g/mL LPS induced a significant increase in ILK expression in comparison to that in the control group ($p < 0.01$ at 24 and 48 h, Figure 3). Incubation of GMCs treated with EPA

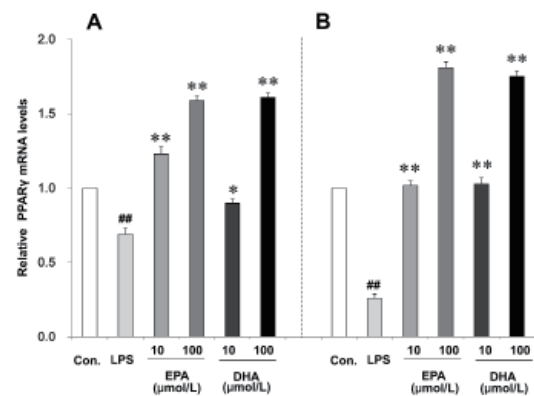


Figure 2. Effects of EPA and DHA on PPAR γ mRNA expression in GMCs. PPAR γ mRNA expression was determined with real-time PCR at 24 h (A) and 48 h (B). The level of mRNA expression was normalized to that of β -actin. # $p < 0.01$, vs. control group. * $p < 0.05$, ** $p < 0.01$, vs. LPS group.

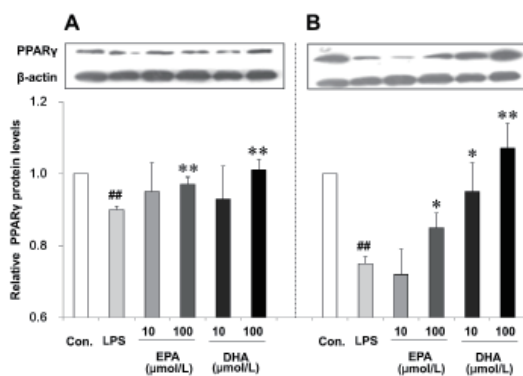


Figure 1. Effects of EPA and DHA on PPAR γ protein expression in GMCs. Expression of PPAR γ was detected using Western blotting at 24 h (A) and 48 h (B). # $p < 0.01$, vs. control group. * $p < 0.05$, ** $p < 0.01$, vs. LPS group.

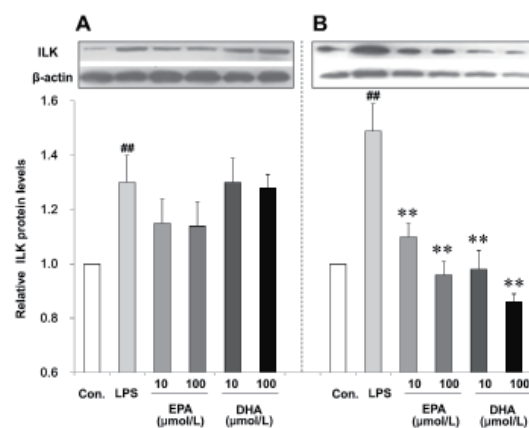


Figure 3. Effects of EPA and DHA on ILK protein expression in GMCs. Expression of ILK was detected using Western blotting at 24 h (A) and 48 h (B). # $p < 0.01$, vs. control group. ** $p < 0.01$, vs. LPS group.

(10 $\mu\text{mol/L}$ and 100 $\mu\text{mol/L}$) or DHA (10 $\mu\text{mol/L}$ and 100 $\mu\text{mol/L}$) for 24 h had no significant effect on ILK protein expression ($p > 0.05$, vs. LPS group, Figure 3A). However, incubation of GMCs treated with 10 $\mu\text{mol/L}$ or 100 $\mu\text{mol/L}$ of EPA or 10 $\mu\text{mol/L}$ or 100 $\mu\text{mol/L}$ of DHA for 48 h significantly decreased the expression of ILK protein ($p < 0.01$, Figure 3B).

Levels of ILK mRNA in GMCs were determined using real-time PCR. As shown in Figure 4, the levels of ILK mRNA dramatically increased in the LPS group ($p < 0.01$ at 24 h and 48 h). Incubation of GMCs treated with EPA (10 $\mu\text{mol/L}$ and 100 $\mu\text{mol/L}$) or DHA (10 $\mu\text{mol/L}$ and 100 $\mu\text{mol/L}$) for 24 h resulted in a significant decrease in ILK mRNA expression in comparison to that in the LPS group ($p < 0.01$, Figure 4A). Incubation of GMCs treated with 100 $\mu\text{mol/L}$ of EPA or 10 $\mu\text{mol/L}$ or 100 $\mu\text{mol/L}$ of DHA for 48 h significantly decreased the expression of ILK mRNA ($p < 0.05$ or $p < 0.01$ vs. LPS group, Figure 4B).

3.3. EPA and DHA reduced integrin $\beta 1$ expression in GMCs

ILK is a downstream mediator of integrin $\beta 1$ activity, and integrin/ILK signal pathways are involved in the regulation of cell adhesion, changes in cell morphology, and ECM deposition. Whether EPA or DHA was able to diminish integrin $\beta 1$ mRNA expression in GMCs was ascertained.

Levels of integrin $\beta 1$ mRNA in GMCs were determined using real-time PCR. As shown in Figure 5, the levels of integrin $\beta 1$ mRNA dramatically increased in LPS-treated cells ($p < 0.01$ at 24 h and 48 h, vs. control group). Incubation of GMCs treated with EPA (100 $\mu\text{mol/L}$) for 24 h resulted in a significant decrease in integrin $\beta 1$ mRNA expression in comparison to that in the LPS group ($p < 0.05$; Figure 5A). Incubation of GMCs treated with 10 $\mu\text{mol/L}$ or 100 $\mu\text{mol/L}$ of EPA or 10 $\mu\text{mol/L}$ or 100 $\mu\text{mol/L}$ of DHA for 48 h significantly decreased the expression of integrin $\beta 1$ mRNA in comparison to that in the LPS group ($p < 0.05$ or $p < 0.01$, Figure 5B).

4. Discussion

This study investigated the mechanisms underlying the renoprotective effect of EPA and DHA in GMCs *in vitro*. Results indicated that EPA and DHA significantly increased the expression of PPAR γ and reduced the expression of ILK and integrin $\beta 1$ in GMCs, and these levels of expression changed dramatically when cells were cultured with LPS. These results suggest that the renoprotective effects of EPA and DHA are possibly related to their effects on the expression of PPAR γ , ILK, and integrin $\beta 1$ in GMCs.

PPAR γ plays an important role in mesangial cells responding to inflammatory stress. PPAR γ protein expression increased dramatically in human mesangial cells stimulated with interleukin-1 β (IL-1 β), and the levels of interleukin-6 (IL-6) and tumor necrosis factor

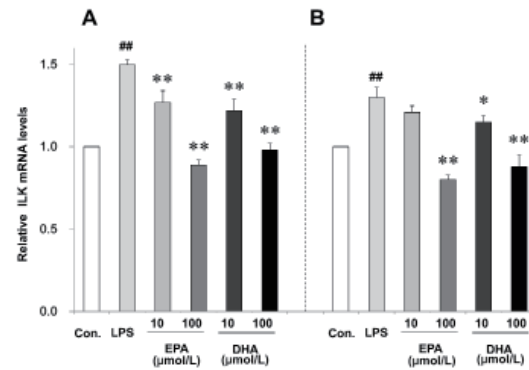


Figure 4. Effects of EPA and DHA on mRNA expression of ILK in GMCs. ILK mRNA expression was determined with real-time PCR at 24 h (A) and 48 h (B). The level of mRNA expression was normalized to that of β -actin. ## $p < 0.01$, vs. control group. * $p < 0.05$, ** $p < 0.01$, vs. LPS group.

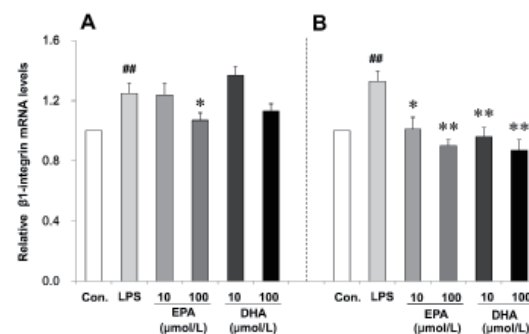


Figure 5. Effects of EPA and DHA on integrin $\beta 1$ mRNA expression in GMCs. Integrin $\beta 1$ mRNA expression was determined with real-time PCR at 24 h (A) and 48 h (B). The level of mRNA expression was normalized to that of β -actin. ## $p < 0.01$, vs. control group. * $p < 0.05$, ** $p < 0.01$, vs. LPS group.

α (TNF α) increased significantly in comparison to those in untreated cells (19). A key finding is that PPAR γ agonists, including troglitazone, rosiglitazone, and prostaglandin J2, significantly decrease the increased expression of TNF α and IL-6 (19). Rosiglitazone inhibits mesangial cell proliferation by blocking reactive oxygen species (ROS)-dependent epidermal growth factor receptor (EGFR) intracellular signaling, and telmisartan has powerful anti-inflammatory action *via* PPAR γ activation in mesangial cells (20). PPAR γ may prove to be a pharmacological target for treatment of glomerulonephritis (19). Fish oil reduced an LPS-induced inflammatory response in HK-2 cells *via* a PPAR γ dependent pathway (21). The current results indicated that both EPA and DHA effectively up-regulated PPAR γ mRNA and protein expression. Thus, fish oil may play a role by activating PPAR γ . PPAR γ agonists are effective in delaying and even preventing the progression of many renal diseases (7). These data suggest that PPAR γ plays an important role in the response of mesangial cells to inflammatory stress. PPAR γ may represent a potential target for the treatment of renal diseases (7).

ILK is a focal adhesion adaptor and a serine/threonine

protein kinase that regulates cell proliferation, survival, epithelial-mesenchymal transition (EMT), and kidney development (22,23). It acts as a central component of a heterotrimer (the PINCH-ILK-parvin complex) at ECM adhesions, mediating interactions with a large number of proteins via multiple sites including its pseudoactive site. ILK links integrins to the actin cytoskeleton and catalytic proteins and thereby regulates focal adhesion assembly, cytoskeleton organization, and signaling (24). Increased activity of ILK and integrin $\beta 1$ in GMCs may contribute to the development of sustained mesangial cell proliferation and lead to glomerular scarring (5). In aging kidneys, integrin $\beta 1$ and ILK may be involved in the process of fibrosis and related senescence (25). ILK also plays an important role in the pathogenesis of nephropathy in GMCs and also in podocytes of the kidney (26,27). In the present study, EPA and DHA decreased the expression of ILK and integrin $\beta 1$ in GMCs stimulated with LPS. This finding confirms the assertion that ILK and integrin $\beta 1$ play a role in lipid-induced kidney injury.

Interestingly, there may be a relationship between PPAR γ and ILK. A study found that fish oil inhibited the proliferation of non-small cell lung carcinoma by suppressing ILK expression via activation of PPAR γ (28).

In summary, the present study suggests that EPA and DHA are capable of increasing PPAR γ expression and decreasing ILK and integrin $\beta 1$ expression in GMCs treated with LPS. This study provides novel insights into the mechanisms of the renoprotective effects of fish oil.

Acknowledgement

This work was supported by a grant from the Shandong Provincial Natural Science Foundation (ZR2013HM099), China.

References

- Mason RM, Wahab NA. Extracellular matrix metabolism in diabetic nephropathy. *J Am Soc Nephrol.* 2003; 14:1358-1373.
- Fielding AB, Dobreva I, Dedhar S. Beyond focal adhesions: Integrin-linked kinase associates with tubulin and regulates mitotic spindle organization. *Cell Cycle (Georgetown, Tex.).* 2008; 7:1899-1906.
- McDonald PC, Fielding AB, Dedhar S. Integrin-linked kinase-essential roles in physiology and cancer biology. *J Cell Sci.* 2008; 121:3121-3132.
- Wu C, Dedhar S. Integrin-linked kinase (ILK) and its interactors: A new paradigm for the coupling of extracellular matrix to actin cytoskeleton and signaling complexes. *J Cell Bio.* 2001; 155:505-510.
- Kagami S, Shimizu M, Kondo S, Kitamura A, Urushihara M, Takamatsu M, Yamaji S, Ishigatsubo Y, Kawachi H, Shimizu F. Up-regulation of integrin-linked kinase activity in rat mesangioproliferative glomerulonephritis. *Life Sci.* 2006; 78:1794-1800.
- Madrazo JA, Kelly DP. The PPAR trio: Regulators of myocardial energy metabolism in health and disease. *J Molec and Cellular Cardiol.* 2008; 44:968-975.
- Yang J, Zhou Y, Guan Y. PPAR γ as a therapeutic target in diabetic nephropathy and other renal diseases. *Curr Opin Nephrol and Hypertens.* 2012; 21:97-105.
- Sarafidis PA, Bakris GL. Protection of the kidney by thiazolidinediones: An assessment from bench to bedside. *Kidney Intl.* 2006; 70:1223-1233.
- Omernik A. Supplementation of n-3 polyunsaturated fatty acids in pulmonary disease. *Pol Merkur Lekarski.* 2012; 32:55-58.
- Harris WS, Miller M, Tighe AP, Davidson MH, Schaefer EJ. Omega-3 fatty acids and coronary heart disease risk: Clinical and mechanistic perspectives. *Atherosclerosis.* 2008; 197:12-24.
- Moertl D, Hammer A, Steiner S, Hutuleac R, Vonbank K, Berger R. Dose-dependent effects of omega-3-polyunsaturated fatty acids on systolic left ventricular function, endothelial function, and markers of inflammation in chronic heart failure of nonischemic origin: A double-blind, placebo-controlled, 3-arm study. *Am Heart J.* 2011; 161:915.e911-919.
- Mizia-Stec K, Haberka M, Mizia M, Chmiel A, Gieszczyk K, Lasota B, Janowska J, Zahorska-Markiewicz B, Gasior Z. N-3 Polyunsaturated fatty acid therapy improves endothelial function and affects adiponectin and resistin balance in the first month after myocardial infarction. *Arch Med Sci.* 2011; 7:788-795.
- Sorice M, Tritto FP, Sordelli C, Gregorio R, Piazza L. N-3 polyunsaturated fatty acids reduces post-operative atrial fibrillation incidence in patients undergoing "on-pump" coronary artery bypass graft surgery. *Monaldi Arch. Chest Dis.* 2011; 76:93-98.
- Lauretani F, Maggio M, Pizzarelli F, Michelassi S, Ruggiero C, Ceda GP, Bandinelli S, Ferrucci L. Omega-3 and renal function in older adults. *Curr Pharm Des.* 2009; 15:4149-4156.
- Fassett RG, Gobe GC, Peake JM, Coombes JS. Omega-3 polyunsaturated fatty acids in the treatment of kidney disease. *Am J Kidney Dis.* 2010; 56:728-742.
- Geng WJ, Liu FE, Jiao B, Cheng YN. Effects of EPA and DHA on the proliferation and apoptosis of glomerular mesangial cells induced by lipopolysaccharide. *J Shandong Univ (Health Sciences).* 2008; 46:57-59.
- Hu XJ, Geng WJ, Jiao B, Liu FE. Protective effects of EPA and DHA on lipopolysaccharide-stimulated rat mesangial cells. *Chin J Pathophysiol.* 2010; 26:513-517.
- Zhao H, Hu XJ, Liu FE, Cheng YN, Jiao B. Effects of EPA and DHA on MMPs, TIMPs and TGF- $\beta 1$ expression by lipopolysaccharide-stimulated rat glomerular mesangial cells. *Chin J Biochem Pharmaceutics.* 2012; 33:221-224.
- Xiong Z, Huang H, Li J, Guan Y, Wang H. Anti-inflammatory effect of PPAR γ in cultured human mesangial cells. *Ren Fail.* 2004; 26:497-505.
- Yuan Y, Zhang A, Huang S, Ding G, Chen R. A PPAR γ agonist inhibits aldosterone-induced mesangial cell proliferation by blocking ROS-dependent EGFR intracellular signaling. *Am J Physiol Renal Physiol.* 2011; 300:F393-402.
- Li H, Ruan XZ, Powis SH, Fernando R, Mon WY, Wheeler DC, Moorhead JF, Varghese Z. EPA and DHA reduce LPS-induced inflammation responses in HK-2 cells: Evidence for a PPAR- γ -dependent mechanism. *Kidney Int.* 2005; 67:867-874.
- Serrano I, McDonald PC, Lock FE, Dedhar S. Role of the integrin-linked kinase (ILK)/Rictor complex in TGF $\beta 1$ -induced epithelial-mesenchymal transition (EMT).

- Oncogene. 2013; 32:50-60.
23. Matsuura S, Kondo S, Suga K, Kinoshita Y, Urushihara M, Kagami S. Expression of focal adhesion proteins in the developing rat kidney. *J Histochem Cytochem.* 2011; 59:864-874.
 24. Qin J, Wu C. ILK: A pseudokinase in the center stage of cell-matrix adhesion and signaling. *Curr Opin Cell Biol.* 2012; 24:607-613.
 25. Li Z, Chen X, Xie Y, Shi S, Feng Z, Fu B, Zhang X, Cai G, Wu C, Wu D, Gu Y. Expression and significance of integrin-linked kinase in cultured cells, normal tissue, and diseased tissue of aging rat kidneys. *J Gerontol. J Gerontol A Biol Sci Med Sci.* 2004; 59:984-996.
 26. Dai C, Stolz DB, Bastacky SI, St-Arnaud R, Wu C, Dedhar S, Liu Y. Essential role of integrin-linked kinase in podocyte biology: Bridging the integrin and slit diaphragm signaling. *J Am Soc of Nephrol.* 2006; 17:2164-2175.
 27. Han SY, Kang YS, Jee YH, Han KH, Cha DR, Kang SW, Han DS. High glucose and angiotensin II increase β 1 integrin and integrin-linked kinase synthesis in cultured mouse podocytes. *Cell Tissue Res.* 2006; 323:321-332.
 28. Han S, Sun X, Ritzenthaler JD, Roman J. Fish oil inhibits human lung carcinoma cell growth by suppressing integrin-linked kinase. *Molec Cancer Res.* 2009; 7:108-117.

(Received March 10, 2014; Revised April 19, 2014; Accepted April 23, 2014)

Substrate specificity of human granzyme 3: Analyses of the P3-P2-P1 triplet using fluorescence resonance energy transfer substrate libraries

Yukiyo Hirata*, Hirofumi Inagaki, Takako Shimizu, Tomoyuki Kawada

Department of Hygiene and Public Health, Nippon Medical School, Tokyo, Japan.

Summary

Granzyme 3 (Gr3) is known as a tryptase-type member of the granzyme family and exists in the granules of immunocompetent cells. Granule proteases including granzymes, are transported into the cytoplasm of tumor cells or virus-infected cells by perforin function, degrade cytoplasmic or nuclear proteins and subsequently cause the death of the target cells. Recently, although several substrates of Gr3 *in vivo* have been reported, these hydrolyzed sites were unclear or lacked consistency. Our previous study investigated the optimal amino acid triplet (P3-P2-P1) as a substrate for Gr3 using a limited combination of amino acids at the P2 and P3 positions. In the present study, new fluorescence resonance energy transfer (FRET) substrate libraries to screen P2 and P3 positions were synthesized, respectively. Using these substrate libraries, the optimal amino acid triplet was shown to be Tyr-Phe-Arg as a substrate for human Gr3. Moreover, kinetic analyses also showed that the synthetic substrate FRETs-YFR had the lowest K_m value for human Gr3. A substantial number of membrane proteins possessed the triplet Tyr-Phe-Arg and some of them might be *in vivo* substrates for Gr3. The results might also be a great help for preparing specific inhibitors to manipulate Gr3 activity both *in vitro* and *in vivo*.

Keywords: Granzyme, serine protease, cytotoxic T lymphocytes

1. Introduction

Granzyme 3 (Gr3; also called granzyme K) is known as a member of the protease family named granzymes, and exists in the cytotoxic granules of cytotoxic cells in the immune-system (1,2). Proteases in the granules of NK cells and cytotoxic T-lymphocytes are introduced into their target cells, such as virus-infected cells and tumor cells, *via* a perforin-mediated mechanism, then hydrolyze cytosolic and/or nuclear proteins, and kill the cells (3). Five kinds of granzymes have been identified in humans. Two of them, granzyme A and Gr3, are known to show tryptase-type specificity and to cleave the peptide bond on the carboxylic side of a basic amino acid, Lys or Arg (4). Recently, some *in vitro* and *in vivo* substrates of Gr3 have been reported, however, some of

their cleavage sites are unclear and the proposed amino acid sequences of the hydrolysis site differ among reports (4-8).

In order to clarify the *in vivo* function of Gr3 and to develop specific inhibitors for the manipulation of enzymatic activity *in vivo*, analysis of the *in vitro* specificity of Gr3 is being attempted.

Fluorescence resonance energy transfer (FRET) is a phenomenon in which electronic excitation energy can be efficiently transferred between a fluorescent energy donor and a suitable energy acceptor. FRET is often applied to determine the distance between a donor fluorophore and an acceptor fluorophore on the basis of intramolecular FRET (9). The FRET substrate (FRETs) contains a fluorescent 2-(*N*-methylamino) benzoyl (NMA) group as a donor fluorophore and a 2,4-dinitrophenyl (DNP) group as an acceptor in the molecule. When an enzyme cleaves any peptide bond between NMA and DNP in the substrate, the fluorescence at 440 nm with excitation at 340 nm increases in proportion to the release of the NMA fluorophore from the internal DNP quencher (10). The

*Address correspondence to:

Dr. Yukiyo Hirata, Department of Hygiene and Public Health, Nippon Medical School, 1-1-5 Sendagi, Bunkyo-ku, Tokyo 113-8602, Japan.
E-mail: yuki-hir@nms.ac.jp

FRET substrate allows us to determine the enzymatic hydrolysis of a peptide bond between amino acids.

We previously investigated the optimal amino acid triplet (P3-P2-P1) as a substrate for Gr3 using FRET libraries. As the P1 residue, Arg, is better than Lys by Gr3. Out of 25 P3-P2 combinations, Phe-Tyr was the sequence that reacted the most with Gr3 (11); however, the result was obtained using a substrate library with limited amino acid sequences. Therefore, in order to elucidate the optimal amino acid sequence of Gr3, new peptide substrate libraries were prepared in the present study. Using the new libraries, the optimal triplet was defined.

2. Materials and Methods

2.1. Materials

FRETS-25Arg, FRETS-F19R, and FRETS-19FR were synthesized by the Peptide Institute, Inc. (Osaka, Japan). FRETS-25-STD1 (*N*-β-[2-(*N*-methylamino)benzoyl]-2,3-diaminopropionyl-glycine) was also purchased from the Peptide Institute, Inc. The micro BCA Protein Assay Reagent kit was obtained from Thermo Fisher Scientific Inc. (Waltham, MA, USA). *N*-α-Benzoyloxycarbonyl-lysine thiobenzyl ester (BLT) was purchased from Sigma-Aldrich Corp. (St. Louis, MO, USA). Trifluoroacetic acid (TFA) and acetonitrile (MeCN) for high performance liquid chromatography (HPLC) analysis were purchased from Kanto Chemical Co. (Tokyo, Japan). Wakosil-II 5C18 RS was purchased from Wako Pure Chemical Ind., Ltd. (Osaka, Japan). Other chemicals used were all of analytical grade.

2.2. Recombinant human Gr3

Recombinant human Gr3 was produced and purified as previously described (11). The protein concentration was determined by a bicinchoninic acid assay (BCA assay). Gr3 activity was determined as the hydrolysis of BLT. Purified protein was dissolved in 10 mM potassium phosphate buffer, pH 6.0, 1 M NaCl, supplemented with 0.1% Triton X-100 to prevent adsorption to the tubes, divided into aliquots in siliconized tubes (Sarstedt K.K., Tokyo, Japan), and stored at -80°C until use.

2.3. FRET substrate (FRETS) libraries

Three sets of libraries were used in this study (Figure 1). The libraries were prepared by the Peptide Institute, Inc. Based on the structure of FRETS-25Arg, which was used in the previous study, new libraries were prepared. These fluorescence resonance energy transfer substrates contain a highly fluorescent NMA group and an efficiently quenched DNP group in the molecule. When an enzyme cleaves any peptide bond between

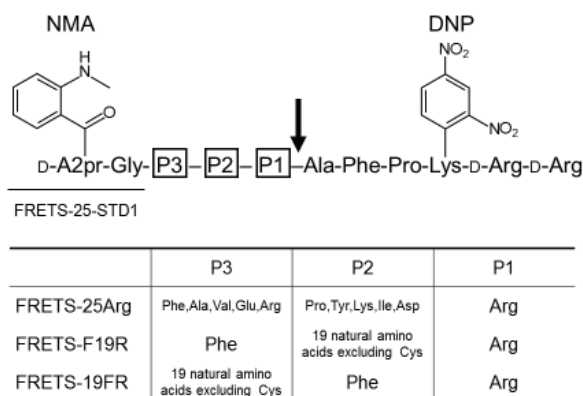


Figure 1. Structure of fluorescence resonance energy transfer substrates (FRETS) used in the present study. The arrow shows the desired hydrolytic site for Gr3. The structure of FRETS-25-STD1 used for the calibration standard is also shown.

NMA and DNP in the substrate, the fluorescence at 440 nm with excitation at 340 nm increases in proportion to the release of the NMA fluorophore from the internal DNP quencher (10).

To analyze the specificity at the P2 position, FRETS-F19R was designed. The P1 position of the substrate sequence was fixed as Arg according to our results using the FRETS-25Xaa series, as described previously (11). Because the substrate carrying the Phe-Tyr-Arg (P3-P2-P1) triplet contained in the FRETS-25Arg library was hydrolyzed the fastest by Gr3 (11), Phe was employed at the P3 position. The P1 and P3 positions were fixed with Arg and Phe, respectively, and each of the 19 amino acids excluding Cys was incorporated in the P2 position in the FRETS-F19R library.

Based on the results obtained with FRETS-F19R, FRETS-19FR was designed to determine the specificity at the P3 position. The P1 and P2 positions were fixed with Arg and Phe, respectively. Each of the 19 amino acids excluding Cys was incorporated at the P3 position.

FRETS-YFR, FRETS-FFR, FRETS-WFR, and FRETS-VFR were isolated from the FRETS-19FR library using reversed-phase HPLC and used for kinetic analyses. The concentration of the purified substrate was determined using FRETS-25-STD1 as a reference standard.

2.4. Enzyme activity with FRET substrates

To 100 nM of purified Gr3 in 0.2 M Tris-HCl buffer (pH 8.0), 0.1 mM (final) FRET substrate was added and incubated for up to 15 min at 37°C. The enzymatic reactions were stopped with the addition of a 9-fold volume of 0.2% TFA. After filtration through a 0.45 μm membrane filter, a 100 μL aliquot was injected into HPLC. HPLC conditions used were the same as described previously (11). Hydrolytic activity was

determined from the peak area of the hydrolyzed product.

The amino-acid sequences of the separated products were identified according to the product description sheets of the libraries. In addition, some amino acid sequences were verified using the combination of absorption spectrometry and fluorescence analysis. The products containing Tyr were identified by detection with absorbance at 280 nm and fluorescence at 440 nm with excitation at 275 nm, which occurred by fluorescence energy transfer from Tyr to NMA. Similarly, a Trp-containing product was confirmed by detection of fluorescence at 440 nm with excitation at 295 nm.

2.5. Kinetic analyses

For determination of the kinetic parameters, Gr3 (5 nM) was incubated with 16 to 80 μ M of each FRET substrate, FRET-S-YFR, FRET-S-FFR, FRET-S-WFR or FRET-S-VFR, for 15 min at 37°C. Then a 9-fold volume of 0.2% TFA was added to stop the reaction. After filtration through a 0.45 μ m membrane filter, a 100 μ L aliquot was injected into HPLC. HPLC conditions used were as follows. The column was Wakosil-II 5C18 RS (4.6 I.D. \times 150 mm) and was maintained at 45°C. Gradient elution was performed with mobile phase A (0.1% TFA in H₂O) and mobile phase B (0.1% TFA in MeCN). The flow-rate was set at 1.0 mL/min and the mobile phase composition was changed from 0% to 44% B over a period of 22 min. The products were detected by absorbance at 254 nm or fluorescence at 440 nm with excitation at 340 nm. The hydrolysis rate was determined as an increase of the peak area of cleaved products. Michaelis constants (K_m), the maximum velocities (V_{max}), k_{cat} values and k_{cat}/K_m values were calculated using Lineweaver-Burk plots (12).

2.6. The protein sequence library search

The proteins possessing YFR tripeptide, the amino acid sequence specifically decomposed by Gr3, were searched in the NCBI transcript sequence database using the gene and transcript searching system called GGRNA ver.1 (<http://ggrna.dbcls.jp/v1/>) (13). This system can quickly retrieve the information on the transcription product registered into the NCBI database according to the existence of short amino acid sequences, such as tripeptides. Multiple transcripts from a single gene and transcripts that are not identified at a protein level were excluded before analysis.

3. Results

3.1. Determination of the P2 position using FRET-S-F19R

To determine the optimal amino acid at the P2 position,

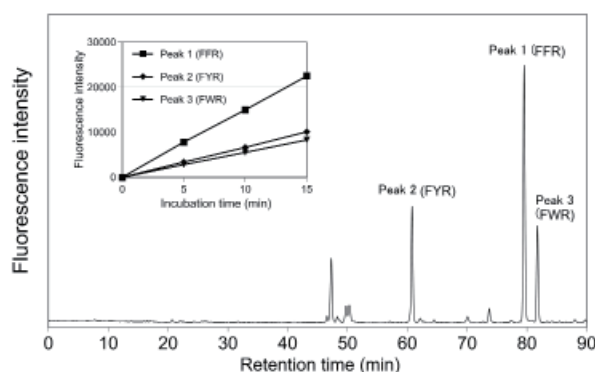


Figure 2. HPLC chromatogram of the hydrolyzed products of FRET-S-F19R by Gr3. FRET-S-F19R was incubated with Gr3 for 15 min at 37°C. Inset shows the peak area of peak 1 (FFR), peak 2 (FYR), and peak 3 (FWR). The amino acid sequence of these products is shown as P3-P2-P1 in one letter notation.

the FRET-S-F19R library was prepared (Figure 1). After reaction with Gr3, three major hydrolyzed products were observed (Figure 2). The peaks increased in a time-dependent manner (Figure 2 inset). By comparing the data with those of unhydrolyzed substrates and of the tryptic digest of FRET-S-F19R, peak 1 to 3 were identified as Phe-Phe-Arg, Phe-Tyr-Arg, and Phe-Trp-Arg, respectively. FRET-S hydrolyzed products were monitored under two conditions, absorption of Phe residue at 254 nm and fluorescence of NMA group at 440 nm with excitation at 340 nm. For the most abundant peak (peak 1), the ratio of absorbance at 254 nm to fluorescence at 440/340 nm was higher than that of other peaks (data not shown). This result showed that peak 1 was confirmed as the Phe-Phe-Arg product which contained more Phe residues than others. The retention time of peak 2 was the same as Phe-Tyr-Arg in the hydrolyzed product of FRET-S-25Arg under the same HPLC conditions; therefore, peak 2 was confirmed as Phe-Tyr-Arg. The third peak, eluted around 82 min, was identified as Phe-Trp-Arg according to the data provided by the manufacturer. In addition, when fluorescence at 440 nm was monitored with excitation at 295 nm, the height of peak 3 was markedly higher than other peaks (data not shown). This is due to the fluorescence energy transfer between Trp and NMA residues. First, Trp residues emit fluorescence at 340 nm by excitation at 295 nm, and the NMA group emits fluorescence at 440 nm by the emission of Trp residue at 340 nm. Thus, the products carrying the Trp residue showed fluorescence at 440 nm and excitation at 295 nm.

3.2. Determination of the P3 position by FRET-S-19FR

The FRET-S-19FR library for screening the optimal amino acid at the P3 position was prepared, in which P1 and P2 positions were fixed as Arg and Phe, respectively, and each of the 19 natural amino acids

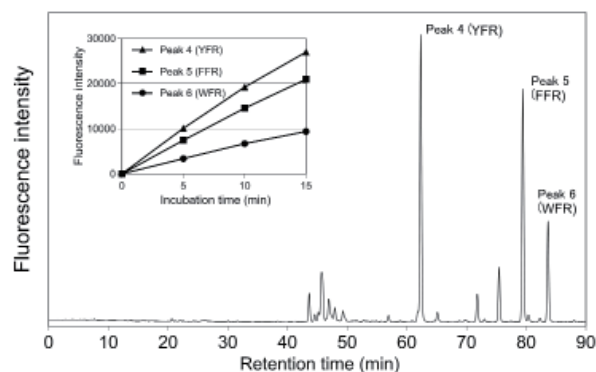


Figure 3. HPLC chromatogram of the hydrolyzed products of FRET-19FR by Gr3. FRET-19FR was incubated with Gr3 for 15 min at 37°C. Inset shows the peak area of peak 4 (YFR), peak 5 (FFR), and peak 6 (WFR).

excluding Cys appeared at the P3 position (Figure 1).

In the same way as FRET-F19R, FRET-19FR was hydrolyzed by Gr3 and analyzed by HPLC. Three major peaks, peaks 4 to 6, were identified as Tyr-Phe-Arg, Phe-Phe-Arg, and Trp-Phe-Arg, respectively (Figure 3).

The highest peak, peak 4, was identified as the Tyr-Phe-Arg product according to the analysis data of unhydrolyzed FRET-19FR. To confirm that peak 4 is a Tyr-carrying product, the HPLC analysis condition was changed; the fluorescence at 440 nm was monitored with excitation at 275 nm instead of 340 nm. Under this condition, peak 4 became higher than other peaks (data not shown). This result confirmed that peak 4 was a Tyr-Phe-Arg product, in which the fluorescence of Tyr residue at around 320 nm upon excitation at 275 nm acted as the excitation light for the NMA group. Retention time of peak 5 in FRET-19FR hydrolyzed products was the same as Phe-Phe-Arg, peak 1 in Figure 2; therefore, peak 5 was confirmed as Phe-Phe-Arg. Peak 6 showed strong fluorescence at 440 nm with excitation at 295 nm, which indicated that the Trp-containing product was eluted at peak 6 (data not shown); thus, peak 6 was confirmed as Trp-Phe-Arg.

All three peaks increased with time and peak 4 (Tyr-Phe-Arg) was the highest (Figure 3 inset). These results indicated that Tyr-Phe-Arg was the most suitable substrate sequence for Gr3 in the FRET-19FR library.

3.3. Kinetic analysis using FRET-YFR, FRET-FFR, FRET-WFR, and FRET-VFR

To analyze the reactivity of Gr3 more precisely, kinetic analyses were carried out using isolated FRET substrates. Four kinds of FRET substrates, FRET-YFR, FRET-FFR, FRET-WFR, and FRET-VFR, carrying Tyr-Phe-Arg, Phe-Phe-Arg, Trp-Phe-Arg, and Val-Phe-Arg, respectively, were isolated from FRET-19FR using HPLC.

Using these purified substrates, Gr3 activity was

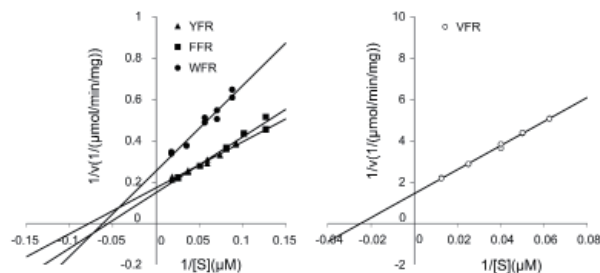


Figure 4. The Lineweaver-Burk plot of the hydrolysis of FRET substrates by Gr3. Gr3 was incubated with 16-80 μM of each FRET substrate for 15 min at 37°C. The hydrolyzed product was analyzed by HPLC. The results of FRET-VFR were separate from others, which are shown in a separate panel.

Table 1. The K_m , k_{cat} , and k_{cat}/K_m values for hydrolysis of FRET substrates by Gr3

Substrates	K_m (μM)	k_{cat} (s^{-1})	k_{cat}/K_m ($\text{s}^{-1}\cdot\text{M}^{-1}$)
FRET-VFR	37.7	0.31	8.23×10^3
FRET-FFR	18.1	3.14	1.74×10^5
FRET-WFR	16.3	1.84	1.13×10^5
FRET-YFR	13.0	2.72	2.11×10^5

assayed and Lineweaver-Burk plots were drawn (Figure 4). From these plots, the kinetic parameters for the four substrates were calculated (Table 1). Among the four, FRET-YFR showed the minimum K_m value of around 13.0 μM and the others were in the following order, WFR < FFR << VFR. On the other hand, FRET-FFR showed the maximum k_{cat} value and the others were in the following order FRET-YFR > WFR >> VFR.

When calculating the k_{cat}/K_m values, the order was FRET-YFR > FFR > WFR >> VFR (Table 1), which coincided with the order of the peak heights of the hydrolyzed FRET-19FR (Figure 3). These results indicated that the Tyr-Phe-Arg (P3-P2-P1) triplet was the most suitable substrate for human Gr3, under both purified and mixed conditions.

3.4. The proteins potentially hydrolyzed by Gr3

As a result of the library search using GGRNA, the number of human proteins that possess YFR tripeptide, the amino acid sequence specifically hydrolyzed by Gr3 were 769. Out of the 769 kinds of proteins, 222 proteins are membrane bound proteins.

4. Discussion

From the results using FRET-F19R, aromatic amino acids were considered more favorable at the P2 position for Gr3 substrate; however, the Phe-Phe-Arg substrate was hydrolyzed much faster than the other two (Phe-Tyr-Arg and Phe-Trp-Arg) and the selectivity of the P2 site amino acid by Gr3 seemed to be high.

Based upon the results with FRET-F19R, another substrate library, FRET-19FR, was prepared for the

analysis of P3 position selectivity.

Similar to the P2 position, Gr3 was shown to prefer aromatic amino acid at P3 position; however, the difference between the fastest Tyr-Phe-Arg and the second Phe-Phe-Arg was smaller than the case of the P2 position, indicating that the stringency of the amino acid specificity at P3 position was lower than at P2 position.

The results described above were obtained using a substrate library, mixtures of the substrates. In order to declare substrate specificity more precisely, kinetic analyses using purified substrates were needed. When comparing the kinetic parameters, Tyr-Phe-Arg substrate showed the smallest K_m value, indicating that human Gr3 showed the highest affinity for the triplet (Table 1). In addition, the k_{cat}/K_m values obtained from the kinetic study coincided well with the results of the hydrolysis pattern of the FRET-19FR library. The Tyr-Phe-Arg substrate proved to be the most favorable for human Gr3 also with purified FRET-19FR in addition to the substrate library mixture.

Mahrus and Craik (5) reported substrate specificity analysis of several granzymes using positional scanning synthetic combinatorial libraries (PS-SCL) of ACC substrates. Their results indicated that Tyr, Arg, Phe, and Lys were the most reactive with human GrK (equal to Gr3) for P4, P3, P2, and P1 positions, respectively. Based on the results, they concluded that the Tyr-Arg-Phe-Lys (P4-P3-P2-P1) quartet was the most suitable for human Gr3. Compared with our present results, only the P2 position was consistent. In particular, the difference of the P1 position was evident. This discrepancy might be due to differences in the structure of the carboxyl side of the P1 position. The FRET substrate used in the present study has an alanine residue at the P1' position, whereas the ACC substrate has a substituted coumarin group. This difference might affect the substrate recognition and/or enzymatic reaction.

Synthetic substrates, those that have *p*-nitroanilide (pNA) or 4-methylcoumarinamide (MCA) as chromogenic groups, were hydrolyzed much slower by Gr3 than by trypsin. Moreover, some of them were hardly hydrolyzed by Gr3 (11). These results suggested that an aromatic ring of pNA and MCA substrates might reduce the binding of these substrates to the active site of Gr3. In contrast, FRETs have oligopeptide structures in the potentially hydrolyzed position. Therefore, FRETs were suitable for analyzing substrate specificity and also for searching for the physiological substrates, because the *in vivo* targets of Gr3 are considered to be proteins.

In addition, in the PS-SCL method, the most suitable amino acid residue, was determined at each position individually and their combination was not analyzed. That might be the reason why their and the present results are not consistent. Their result for the

P3 position is similar to our previous results that Arg residue was the second choice for P3 position after Phe out of 5 amino acids (Phe, Arg, Ala, Val, Glu) (11).

Another *in vitro* specificity analysis of human Gr3 was carried out using the PepChip protease array, which consisted of more than 1,000 randomized 15 amino acid polypeptides (7). The results indicated that Gr3 preferred polypeptides which had Arg, aromatic and hydrophobic amino acids at P1, P2, and P4 positions, respectively. The results were approximately consistent with our results.

On the other hand, several candidates for an *in vivo* substrate for Gr3 have been reported. Gr3 reportedly hydrolyzes the nuclear SET complex of the target cells in a similar manner to granzyme A (7,14,15). This is considered to result in the release of NM23-H1 and degradation of ssDNA. Moreover, Gr3 was investigated to degrade hnRNP K (16) and Bid, which related to mitochondria-mediated apoptosis of the cells (17).

Recently, the degradation site of several cellular proteins by human Gr3 was reported. It was investigated whether Gr3 hydrolyzed DLWK²⁴↓L and GSTK³⁰⁵↓R of p53 protein (6), YVPR⁶²↓A and QQYR²⁸²↓A of β -tubulin (7) and ERER⁷¹³↓Q of valosin-containing protein (8); however, it is very difficult to find some regularity in these results. Similarity to our results from these reports is also hardly found.

Gr3 is stored in intracellular granules as an inactive precursor and transformed to its enzymatically active form by cathepsin C (18). The activated enzymes including Gr3 are considered to be transported into the cytoplasm of the target cells, degrade various proteins and cause the subsequent death of the target cells. To determine expression of Gr3 in activated lymphocytes, human lymphokine-activated killer (LAK) cells were prepared by incubating isolated lymphocytes from peripheral blood with IL-2 for 7 days. When the culture supernatant and cell lysates of LAK cells were analyzed using Gr3 ELISA, Gr3 was detected in culture supernatant as well as in cell lysates (data not shown). Therefore, Gr3 might function not only in the target cells but also outside of the cells, such as attacking plasma membrane proteins in blood plasma.

Human Gr3 is a positively charged protein due to its high content of Arg and Lys. Therefore, it can be considered that Gr3 tends to associate with negatively charged biomolecules such as sulfated carbohydrates and phospholipids. In fact, intracellular Gr3 was hardly extracted with physiological saline solution containing some detergents but with buffers containing 1 M NaCl (data not shown). Gr3 binds to negatively charged proteoglycans along with other granzymes when stored in cytotoxic granules in lymphocytes. Once excreted from lymphocytes, Gr3 might bind to a negatively charged cell surface and have some cytotoxic effect by hydrolyzing cell surface proteins. In addition, we considered that the sequence YFR in the membrane

bound protein is likely to be located at a boundary of the membrane surface, because the former two aromatic amino acids are buried in a hydrophobic atmosphere and the positively charged Arg acts as an anchor by interacting with polar residues of membrane phospholipids. Gr3 may hydrolyze membrane bound proteins after invading target cells.

When GGRNA was used to search human proteins that contained YFR sequence, 769 kinds of proteins were found in the NCBI protein database (13). Among those proteins, 222 were known to locate on a cellular membrane including nuclear and mitochondrial membranes. Therefore, degradation of membrane proteins by Gr3 might be a potential mechanism of its cytotoxic activity. The involvement of the hydrolysis of membrane bound proteins is not known in the induction of apoptosis by granzymes including granzyme A and granzyme B. Bovenschen *et al.* identified cellular proteins that could be hydrolyzed by Gr3 (7). However, they analyzed only cytoplasmic proteins of Jurkat cells. Therefore, membrane bound substrate proteins were not considered in their study. Whether membrane bound proteins are hydrolyzed by Gr3 in the target cells remains to be understood.

This study clearly showed the optimal substrate sequence for Gr3, Tyr-Phe-Arg, by determining the order of the hydrolysis rate. Inhibitors prepared using this sequence might be useful for distinguishing Gr3 from other granzymes *in vitro* and possibly valuable for controlling disease progression, which might involve Gr3 malfunction.

Acknowledgements

The authors thank the laboratory members of our department for their skillful technical assistance.

References

- Hameed A, Lowrey DM, Lichtenheld M, Podack ER. Characterization of three serine esterases isolated from human IL-2 activated killer cells. *J Immunol.* 1988; 141:3142-3147.
- Bovenschen N, Kummer JA. Orphan granzymes find a home. *Immunol Rev.* 2010; 235:117-127.
- Krzewski K, Coligan JE. Human NK cell lytic granules and regulation of their exocytosis. *Front Immunol.* 2012; 3:335.
- Susanto O, Trapani JA, Brasacchio D. Controversies in granzyme biology. *Tissue Antigens.* 2012; 80:477-487.
- Mahrus S, Craik CS. Selective chemical functional probes of granzymes A and B reveal granzyme B is a major effector of natural killer cell-mediated lysis of target cells. *Chem Biol.* 2005; 12:567-577.
- Hua G, Wang S, Zhong C, Xue P, Fan Z. Ignition of p53 bomb sensitizes tumor cells to granzyme K-mediated cytotoxicity. *J Immunol.* 2009; 182:2152-2159.
- Bovenschen N, Quadir R, van den Berg AL, Brenkman AB, Vandenberghe I, Devreese B, Joore J, Kummer JA. Granzyme K displays highly restricted substrate specificity that only partially overlaps with granzyme A. *J Biol Chem.* 2009; 284:3504-3512.
- Guo Y, Chen J, Shi L, Fan Z. Valosin-containing protein cleavage by granzyme K accelerates an endoplasmic reticulum stress leading to caspase-independent cytotoxicity of target tumor cells. *J Immunol.* 2010; 185:5348-5359.
- Stryer L. Fluorescence energy transfer as a spectroscopic ruler. *Annu Rev Biochem.* 1978; 47:819-846.
- Tanskul S, Oda K, Oyama H, Noparatnaraporn N, Tsunemi M, Takada K. Substrate specificity of alkaline serine proteinase isolated from photosynthetic bacterium, *Rubrivivax gelatinosus* KDDS1. *Biochem Biophys Res Commun.* 2003; 309:547-551.
- Hirata Y, Inagaki H, Shimizu T, Li Q, Nagahara N, Minami M, Kawada T. Expression of enzymatically active human granzyme 3 in *Escherichia coli* for analysis of its substrate specificity. *Arch Biochem Biophys.* 2006; 446:35-43.
- Lineweaver H, Burk D. The determination of enzyme dissociation constants. *J Am Chem Soc.* 1934; 56:658-666.
- Naito Y, Bono H. GGRNA: an ultrafast, transcript-oriented search engine for genes and transcripts. *Nucleic Acids Res.* 2012; 40:W592-596.
- Zhao T, Zhang H, Guo Y, Zhang Q, Hua G, Lu H, Hou Q, Liu H, Fan Z. Granzyme K cleaves the nucleosome assembly protein SET to induce single-stranded DNA nicks of target cells. *Cell Death Differ.* 2007; 14:489-499.
- Beresford PJ, Zhang D, Oh DY, Fan Z, Greer EL, Russo ML, Jaju M, Lieberman J. Granzyme A activates an endoplasmic reticulum-associated caspase-independent nuclease to induce single-stranded DNA nicks. *J Biol Chem.* 2001; 276:43285-43293.
- van Domselaar R, Quadir R, van der Made AM, Broekhuizen R, Bovenschen N. All human granzymes target hnRNP K that is essential for tumor cell viability. *J Biol Chem.* 2012; 287:22854-22864.
- Zhao T, Zhang H, Guo Y, Fan Z. Granzyme K directly processes bid to release cytochrome c and endonuclease G leading to mitochondria-dependent cell death. *J Biol Chem.* 2007; 282:12104-12111.
- Hirata Y, Inagaki H, Kawada T. Recombinant human progranzyme 3 expressed in *Escherichia coli* for analysis of its activation mechanism. *Microbiol Immunol.* 2010; 54:98-104.

(Received December 24, 2013; Revised February 21, 2014; Accepted March 15, 2014)

A high-carbohydrate diet lowered blood pressure in healthy Chinese male adolescents

Xingchun Zhu^{1,2}, Jia Lin¹, Yongyan Song¹, Hui Liu¹, Rongrong Zhang¹, Mei Fan¹, Yuanhao Li¹, Rong Tian³, Dingzhi Fang^{1,*}

¹ Department of Biochemistry and Molecular Biology, West China School of Preclinical and Forensic Medicine, Sichuan University, Chengdu, Sichuan, China;

² Clinical Laboratory, Affiliated Hospital of North Sichuan Medical College, Nanchong, Sichuan, China;

³ Mitochondria and Metabolism Center, University of Washington, Seattle, WA, USA.

Summary

Different diets consumed by individuals of different ethnicities, gender, and age may cause changes in blood pressure. The current study sought to investigate changes in blood pressures after consumption of a high-carbohydrate (high-CHO) diet by healthy Chinese adolescents. As a population, the Chinese consume a diet with a high carbohydrate content and they have a low incidence of hypertension and coronary artery disease. Dietary data were collected using a 3-day diet diary. Subjects were 672 high school students who were divided into a high-CHO diet group ($\geq 55\%$ carbohydrates) and a non-high-CHO diet group ($< 55\%$ carbohydrates, $< 40\%$ fats). Plasma glucose levels, heart rate, systolic blood pressure (SBP), and diastolic blood pressure (DBP) were measured. Body mass index (BMI), waist-to-hip ratio (WHR), pulse pressure (PP), and mean arterial pressure (MAP) were calculated. Results indicated that males had a higher BMI, glucose level, SBP, DBP, PP, and MAP than females. When diet was taken into account, males in the non-high-CHO diet group had a higher SBP and PP than females. Males in the high-CHO diet group had a higher glucose level than females. Males in the high-CHO diet group had a lower SBP ($p = 0.004$) and PP ($p = 0.002$) than males in the non-high-CHO diet group and females in the high-CHO diet group had a lower glucose level ($p = 0.003$) than females in the non-high-CHO diet group. After adjusting for age, BMI, WHR, heart rate, the total daily energy intake, and the intake of vitamin C, calcium, sodium, potassium and magnesium, significant differences in SBP and PP were noted in males. These results indicate that male adolescents consuming a high-CHO diet had a lower SBP and PP than males consuming a non-high-CHO diet.

Keywords: Diastolic blood pressure, high-carbohydrate diet, mean arterial pressure, pulse pressure, systolic blood pressure

1. Introduction

Coronary artery disease (CAD) is the leading cause of death worldwide (1). A series of risk factors for CAD, including age, gender, obesity, hypertension, and dyslipoproteinemia, has been identified over the past

few decades (2). Hypertension, a common condition in many countries (3), is closely associated with an increased risk of CAD (4) and seriously affects the health and the quality of life of both the elderly and children. In China, the overall prevalence of a relatively high blood pressure among children aged 7-17 years has increased markedly, rising from 19.29% for boys and 14.69% for girls in 2000 to 26.16% for boys and 19.77% for girls in 2010 (5). The increased prevalence of hypertension may be one explanation for the steadily increasing risk of CAD in younger populations over the past few decades (6). The treatment and control of hypertension is a crucial and effective intervention

*Address correspondence to:

Dr. Dingzhi Fang, Department of Biochemistry and Molecular Biology, West China School of Preclinical and Forensic Medicine, Sichuan University, 17 Section 3, South Renmin Rd, Chengdu 610041, China.
E-mail: dzfang@scu.edu.cn

to deal with CAD. A reduction of 3 mmHg in systolic blood pressure (SBP) has been found to result in a 5% reduction in CAD mortality (7). Pulse pressure (PP) is a well-established independent predictor for cardiovascular outcomes (8). However, hypertension control in younger individuals has received less attention than that in middle-aged individuals and the elderly (9). Therefore, further efforts must be made to understand the development of hypertension and to identify more effective ways to control it in youth.

Studies have indicated that there is a significantly lower risk of hypertension (10) and CAD (11) in the Chinese population. Interestingly, more than 67% of this population's dietary energy is derived from carbohydrates (12,13). A study of this traditional diet has found that a higher percentage of energy intake in the form of carbohydrates is significantly associated with a lower risk of hypertension (14). In fact, a host of studies suggests that high-carbohydrate (high-CHO) diets can lower blood pressure levels (15-17). However, data also indicate that there are no significant changes in blood pressures after a high-CHO dietary intervention (18). A meta-analysis of intervention trials shows that high-CHO diets may be associated with slightly higher blood pressure than high-cis-monounsaturated fat diets (19). This inconsistency may be the result of different genetic and environmental backgrounds (20) and ethnicities (21) or even gender. However, few studies have been sought to investigate the effects of high-CHO diets on blood pressure in healthy adolescents of different genders. These effects have not been reported yet in healthy boys and girls, much less in Chinese, despite the fact that this population consumes a diet with a high carbohydrate content and this population has a lower incidence of hypertension and CAD. Therefore, a cross-sectional study was conducted to investigate changes in blood pressure induced by the high-CHO diet in healthy Chinese Han adolescents of different genders.

2. Methods

This study was *i)* approved by The Ethical Committee of Sichuan University, and *ii)* was conducted with the understanding and the written consent of each high school participant and her/his guardian.

2.1. Subjects

This study was conducted at a boarding high school (grades 11 and 12) located on the outskirts of the City of Chengdu, Sichuan Province, the People's Republic of China. This western province has been influenced by industrialization far less than China's eastern provinces. Volunteers were recruited via advertisements seeking healthy students. Students with health problems and students taking medication that might affect their blood

pressure were excluded from final analysis. In total, 672 students (280 males and 392 females) aged 15-18 years served as subjects. These individuals were apparently healthy, as indicated by medical questionnaires and physical examinations. All of the students were of the Chinese Han ethnic group.

2.2. Dietary data collection

Based on the results of a preliminary study at this high school, dietary data were collected in a 3-day diet diary for the 3 days before blood samples were taken and anthropometric variables were determined. Actual foods by item and amount were displayed on a table in front of each classroom to help the students more accurately estimate what and how much they consumed during each meal. The students were instructed to complete questionnaires in their classrooms. Dietary components were calculated using computer software developed by the Department of Nutrition and Food Safety of the Chinese Center for Disease Control (Beijing, China). Dietary intake by the students was categorized as a high-CHO diet and a non-high-CHO diet on the basis of fat and carbohydrate contributions to total energy. A high-CHO diet was defined as no less than 55% of total energy derived from carbohydrates (22) while a non-high-CHO diet was defined as less than 55% of total energy derived from carbohydrates and less than 40% of total energy derived from fats.

2.3. Physical examinations and laboratory analyses

Venous blood samples were collected after fasting for 12 hours. Collection took place between 7:00 and 8:00 a.m. after which the subject's height, weight, waist circumference, hip circumference, heart rate, SBP, and diastolic blood pressure (DBP) were measured (blood pressure was measured using a standard mercury sphygmomanometer with 1 of 5 cuff sizes chosen on the basis of the circumference of the participant's arm).

Plasma glucose levels were determined using an enzymatic method as previously described (23). Inter- and intra-assay coefficients of variation were less than 6%. Each variable was measured three times independently, and the average of the three measurements was used for statistical analyses. Each subject's body mass index {BMI, =weight (kg)/[height (m)]²}, waist-to-hip ratio [WHR, = waist circumference (cm)/hip circumference (cm)], pulse pressure [PP, =SBP (mmHg)-DBP (mmHg)], and mean arterial pressure [MAP, =1/3SBP (mmHg)+2/3DBP (mmHg)] were calculated.

2.4. Statistical analyses

The normality of the data for each variable was tested using a Shapiro-Wilk test. Subjects consuming the high-

CHO diet (denoted here as the "high-CHO diet group") and those consuming the non-high-CHO diet (denoted here as the "non-high-CHO diet group") were compared using the mean values of variables and both genders were compared using an independent-samples *t*-test. Multiple linear regression analysis was used to adjust for confounding variables. Statistical significance was defined as $p \leq 0.05$. Results are expressed as the mean \pm standard deviation (S.D.) unless stated otherwise.

3. Results

3.1. Characteristics of the two diets

Characteristics of the non-high-CHO diet and the high-CHO diet consumed by the subjects in this study are shown in Table 1. The non-high-CHO diet group consumed a diet consisting of 12.75% proteins, 36.08% fats, and 51.51% carbohydrates while the high-CHO diet group consumed a diet consisting of 11.76% proteins, 27.00% fats, and 61.58% carbohydrates. There were significant differences between the two groups in terms of total daily energy intake and the intake of calcium, sodium, potassium, and magnesium except for vitamin C intake ($p = 0.068$).

3.2. Subject characteristics

The baseline characteristics of the subjects are shown in Table 2. All of the subjects were of the Chinese Han

ethnicity and all were high school students aged 16.85 ± 0.59 years. Males were older, they had a greater BMI, they had higher plasma glucose levels, they had a higher SBP, PP, and MAP, and they had a lower WHR and heart rate than females.

3.3. Blood pressure of the high-CHO diet group and the non-high-CHO diet group

The blood pressure of subjects consuming the high-CHO diet or the non-high-CHO diet is shown in Table 3, along with their age, BMI, WHR, heart rate, and plasma glucose levels. Males who consumed the non-high-CHO diet were older and had a higher SBP and PP compared to females who consumed the same diet. Males who consumed the high-CHO diet were older and had higher plasma glucose levels than females who consumed the same diet. In addition, females had a higher WHR and heart rate than males, regardless of the diet.

Subjects consuming the high-CHO diet had significantly lower glucose levels and a lower SBP, PP, and MAP than subjects consuming the non-high-CHO diet. After adjusting for age, gender, BMI, WHR, heart rate, the total daily energy intake, and the intake of vitamin C, calcium, sodium, potassium, magnesium, significant differences in SBP, PP, and MAP were noted. After adjusting for age, gender, BMI and the total daily energy intake, significant differences in glucose levels were not noted. When gender was taken into account, males in the

Table 1. Dietary characteristics of the non- high-CHO diet and the high-CHO diet consumed by subjects in this study

Variables	Non-high-CHO diet	High-CHO diet	<i>p</i>
Number of subjects	<i>n</i> = 266	<i>n</i> = 406	
Total energy (kilocalories/d)	3.129 \pm 1.469	2.346 \pm 1.065	< 0.001
Proteins (% of total energy intake)	12.75 \pm 2.58	11.76 \pm 2.85	< 0.001
Fats (% of total energy intake)	36.08 \pm 2.50	27.00 \pm 5.70	< 0.001
Carbohydrates (% of total energy intake)	51.51 \pm 2.64	61.58 \pm 5.57	< 0.001
Vitamin C (mg/d)	62.84 \pm 45.30	56.51 \pm 42.82	0.068
Calcium (mg/d)	427.3 \pm 340.2	319.8 \pm 253.0	< 0.001
Potassium (g/d)	2.086 \pm 1.426	1.619 \pm 1.142	< 0.001
Sodium (g/d)	3.812 \pm 1.777	2.732 \pm 1.580	< 0.001
Magnesium (mg/d)	349.9 \pm 205.4	275.5 \pm 156.6	< 0.001

Data are the mean \pm S.D. *p* represents the non-high-CHO diet vs. the high-CHO diet in an independent-samples *t*-test.

Table 2. Baseline characteristics of the subjects in this study

Variables	Total (<i>n</i> = 672)	Males (<i>n</i> = 280)	Females (<i>n</i> = 392)	<i>p</i>
Age (years)	16.85 \pm 0.59	16.95 \pm 0.61	16.78 \pm 0.56	< 0.001
BMI (Kg/m ²)	20.46 \pm 3.19	20.80 \pm 3.28	20.21 \pm 3.10	0.019
WHR	0.78 \pm 0.05	0.77 \pm 0.04	0.79 \pm 0.05	0.001
Heart rate (bpm)	82.29 \pm 11.06	79.53 \pm 10.64	84.27 \pm 10.94	< 0.001
Glucose (mg/dL)	90.94 \pm 7.60	92.53 \pm 8.03	89.81 \pm 7.07	< 0.001
SBP (mmHg)	118.5 \pm 11.80	120.80 \pm 11.97	116.86 \pm 11.41	< 0.001
DBP (mmHg)	72.42 \pm 10.63	73.24 \pm 10.33	71.84 \pm 10.81	0.092
PP (mmHg)	46.08 \pm 9.19	47.56 \pm 8.85	45.02 \pm 9.30	< 0.001
MAP (mmHg)	87.78 \pm 10.14	89.09 \pm 10.07	86.85 \pm 10.10	0.005

Data are the mean \pm S.D. *p* represents females vs. males in an independent-samples *t*-test.

high-CHO diet group had a significantly lower SBP and PP than males in the non-high-CHO diet group (Table 3). Females in the high-CHO diet group had a lower glucose level (Table 3). After adjusting for various variables, significant differences were still noted (Table 3).

4. Discussion

The lower prevalence of hypertension and CAD in the Chinese population has been well documented (10,11). The traditional Chinese diet has a high carbohydrate content (12,13) that may help to limit risk factors for hypertension and CAD. The current results showed that in the healthy Chinese adolescents of this study, the male subjects taking the high-CHO diet had lower SBP and PP than the males taking the non-high-CHO diet.

The results of most observational studies that investigated the effects of both type and amount of carbohydrate intake on blood pressure are contradictory (15,16,18). For example, diets with a high carbohydrate content coming mainly from sucrose and fructose are reported to raise blood pressure (24-26). However, results of the International Population Study on Macronutrients and Blood Pressure (INTERMAP), which included 4,680 subjects aged 40-59 years from 4 countries (the People's Republic of China, Japan, the United Kingdom, and the United States), have suggested a weakly inverse or even an indirect relationship between blood pressure and starch intake (27). In contrast, results of the Multiple Risk Factor Intervention Trial (MRFIT) indicated that dietary starch consumption was positively associated with blood pressure (28). The traditional Chinese diet mainly consists of white rice, and most of the carbohydrates in white rice are starch (29). The current results provide significant evidence that male adolescents in the high-CHO diet group had a significantly lower SBP and PP than male adolescents in the non-high-CHO diet group after adjusting for confounding variables that might influence blood pressure. Since high-CHO diets have a lower proportion of energy from fats, a lower blood pressure may be the result of reduced fat since a lower blood pressure after consuming a high-CHO diet is independent of changes in plasma insulin levels (30). Similarly, males in the current study who did not have lower plasma glucose levels nonetheless had a lower SBP and PP compared to males in the non-high-CHO diet group. However, females in the high-CHO diet group who did not have a lower blood pressure had even lower plasma glucose levels.

The current findings indicate that the high-CHO diet affected blood pressure differently in males and females. A significant decrease in blood pressure after consuming a high-CHO diet was noted only in males and not in females. The different outcomes resulting from a high-CHO diet might be due, at least in part, to physiological (31), pathological (32), or psychological

Table 3. Age, BMI, glucose levels, and blood pressure of subjects on the non-high-CHO diet or the high-CHO diet

Variables	Total (n = 406)		Males (n = 127)		Females (n = 279)		P	p ^a
	Non-high-CHO diet (n = 266)	High-CHO diet (n = 140)	Non-high-CHO diet (n = 153)	High-CHO diet (n = 74)	Non-high-CHO diet (n = 113)	High-CHO diet (n = 166)		
Age (years)	16.86 ± 0.58	16.85 ± 0.59	16.97 ± 0.59	16.94 ± 0.63	16.72 ± 0.53 ^g	16.81 ± 0.57 ^f	0.136	-
BMI (kg/m ²)	20.72 ± 2.99	20.28 ± 3.30	20.96 ± 2.97	20.61 ± 3.63	20.41 ± 3.00	20.13 ± 3.14	0.428	-
WHR	0.78 ± 0.05	0.78 ± 0.05	0.77 ± 0.04	0.77 ± 0.04	0.79 ± 0.05 ^f	0.79 ± 0.05 ^f	0.507	-
Heart rate (bpm)	82.04 ± 12.04	82.46 ± 10.38	79.24 ± 10.28	79.87 ± 11.10	85.84 ± 13.20 ^g	83.64 ± 9.84 ^g	0.111	-
Glucose (mg/dL)	92.34 ± 8.50	90.03 ± 6.80	92.96 ± 8.68	92.01 ± 7.17	91.49 ± 8.21	89.13 ± 6.44 ^g	0.003	0.023 ^c
SBP (mmHg)	120.83 ± 12.42	116.97 ± 11.12	122.68 ± 12.22	118.53 ± 11.29	118.34 ± 12.31 ^f	116.26 ± 11.00	0.103	0.109 ^c
DBP (mmHg)	73.21 ± 10.66	71.91 ± 10.59	73.68 ± 10.18	72.71 ± 10.53	72.57 ± 11.29	71.54 ± 10.61	0.397	0.316 ^c
PP (mmHg)	47.63 ± 9.47	45.06 ± 8.87	49.00 ± 9.66	45.82 ± 7.44	45.77 ± 8.92 ^f	44.72 ± 9.46	0.310	0.445 ^c
MAP (mmHg)	89.08 ± 10.36	86.93 ± 9.92	90.01 ± 9.90	87.98 ± 10.21	87.82 ± 10.86	86.45 ± 9.77	0.224	0.185 ^c

Data are the mean ± S.D. *p* represents the Non-high-CHO diet vs. High-CHO diet in an independent-samples *t*-test. ^a Adjusted *p* value obtained from multiple linear regression; ^b After adjusting for age, gender, BMI, and energy intake; ^c After adjusting for age, BMI, and energy intake; ^d After adjusting for age, gender, BMI, WHR, heart rate, energy intake, and intake of vitamin C, calcium, sodium, potassium, and magnesium; ^e After adjusting for age, BMI, WHR, heart rate, energy intake, and intake of vitamin C, calcium, sodium, potassium, and magnesium; ^f *p* ≤ 0.05 compared to males in the group on the same diet according to an independent-samples *t*-test; ^g *p* ≤ 0.001 compared to males in the group on the same diet according to an independent-samples *t*-test.

variation or to different hormonal effects (33,34). For example, previous studies have indicated that estrogen can lead to a lower level of serum angiotensin-converting-enzyme (ACE) activity (33) and higher level of ACE2 activity (34), leading to higher blood pressure in male mice (34). The detailed mechanism by which a high-CHO diet affects blood pressure needs to be elucidated in further studies.

A 3-day diet diary was used to collect dietary information in the present study. The total daily energy intake, the intake of vitamin C, calcium, sodium, potassium, and magnesium, and the proportion of energy derived from carbohydrates, fats, and proteins with respect to the total energy intake was calculated using software. The data obtained by these methods may not accurately reflect the dietary habits of the individuals studied. Therefore, this limitation should be taken into account when the results of the present study are cited.

In summary, the current results indicate that healthy Chinese male adolescents consuming a high-CHO diet had a lower SBP and PP than males consuming a non-high-CHO diet. The beneficial effects on blood pressure of the high-CHO diet may be one explanation for the lower prevalence of hypertension and CAD as has been documented in the Chinese population. Further studies have the potential to reveal the underlying mechanisms of a high-CHO diet, which may reduce the risk of hypertension and CAD.

Acknowledgements

This study was supported by a grant from the National Natural Science Foundation of China (Grant No. 81370375) to Dr. Ding Zhi Fang.

References

- Peden JF, Farrall M. Thirty-five common variants for coronary artery disease: The fruits of much collaborative labour. *Hum Mol Genet.* 2011; 20:R198-205.
- Cheng TO. Cardiovascular health, risks and diseases in contemporary China. *Int J Cardiol.* 2011; 152:285-294.
- Conroy RM, Pyörälä K, Fitzgerald AP, *et al.* Estimation of ten-year risk of fatal cardiovascular disease in Europe: The SCORE project. *European Heart J.* 2003; 11:987-1003.
- Foody J, Huo Y, Ji L, Zhao D, Boyd D, Meng HJ, Shiff S, Hu D. Unique and varied contributions of traditional CVD risk factors: A systematic literature review of CAD risk factors in China. *Clin Med Insights Cardiol.* 2013; 7:59-86.
- Zhang YX, Zhao JS, Sun GZ, Lin M, Chu ZH. Prevalent trends in relatively high blood pressure among children and adolescents in Shandong, China. *Ann Hum Biol.* 2012; 39:259-263.
- Saleheen D, Frossard P. CAD risk factors and acute myocardial infarction in Pakistan. *Acta Cardiol.* 2004; 59:417-424.
- Stamler R. Implications of the INTERSALT study. *Hypertension.* 1991; 17:116-20.
- Dart AM, Kingwell BA. Pulse pressure. A review of mechanisms and clinical relevance. *J Am Coll Cardiol.* 2001; 37:975-984.
- Egan BM, Zhao Y, Axon RN. US trends in prevalence, awareness, treatment, and control of hypertension, 1988-2008. *JAMA.* 2010; 303:2043-2050.
- Pereira M, Lunet N, Azevedo A, Barros H. Differences in prevalence, awareness, treatment and control of hypertension between developing and developed countries. *J Hypertens.* 2009; 27:963-975.
- Gaziano TA, Bitton A, Anand S, Abrahams-Gessel S, Murphy A. Growing epidemic of coronary heart disease in low- and middle-income countries. *Curr Probl Cardiol.* 2010; 35:72-115.
- Lee MM, Wu-Williams A, Whittemore AS, *et al.* Comparison of dietary habits, physical activity and body size among Chinese in North America and China. *Int J Epidemiol.* 1994; 23:984-990.
- Chen Z, Shu XO, Yang G, Li H, Li Q, Gao YT, Zheng W. Nutrient intake among Chinese women living in Shanghai, China. *Br J Nutr.* 2006; 96:393-399.
- Chen CM, Zhao W, Yang Z, Zhai Y, Wu Y, Kong L. The role of dietary factors in chronic disease control in China. *Obes Rev.* 2008; 9:100-103.
- Muzio F, Mondazzi L, Harris WS, Sommariva D, Branchi A. Effects of moderate variations in the macronutrient content of the diet on cardiovascular disease risk factors in obese patients with the metabolic syndrome. *Am J Clin Nutr.* 2007; 86:946-951.
- Lim SS, Noakes M, Keogh JB, Clifton PM. Long-term effects of a low carbohydrate, low fat or high unsaturated fat diet compared to a no-intervention control. *Nutr Metab Cardiovasc Dis.* 2010; 20:599-607.
- Appel LJ, Sacks FM, Carey VJ, Obarzanek E, Swain JF, Miller ER 3rd, Conlin PR, Erlinger TP, Rosner BA, Laranjo NM, Charleston J, McCarron P, Bishop LM; OmniHeart Collaborative Research Group. Effects of protein, monounsaturated fat, and carbohydrate intake on blood pressure and serum lipids: Results of the OmniHeart randomized trial. *JAMA.* 2005; 294:2455-2464.
- Brehm BJ, Seeley RJ, Daniels SR, D'Alessio DA. A randomized trial comparing a very low carbohydrate diet and a calorie-restricted low fat diet on body weight and cardiovascular risk factors in healthy women. *J Clin Endocrinol Metab.* 2003; 88:1617-1623.
- Shah M, Adams-Huet B, Garg A. Effect of high-carbohydrate or high-cis-monounsaturated fat diets on blood pressure: A meta-analysis of intervention trials. *Am J Clin Nutr.* 2007; 85:1251-1256.
- Appel LJ, Brands MW, Daniels SR, Karanja N, Elmer PJ, Sacks FM; American Heart Association. Dietary approaches to prevent and treat hypertension: A scientific statement from the American Heart Association. *Hypertension.* 2006; 47:296-308.
- Svetkey LP, Erlinger TP, Vollmer WM, Feldstein A, Cooper LS, Appel LJ, Ard JD, Elmer PJ, Harsha D, Stevens VJ. Effect of lifestyle modifications on blood pressure by race, sex, hypertension status, and age. *J Hum Hypertens.* 2005; 19:21-31.
- Parks EJ, Hellerstein MK. Carbohydrate-induced hypertriacylglycerolemia: Historical perspective and review of biological mechanisms. *Am J Clin Nutr.* 2000;

- 71:412-433.
23. Fang DZ, Liu BW. Polymorphism of HL +1075C, but not -480T, is associated with plasma high density lipoprotein cholesterol and apolipoprotein AI in men of a Chinese population. *Atherosclerosis*. 2002; 161:417-424.
 24. Jalas DI, Smits G, Johnson RJ, Chonchol M. Increased fructose associates with elevated blood pressure. *J Am Soc Nephrol*. 2010; 21:1543-1549.
 25. Hulman S, Falkner B. The effect of excess dietary sucrose on growth, blood pressure, and metabolism in developing Sprague-Dawley rats. *Pediatr Res*. 1994; 36:95-101.
 26. Daly ME, Vale C, Walker M, Alberti KG, Mathers JC. Dietary carbohydrates and insulin sensitivity: A review of the evidence and clinical implication. *Am J Clin Nutr*. 1997; 66:1072-1085.
 27. Brown IJ, Elliott P, Robertson CE, Chan Q, Daviglus ML, Dyer AR, Huang CC, Rodriguez BL, Sakata K, Ueshima H, Van Horn L, Zhao L, Stamler J; INTERMAP Research Group. Dietary starch intake of individuals and their blood pressure: The International Study of Macronutrients and Micronutrients and Blood Pressure. *J Hypertens*. 2009; 27:231-236.
 28. Stamler J, Caggiula A, Grandits GA, Kjelsberg M, Cutler JA. Relationship to blood pressure of combinations of dietary macronutrients. Findings of the Multiple Risk Factor Intervention Trial (MRFIT). *Circulation*. 1996; 94:2417-2423.
 29. Chen CM, Zhao W, Yang Z, Zhai Y, Wu Y, Kong L. The role of dietary factors in chronic disease control in China. *Obes Rev*. 2008; 9:100-103.
 30. Straznicky NE, O'Callaghan CJ, Barrington VE, Louis WJ. Hypotensive effect of low-fat, high-carbohydrate diet can be independent of changes in plasma insulin concentrations. *Hypertension*. 1999; 34:580-585.
 31. Reik W, Walter J. Evolution of imprinting mechanisms: The battle of the sexes begins in the zygote. *Nat Genet*. 2001; 27:255-256.
 32. Koskinen J, Magnussen CG, Viikari JS, Kähönen M, Laitinen T, Hutri-Kähönen N, Lehtimäki T, Jokinen E, Raitakari OT, Juonala M. Effect of age, gender and cardiovascular risk factors on carotid distensibility during 6-year follow-up. The Cardiovascular Risk in Young Finns study. *Atherosclerosis*. 2012; 224:474-479.
 33. Proudler AJ, Ahmed AI, Crook D, Fogelman I, Rymer JM, Stevenson JC. Hormone replacement therapy and serum angiotensin-converting-enzyme activity in postmenopausal women. *Lancet*. 1995; 346:89-90.
 34. Gupte M, Thatcher SE, Boustany-Kari CM, Shoemaker R, Yiannikouris F, Zhang X, Karounos M, Cassis LA. Angiotensin converting enzyme 2 contributes to sex differences in the development of obesity hypertension in C57BL/6 mice. *Arterioscler Thromb Vasc Biol*. 2012; 32:1392-1399.

(Received October 19, 2013; Revised December 31, 2013; Accepted February 4, 2014)

Guide for Authors

1. Scope of Articles

BioScience Trends is an international peer-reviewed journal. BioScience Trends devotes to publishing the latest and most exciting advances in scientific research. Articles cover fields of life science such as biochemistry, molecular biology, clinical research, public health, medical care system, and social science in order to encourage cooperation and exchange among scientists and clinical researchers.

2. Submission Types

Original Articles should be well-documented, novel, and significant to the field as a whole. An Original Article should be arranged into the following sections: Title page, Abstract, Introduction, Materials and Methods, Results, Discussion, Acknowledgments, and References. Original articles should not exceed 5,000 words in length (excluding references) and should be limited to a maximum of 50 references. Articles may contain a maximum of 10 figures and/or tables.

Brief Reports definitively documenting either experimental results or informative clinical observations will be considered for publication in this category. Brief Reports are not intended for publication of incomplete or preliminary findings. Brief Reports should not exceed 3,000 words in length (excluding references) and should be limited to a maximum of 4 figures and/or tables and 30 references. A Brief Report contains the same sections as an Original Article, but the Results and Discussion sections should be combined.

Reviews should present a full and up-to-date account of recent developments within an area of research. Normally, reviews should not exceed 8,000 words in length (excluding references) and should be limited to a maximum of 100 references. Mini reviews are also accepted.

Policy Forum articles discuss research and policy issues in areas related to life science such as public health, the medical care system, and social science and may address governmental issues at district, national, and international levels of discourse. Policy Forum articles should not exceed 2,000 words in length (excluding references).

Case Reports should be detailed reports of the symptoms, signs, diagnosis, treatment, and follow-up of an individual patient. Case reports may contain a demographic profile of the patient but usually describe an unusual or novel occurrence. Unreported or unusual

side effects or adverse interactions involving medications will also be considered. Case Reports should not exceed 3,000 words in length (excluding references).

News articles should report the latest events in health sciences and medical research from around the world. News should not exceed 500 words in length.

Letters should present considered opinions in response to articles published in BioScience Trends in the last 6 months or issues of general interest. Letters should not exceed 800 words in length and may contain a maximum of 10 references.

3. Editorial Policies

Ethics: BioScience Trends requires that authors of reports of investigations in humans or animals indicate that those studies were formally approved by a relevant ethics committee or review board.

Conflict of Interest: All authors are required to disclose any actual or potential conflict of interest including financial interests or relationships with other people or organizations that might raise questions of bias in the work reported. If no conflict of interest exists for each author, please state "There is no conflict of interest to disclose".

Submission Declaration: When a manuscript is considered for submission to BioScience Trends, the authors should confirm that 1) no part of this manuscript is currently under consideration for publication elsewhere; 2) this manuscript does not contain the same information in whole or in part as manuscripts that have been published, accepted, or are under review elsewhere, except in the form of an abstract, a letter to the editor, or part of a published lecture or academic thesis; 3) authorization for publication has been obtained from the authors' employer or institution; and 4) all contributing authors have agreed to submit this manuscript.

Cover Letter: The manuscript must be accompanied by a cover letter signed by the corresponding author on behalf of all authors. The letter should indicate the basic findings of the work and their significance. The letter should also include a statement affirming that all authors concur with the submission and that the material submitted for publication has not been published previously or is not under consideration for publication elsewhere. The cover letter should be submitted in PDF format. For example of Cover Letter, please visit <http://www.biosciencetrends.com/downcentre.php> (Download Centre).

Copyright: A signed JOURNAL PUBLISHING AGREEMENT (JPA) form must be provided by post, fax, or as a scanned file before acceptance of the article. Only forms with a hand-written signature are accepted. This copyright will ensure the widest possible dissemination of information. A form facilitating transfer of copyright can be downloaded by clicking the

appropriate link and can be returned to the e-mail address or fax number noted on the form (Please visit [Download Centre](#)). Please note that your manuscript will not proceed to the next step in publication until the JPA Form is received. In addition, if excerpts from other copyrighted works are included, the author(s) must obtain written permission from the copyright owners and credit the source(s) in the article.

Suggested Reviewers: A list of up to 3 reviewers who are qualified to assess the scientific merit of the study is welcomed. Reviewer information including names, affiliations, addresses, and e-mail should be provided at the same time the manuscript is submitted online. Please do not suggest reviewers with known conflicts of interest, including participants or anyone with a stake in the proposed research; anyone from the same institution; former students, advisors, or research collaborators (within the last three years); or close personal contacts. Please note that the Editor-in-Chief may accept one or more of the proposed reviewers or may request a review by other qualified persons.

Language Editing: Manuscripts prepared by authors whose native language is not English should have their work proofread by a native English speaker before submission. If not, this might delay the publication of your manuscript in BioScience Trends.

The Editing Support Organization can provide English proofreading, Japanese-English translation, and Chinese-English translation services to authors who want to publish in BioScience Trends and need assistance before submitting a manuscript. Authors can visit this organization directly at <http://www.iacmhr.com/iac-eso/support.php?lang=en>. IAC-ESO was established to facilitate manuscript preparation by researchers whose native language is not English and to help edit works intended for international academic journals.

4. Manuscript Preparation

Manuscripts should be written in clear, grammatically correct English and submitted as a Microsoft Word file in a single-column format. Manuscripts must be paginated and typed in 12-point Times New Roman font with 24-point line spacing. Please do not embed figures in the text. Abbreviations should be used as little as possible and should be explained at first mention unless the term is a well-known abbreviation (e.g. DNA). Single words should not be abbreviated.

Title Page: The title page must include 1) the title of the paper (Please note the title should be short, informative, and contain the major key words); 2) full name(s) and affiliation(s) of the author(s), 3) abbreviated names of the author(s), 4) full name, mailing address, telephone/fax numbers, and e-mail address of the corresponding author; and 5) conflicts of interest (if you have an actual or potential conflict of interest to disclose, it must be included as a footnote on the title page of the manuscript; if no conflict of

interest exists for each author, please state "There is no conflict of interest to disclose"). Please visit [Download Centre](#) and refer to the title page of the manuscript sample.

Abstract: The abstract should briefly state the purpose of the study, methods, main findings, and conclusions. For article types including Original Article, Brief Report, Review, Policy Forum, and Case Report, a one-paragraph abstract consisting of no more than 250 words must be included in the manuscript. For News and Letters, a brief summary of main content in 150 words or fewer should be included in the manuscript. Abbreviations must be kept to a minimum and non-standard abbreviations explained in brackets at first mention. References should be avoided in the abstract. Key words or phrases that do not occur in the title should be included in the Abstract page.

Introduction: The introduction should be a concise statement of the basis for the study and its scientific context.

Materials and Methods: The description should be brief but with sufficient detail to enable others to reproduce the experiments. Procedures that have been published previously should not be described in detail but appropriate references should simply be cited. Only new and significant modifications of previously published procedures require complete description. Names of products and manufacturers with their locations (city and state/country) should be given and sources of animals and cell lines should always be indicated. All clinical investigations must have been conducted in accordance with Declaration of Helsinki principles. All human and animal studies must have been approved by the appropriate institutional review board(s) and a specific declaration of approval must be made within this section.

Results: The description of the experimental results should be succinct but in sufficient detail to allow the experiments to be analyzed and interpreted by an independent reader. If necessary, subheadings may be used for an orderly presentation. All figures and tables must be referred to in the text.

Discussion: The data should be interpreted concisely without repeating material already presented in the Results section. Speculation is permissible, but it must be well-founded, and discussion of the wider implications of the findings is encouraged. Conclusions derived from the study should be included in this section.

Acknowledgments: All funding sources should be credited in the Acknowledgments section. In addition, people who contributed to the work but who do not meet the criteria for authors should be listed along with their contributions.

References: References should be numbered in the order in which they appear in the text. Citing of unpublished results, personal communications, conference abstracts, and theses in the reference list is not recommended but these sources may be mentioned in the text. In the reference list,

cite the names of all authors when there are fifteen or fewer authors; if there are sixteen or more authors, list the first three followed by *et al.* Names of journals should be abbreviated in the style used in PubMed. Authors are responsible for the accuracy of the references. Examples are given below:

Example 1 (Sample journal reference): Inagaki Y, Tang W, Zhang L, Du GH, Xu WF, Kokudo N. Novel aminopeptidase N (APN/CD13) inhibitor 24F can suppress invasion of hepatocellular carcinoma cells as well as angiogenesis. *Biosci Trends*. 2010; 4:56-60.

Example 2 (Sample journal reference with more than 15 authors): Darby S, Hill D, Auvinen A, *et al.* Radon in homes and risk of lung cancer: Collaborative analysis of individual data from 13 European case-control studies. *BMJ*. 2005; 330:223.

Example 3 (Sample book reference): Shalev AY. Post-traumatic stress disorder: diagnosis, history and life course. In: Post-traumatic Stress Disorder, Diagnosis, Management and Treatment (Nutt DJ, Davidson JR, Zohar J, eds.). Martin Dunitz, London, UK, 2000; pp. 1-15.

Example 4 (Sample web page reference): Ministry of Health, Labour and Welfare of Japan. Dietary reference intakes for Japanese. <http://www.mhlw.go.jp/houdou/2004/11/h1122-2a.html> (accessed June 14, 2010).

Tables: All tables should be prepared in Microsoft Word or Excel and should be arranged at the end of the manuscript after the References section. Please note that tables should not be image format. All tables should have a concise title and should be numbered consecutively with Arabic numerals. If necessary, additional information should be given below the table.

Figure Legend: The figure legend should be typed on a separate page of the main manuscript and should include a short title and explanation. The legend should be concise but comprehensive and should be understood without referring to the text. Symbols used in figures must be explained.

Figure Preparation: All figures should be clear and cited in numerical order in the text. Figures must fit a one- or two-column format on the journal page: 8.3 cm (3.3 in.) wide for a single column, 17.3 cm (6.8 in.) wide for a double column; maximum height: 24.0 cm (9.5 in.). Please make sure that the symbols and numbers appeared in the figures should be clear. Please make sure that artwork files are in an acceptable format (TIFF or JPEG) at minimum resolution (600 dpi for illustrations, graphs, and annotated artwork, and 300 dpi for micrographs and photographs). Please provide all figures as separate files. Please note that low-resolution images are one of the leading causes of article resubmission and schedule delays. All color figures will be reproduced in full color in the online edition of the journal at no cost to authors.

Units and Symbols: Units and symbols

conforming to the International System of Units (SI) should be used for physicochemical quantities. Solidus notation (*e.g.* mg/kg, mg/mL, mol/mm²/min) should be used. Please refer to the SI Guide www.bipm.org/en/si/ for standard units.

Supplemental data: Supplemental data might be useful for supporting and enhancing your scientific research and BioScience Trends accepts the submission of these materials which will be only published online alongside the electronic version of your article. Supplemental files (figures, tables, and other text materials) should be prepared according to the above guidelines, numbered in Arabic numerals (*e.g.*, Figure S1, Figure S2, and Table S1, Table S2) and referred to in the text. All figures and tables should have titles and legends. All figure legends, tables and supplemental text materials should be placed at the end of the paper. Please note all of these supplemental data should be provided at the time of initial submission and note that the editors reserve the right to limit the size and length of Supplemental Data.

5. Submission Checklist

The Submission Checklist will be useful during the final checking of a manuscript prior to sending it to BioScience Trends for review. Please visit [Download Centre](#) and download the Submission Checklist file.

6. Online Submission

Manuscripts should be submitted to BioScience Trends online at <http://www.biosciencetrends.com>. The manuscript file should be smaller than 5 MB in size. If for any reason you are unable to submit a file online, please contact the Editorial Office by e-mail at office@biosciencetrends.com.

7. Accepted Manuscripts

Proofs: Galley proofs in PDF format will be sent to the corresponding author via e-mail. Corrections must be returned to the editor (proof-editing@biosciencetrends.com) within 3 working days.

Offprints: Authors will be provided with electronic offprints of their article. Paper offprints can be ordered at prices quoted on the order form that accompanies the proofs.

Page Charge: Page charges will be levied on all manuscripts accepted for publication in BioScience Trends (\$140 per page for black white pages; \$340 per page for color pages). Under exceptional circumstances, the author(s) may apply to the editorial office for a waiver of the publication charges at the time of submission.

(Revised February 2013)

Editorial and Head Office:

Pearl City Koishikawa 603
2-4-5 Kasuga, Bunkyo-ku
Tokyo 112-0003 Japan
Tel: +81-3-5840-8764
Fax: +81-3-5840-8765
E-mail: office@biosciencetrends.com

JOURNAL PUBLISHING AGREEMENT (JPA)

Manuscript No.:

Title:

Corresponding Author:

The International Advancement Center for Medicine & Health Research Co., Ltd. (IACMHR Co., Ltd.) is pleased to accept the above article for publication in BioScience Trends. The International Research and Cooperation Association for Bio & Socio-Sciences Advancement (IRCA-BSSA) reserves all rights to the published article. Your written acceptance of this JOURNAL PUBLISHING AGREEMENT is required before the article can be published. Please read this form carefully and sign it if you agree to its terms. The signed JOURNAL PUBLISHING AGREEMENT should be sent to the BioScience Trends office (Pearl City Koishikawa 603, 2-4-5 Kasuga, Bunkyo-ku, Tokyo 112-0003, Japan; E-mail: office@biosciencetrends.com; Tel: +81-3-5840-8764; Fax: +81-3-5840-8765).

1. Authorship Criteria

As the corresponding author, I certify on behalf of all of the authors that:

- 1) The article is an original work and does not involve fraud, fabrication, or plagiarism.
- 2) The article has not been published previously and is not currently under consideration for publication elsewhere. If accepted by BioScience Trends, the article will not be submitted for publication to any other journal.
- 3) The article contains no libelous or other unlawful statements and does not contain any materials that infringes upon individual privacy or proprietary rights or any statutory copyright.
- 4) I have obtained written permission from copyright owners for any excerpts from copyrighted works that are included and have credited the sources in my article.
- 5) All authors have made significant contributions to the study including the conception and design of this work, the analysis of the data, and the writing of the manuscript.
- 6) All authors have reviewed this manuscript and take responsibility for its content and approve its publication.
- 7) I have informed all of the authors of the terms of this publishing agreement and I am signing on their behalf as their agent.

2. Copyright Transfer Agreement

I hereby assign and transfer to IACMHR Co., Ltd. all exclusive rights of copyright ownership to the above work in the journal BioScience Trends, including but not limited to the right 1) to publish, republish, derivate, distribute, transmit, sell, and otherwise use the work and other related material worldwide, in whole or in part, in all languages, in electronic, printed, or any other forms of media now known or hereafter developed and the right 2) to authorize or license third parties to do any of the above.

I understand that these exclusive rights will become the property of IACMHR Co., Ltd., from the date the article is accepted for publication in the journal BioScience Trends. I also understand that IACMHR Co., Ltd. as a copyright owner has sole authority to license and permit reproductions of the article.

I understand that except for copyright, other proprietary rights related to the Work (e.g. patent or other rights to any process or procedure) shall be retained by the authors. To reproduce any text, figures, tables, or illustrations from this Work in future works of their own, the authors must obtain written permission from IACMHR Co., Ltd.; such permission cannot be unreasonably withheld by IACMHR Co., Ltd.

3. Conflict of Interest Disclosure

I confirm that all funding sources supporting the work and all institutions or people who contributed to the work but who do not meet the criteria for authors are acknowledged. I also confirm that all commercial affiliations, stock ownership, equity interests, or patent-licensing arrangements that could be considered to pose a financial conflict of interest in connection with the article have been disclosed.

Corresponding Author's Name (Signature):

Date:

